

Medical University of South Carolina

MEDICA

MUSC Theses and Dissertations

1-1-2018

The Roles of Macrophages and Alternative Complement Signaling in Auditory Nerve Development and Function

LaShardai Neniara Brown
Medical University of South Carolina

Follow this and additional works at: <https://medica-musc.researchcommons.org/theses>

Recommended Citation

Brown, LaShardai Neniara, "The Roles of Macrophages and Alternative Complement Signaling in Auditory Nerve Development and Function" (2018). *MUSC Theses and Dissertations*. 940.
<https://medica-musc.researchcommons.org/theses/940>

This Dissertation is brought to you for free and open access by MEDICA. It has been accepted for inclusion in MUSC Theses and Dissertations by an authorized administrator of MEDICA. For more information, please contact medica@musc.edu.

**The Roles of Macrophages and Alternative Complement Signaling in Auditory Nerve
Development and Function**

by

LaShardai Neniara Brown

A dissertation submitted to the faculty of the Medical University of South Carolina in partial fulfillment of the requirements for the degree of Doctor of Philosophy in the College of Graduate Studies

Department of Pathology and Laboratory Medicine

2018

Approved by:

Chairman, Advisory Committee:

Advisory Committee:



Hainan Lang



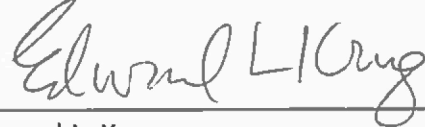
Carl Atkinson



Jeremy L. Barth



Judy R. Dubno



Edward L. Krug



Stephen P. Ethier



Dennis K. Watson

'LASHARDAI NENIARA BROWN. The Roles of Macrophages and Alternative Complement Signaling in Auditory Nerve Development and Function. (Under the direction of Hainan Lang)'

TABLE OF CONTENTS

Dedication.....	iii
Acknowledgements.....	iv
List of Abbreviations.....	vi
List of Figures.....	viii
List of Tables.....	x
Abstract.....	xi
Chapter One: Introduction	
A. Hearing and Cells of the Auditory Nerve.....	1
B. Auditory Nerve Refinement.....	14
C. Macrophages and Complement Signaling.....	19
D. Rationale, Significant and Specific Aims.....	27
Chapter Two: Materials and Methods.....	31
Chapter Three: macrophage-mediated glial cell elimination in the postnatal mouse cochlea.....	44
Introduction.....	45
Results.....	48
Glial cell numbers decrease after the second postnatal week.....	48
Immune-related and axon guidance gene expression correlate with auditory nerve maturation.....	52
Macrophage numbers increase during auditory nerve maturation.....	58
Postnatal macrophages display activated phenotypes.....	61
Macrophages phagocytose glial cells and axonal fragments.....	65

Transient depletion of postnatal macrophages increases glial cell numbers.....	71
Transient depletion of macrophages results in dysfunction of myelinating glial cells.....	77
Macrophage depletion impairs auditory function of postnatal and young adult mice.....	82
Discussion.....	87
Chapter Four: Cochlear Pathophysiological Alterations in fB ^{-/-} Mice.....	94
Introduction	95
Results.....	98
Complement gene expression in the auditory nerve.....	98
Mice deficient in fB signaling have impaired auditory function.....	100
Characterization of gross morphology of HCs and SGNs in fB ^{-/-} mice.....	103
fB ^{-/-} mice display reduced glial cell numbers and potassium channel dysfunction in auditory nerve.....	106
Macrophages are found in the auditory nerves of fB deficient mice.....	111
A loss of cochlear lateral wall integrity in fB ^{-/-} mice.....	113
Discussion.....	116
Chapter Five: Summary and Future Directions.....	120
References.....	131

DEDICATION

But thanks be to God, who gives us the victory through our Lord Jesus Christ.

-1 Corinthians 15:57

And we know that in all things God works together for the good of those who love Him, who have been called to his purpose.

- Romans 8:28

This work is dedicated to my loving husband, Lonnie Brown Jr, and my beautiful daughter, Averie Brown. Lonnie, this is to you for all of the late nights you joined me at the lab, the times you helped me practice talks and for those times you lifted my heavy heart after failed experiments. Thank you for being my steady rock of encouragement and my example of endurance. Averie, it was with you in mind that I was able to see this to completion. Thank you for your smiles and giggles. Know that you are able to do anything.

ACKNOWLEDGMENTS

First, I would like to thank my wonderful mentor, Dr. Hainan Lang, for guiding me through this process. Hainan, thank you for your inspiration, support and encouragement. I appreciate you for cultivating me to be the scientist that I am today. Without you, I would not know my potential and would not know there is “never a dead end in science, only new possibilities”.

Also, thank you to the members of my dissertation advisory committee: Drs. Judy Dubno, Edward Krug, Jeremy Barth, Stephen Ethier, Dennis Watson, and Carl Atkinson. I am extremely appreciative to Dr. Dubno for her encouragement and for extra support by serving as a co-sponsor for my National Research Service Award (NRSA) fellowship from NIH NIDCD (F31DC015741) and providing support with my T32 appointment (T32DC014435). My deepest gratitude is to Dr. Krug for always offering me an open-door policy and for stimulating my career development. I am exceptionally grateful to Dr. Barth for his great feedback and for training me in gene regulation and bioinformatics. I truly appreciate Dr. Ethier for providing helpful discussions and thoughtful questions that have advanced my research. My gratitude is also extended to Dr. Watson for improving the depth of my molecular explorations. I also am extremely grateful to Dr. Atkinson for introducing me to the amazing world of complement and for serving as a co-sponsor for my NRSA fellowship.

I also wish to thank all of the current members of the Lang lab and lab alumni, including Dr. Yazhi Xing, Clarisse Panganiban, Kenyaria Noble, Juhong Zhu, Ting Liu, Nancy Smythe, Catherine Bridges, Dr. Hui Li, Dr. Xingping Hao,

and the many visiting ENT fellows. I am also grateful to faculty members of the Department of Pathology, the Department of Otolaryngology-Head and Neck Surgery and Laboratory Medicine and to the College of Graduate Studies. I owe many thanks to the MUSC IMSD group for providing a sense of community. Additionally, special thanks are extended to Dr. Cynthia Wright for all of her encouragement. Thank you to my many friends and classmates for the laughs and fun times. I am also forever thankful to Pastor Abraham Belanger, First Lady Ty Belanger and my amazing family at First Fruits Community Church for their prayers and love.

I want to express my greatest gratitude to my extraordinary family. Thank you, to the most amazing parents, Troy and Sheila Conaway. Thank you for sculpting me to be an inquisitive and strong woman. You both have always been my biggest supporters and my loudest cheerleaders. Thank you to my adoring and beautiful sisters, LaKisha and LaTroya, along with my brothers- and sister-in-law, Tony, Mike and Kalima. My love extends to all of you for the emotional support you have provided.

Finally, I could not have completed the work required for this dissertation without my wonderful husband, Lonnie Brown Jr. Thank you for your help with graphics and for always serving as my audience for presentations. Thank you for walking by my side throughout this journey. To my sweet Averie, thank you for being my sweet sunshine in these last months. You will forever be my motivation.

LIST OF ABBREVIATIONS

ABR- Auditory Brainstem Response

BDNF- Brain-derived Neurotrophic Factor

BrdU- Bromodeoxyuridine

C1q- Complement Component 1 subunit q

C3- Complement Component 3

CD11b- Cluster of Differentiation 11b

CD68- Cluster of Differentiation 68

cDNA- Complementary Deoxyribonucleic Acid

CMT- Charcot-Marie-Tooth

CNS- Central Nervous System

DAPI- 4'6-diamidino-2-Phenylindole Dihydrochloride

dB SPL- Decibel Sound Pressure Level

dLGN- Dorsal Lateral Geniculate Nucleus

DPOAE- Distortion Product Otoacoustic Emission

DTX- Diphtheria Toxin

E- Embryonic Day

EDTA- Ethylenediaminetetraacetic

EM- Electron Microscopy

EP- Endocochlear Potential

fB- Complement Factor B

H2-D1- Histocompatibility 2, D region

H2-K1- Histocompatibility 2, K region

IBA1- Ionized Calcium-Binding Adapter Molecule

IHC- Inner Hair Cell

kHz- Kilohertz

LW-Lateral Wall

MAC- Membrane Attack Complex

NCC- Neural Crest Cell

NF200- Neurofilament 200

NT3- Neurotrophin 3

mRNA- Messenger Ribonucleic Acid

MS- Multiple Sclerosis

OHC- Outer Hair Cell

OSL- Osseous Spiral Lamina

P- Postnatal Day

PI- Propidium Iodide

RC- Rosenthal's Canal

RM- Reissner's Membrane

SGN- Spiral Ganglion Neuron

Sox2- SRY-related HMG-box 2

Sox10- SRY-related HMG-box 10

SEM- Standard Error Mean

TM- Tectorial Membrane

μ L- Microliter

μ m- Micrometer

LIST OF FIGURES

Figure 1-1. Anatomy of the ear.....	3
Figure 1-2. Human cochlear frequency map.....	7
Figure 1-3. Microenvironment of the auditory nerve.....	13
Figure 1-4. Innervation of the developing and adult cochlea.....	17
Figure 1-5. The three pathways of complement activation.....	25
Figure 2-1. Characterization of fB ^{-/-} mice.....	33
Figure 2-2. Diphtheria toxin administration to CD11b mice via intraperitoneal injection.....	34
Figure 3-1. Increased glial cell numbers and proliferation correlate with auditory nerve refinement in postnatal mouse cochleae.....	50
Figure 3-2. Genes associated with axonal guidance and immune responses are differentially expressed in the postnatal auditory nerve.....	55
Figure 3-3. Iba1 ⁺ macrophage numbers and proliferation peak in the first postnatal week.....	59
Figure 3-4. Macrophage activation occurs in the developing auditory nerve.....	63
Figure 3-5. Macrophages engulf glial cells and the fragments of auditory nerve fibers.....	67
Figure 3-6. Ultrastructure of cochlea shows macrophages engulf degenerating axons and glial cells.....	69
Figure 3-7. DTX treatment results in decreased macrophages and increased glial cells in the auditory nerve of postnatal CD11b ^{DTR/EGFP} mice.....	73

Figure 3-8. DTX-treated mice have relatively normal neuronal cells, hair cells and afferent synapses.....75

Figure 3-9. Depletion of macrophages results in transient myelin and LW-related abnormalities.....79

Figure 3-10. Macrophage depletion impairs auditory function in DT-treated CD11b^{DTR/EGFP} mice.....84

Figure 4-1. Complement gene expression in postnatal CBA/CaJ mouse auditory nerve.....99

Figure 4-2. Auditory Brainstem Response (ABR) Measurements in fB deficient mice..... 101

Figure 4-3. fB^{-/-} mice display decreased amplitudes and increased latencies of auditory nerve fibers..... 102

Figure 4-4. Organ of Corti is comparable in fB^{-/-} and WT mice.....104

Figure 4-5. Neuron densities are not significantly altered in fB^{-/-} mouse cochleae.....105

Figure 4-6. Ultrastructure analysis of fB^{-/-} mouse cochleae reveal myelin pathologies.....108

Figure 4-7. Glial cell numbers are increased in fB^{-/-} mouse cochlear nerves and demonstrate potassium channel dysfunction.....110

Figure 4-8. Macrophage densities in the auditory nerves of fB deficient mice.....112

Figure 4-9. fB deficiency results in cochlear LW pathologies.....114

LIST OF TABLES

Table 1. Ingenuity pathway analysis of canonical pathways identified by differentially expressed genes.....	57
--	----

ABSTRACT

Hearing relies on the transmission of auditory information from sensory hair cells to the brain through the auditory nerve. This relay of information requires hair cells to be innervated by spiral ganglion neurons (SGNs) in an exclusive manner and for SGNs and their axons to be ensheathed by myelinating and non-myelinating glial cells. In the developing auditory nerve, mistargeted SGN axons undergo retraction or pruning, and excessive neural cells are eliminated to obtain the characteristic innervation pattern seen in the mature cochlea. The mechanisms governing auditory nerve maturation remain unclear. However, in peripheral nerves, key contributors to the establishment of mature nerve circuitry are immune cells, such as macrophages. The major goal of this dissertation was to determine if macrophages are beneficial for the structure and function of the developing auditory nerve. Using postnatal mice, we examined macrophage distribution and activation in the developing auditory nerve and explored the relationship between macrophages and glial cells. In the developing auditory nerve, the number of macrophages and glial cells peaked during the first postnatal week, concurrent with the period of SGN refinement. Macrophage and glial cell numbers were significantly reduced by the second postnatal week, when SGN pruning is complete. Macrophages also phagocytosed glial cells, suggesting a role for macrophages in regulating glial cell numbers. Transient depletion of macrophages in postnatal mice resulted in cochlear pathologies, including increased glial cell numbers, temporary cochlear lateral wall alterations and diminished auditory function.

Another goal of this dissertation was to investigate the role of immune-related pathways in the auditory nerve. Complement proteins localize to the surface of nerves during developmental refinement and injury-related regeneration. Using adult complement fB^{-/-} mice, we examined the role of alternative complement signaling in the auditory nerve. Similar with our findings in macrophage-depleted mice, factor B deficient mice demonstrated diminished auditory function and exhibited increased glial cell numbers and myelin dysfunction. These common pathologies indicate that macrophages and the alternative complement signaling pathway regulate glial cell numbers and function, demonstrating that macrophages and specified immune signals are beneficial and required for auditory nerve development by supporting glial cell function.

CHAPTER ONE: INTRODUCTION

A. HEARING AND CELLS OF THE AUDITORY NERVE

A.1 ANATOMY OF THE HUMAN EAR

The ear collects and amplifies acoustic information from the environment and utilizes intricate processes to convert external acoustic stimuli into interpretable auditory information. The cochlea perceives, amplifies, transduces and conducts sound wave vibrations into electrical impulses and neural inputs. The neural inputs are sent along the auditory nerve to the central auditory system. The mammalian ear has three main parts: 1) the outer ear, including the auricle and tympanic canal (ear canal), 2) the middle ear, containing the tympanic membrane (ear drum) and three ossicles, and 3) the inner ear, consisting of the cochlea, auditory nerve, vestibular organs, and vestibular nerve (Figure 1-1). Cooperation and functioning of these intricate structures is required for hearing, sound perception and balance.

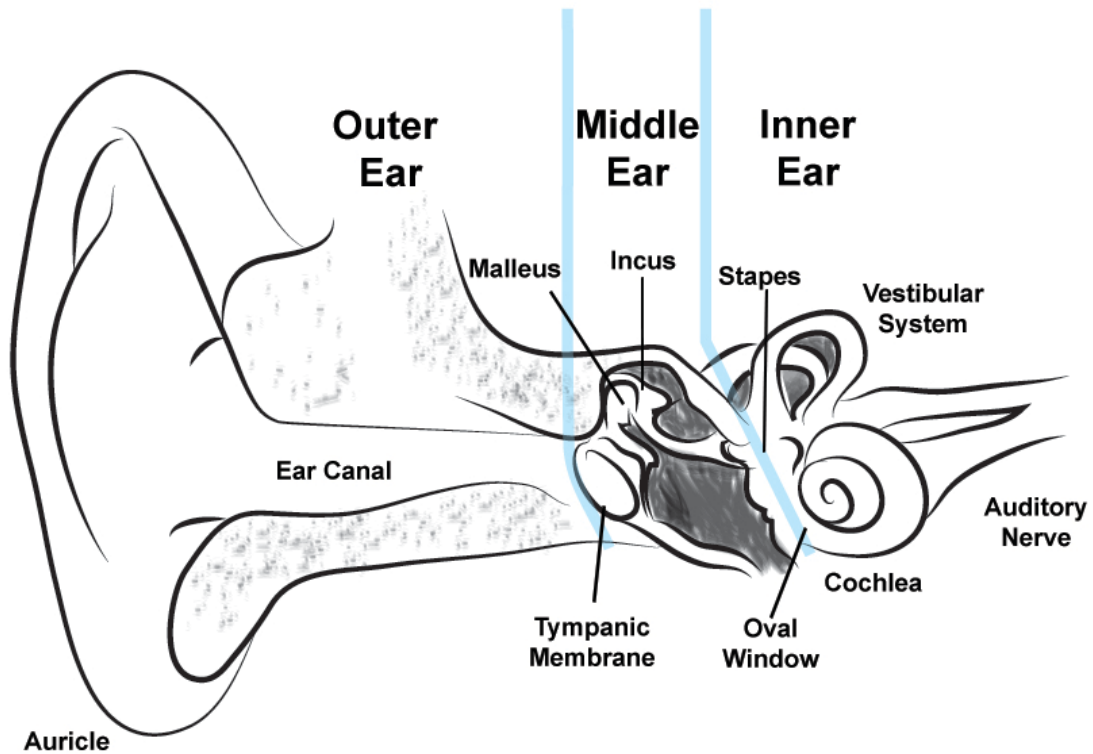


Figure 1-1. Anatomy of the ear. The ear is partitioned into 3 regions: the outer, middle and inner ear. The outer ear is comprised of the auricle and ear canal. The middle ear contains the tympanic membrane and 3 ossicles: the malleus, incus and stapes. The oval window is the location where the middle ear ossicles meet with the cochlea. The inner ear consists of the cochlea, vestibular organs, auditory nerve and vestibular nerve. The cochlea is responsible for hearing function, whereas the vestibular organs are responsible for balance.

A.2 FUNCTIONS OF THE OUTER AND MIDDLE EAR

The auricle, or pinna, is the external portion of the ear that connects to the ear canal, a hollow tube that opens to the external environment and flanks the tympanic membrane. The auricle plays an important role in distinguishing the frequencies that enter the ear canal. Low-frequency sound waves are discriminated out, allowing the passing of middle and higher frequencies to travel through the ear canal [1, 2]. This discrimination of passing frequencies is important for human speech, sound perception and directional cues [1, 2]. Anatomical curvatures and length differences of the ear canal influence variations in the internal pressure of the outer ear [2]. These anatomical distinctions and pressure changes are required for the movement of sound waves through the air-filled environment of the outer ear [3, 4]. In this environment, sound waves travel with low impedance or low resistance to movement. However, the impedance levels of the fluid-filled cochlea are significantly higher. To overcome the high impedance of the cochlea, the middle ear increases the pressure of traveling sound waves by nearly 200-fold [5]. The middle ear is covered by the auditory bulla and contains the tympanic membrane along with three bony structures (ossicles): the malleus, incus and stapes (Figure 1-1) [6]. As sound waves travel from the ear canal they converge on the tympanic membrane. Movement of sound waves from the large surface of the tympanic membrane to the smaller oval window, the spot where the interconnected ossicles fuse to the inner ear, causes intense pressurization of

sound waves. This increased pressure is needed for sound waves to travel through the cochlear fluid [6, 7].

A.3 THE INNER EAR

The inner ear includes the cochlea and vestibular system. The vestibular system is responsible for spatial orientation and the sense of balance. The cochlea is a spiraled structure divided into three fluid-filled membranous ducts, the scala vestibule, scala media and scala tympani. The scala vestibule and scala tympani are filled with cerebrospinal fluid-like liquid known as perilymph [8]. The perilymph is made of high levels of sodium (Na^+) and low levels of potassium (K^+). The fluids supplying the scala media, the endolymph, contains high levels of K^+ and low levels of Na^+ and calcium (Ca^{2+}). This difference in ionic composition results in differences in electrical properties between the cochlear partitions, generating a positive potential, the endocochlear potential (EP). EP is the driving potential that increases the influx of K^+ receptor current into the hair cells of the organ of Corti [9].

An elastic strip called Reissner's membrane separates the scala vestibule from the scala media. The scala media and scala tympani are separated by the basilar membrane, a membrane with graded stiffness and mass. As the middle ear ossicles vibrate against the oval window, the perilymph within the scala vestibule is displaced, causing the basilar membrane to bow, beginning the mechanotransduction of sound waves into neural information [5, 7]. The physical properties of the basilar membrane vary from the base, or the portion closest to

the oval window, to the apex. At basal regions, the membrane is more narrow and stiffer in comparison to the apex of the basilar membrane. As sound waves travel along the basilar membrane, high-frequency waves produce maximal displacement at the basal region, whereas low frequencies impinge on the basilar membrane at apical regions (Figure 1-2) [10].

A.4. DEVELOPMENT OF OTIC PLACODE

The otic placode is a thickened layer of ectodermal cells that give rise to the sensory cells of the cochlea. In rodents, the otic placode can be seen as early as E8 [11]. This dense layer of cells produce pro-neurosensory cells that differentiate into neuronal precursors by the expression of several regulation genes, including Sex determining region Y-related high mobility group-box 2, Sox2, and the transcription factor, Oct6 [12]. The cells of the otic placode invaginate and proliferate to form the otocyst. The otocyst later gives rise to the cochlear duct, a sealed sac that houses the organ of Corti [13].

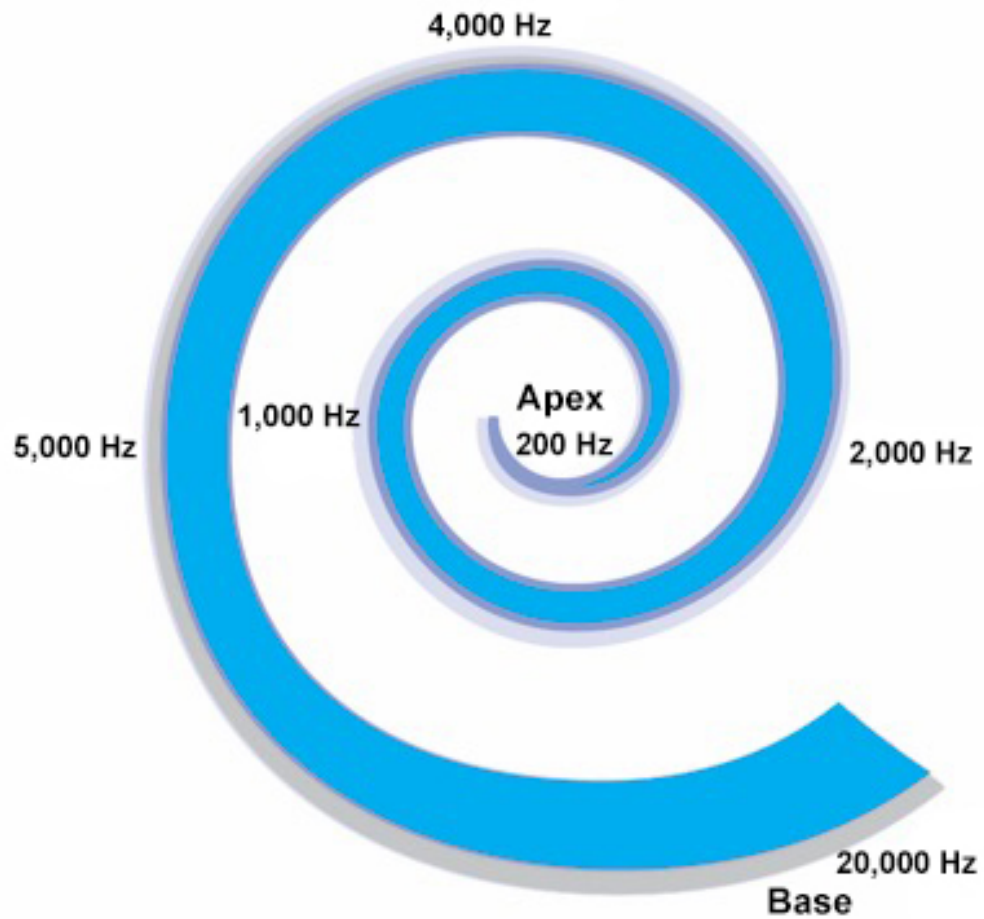


Figure 1-2. Human cochlear frequency map. The hair cells of the cochlea are arranged along the basilar membrane in a frequency gradient. Hair cells that respond to high frequencies are located at wide base, closest to the oval window. Hair cells that respond to low frequencies can be found toward the apex of the membrane coil. Humans can respond to frequencies between 200-20,000 Hz. Rodents can respond to frequencies between 1000-70,000 Hz.

A.5 HAIR CELLS- SENSORY CELLS OF THE COCHLEA

The sensory epithelium, located on the basilar membrane, contains the specialized hair cells and non-sensory cells. Cochlear hair cells are mechanosensory cells that transduce the mechanical movement of the basilar membrane caused by sound waves into neural signals. Hair cells are tightly juxtaposed with an underlying layer of non-sensory supporting cells and are housed in the organ of Corti [10]. There are two populations of hair cells, inner hair cells (IHCs) and outer hair cells (OHCs), which extend along the basilar membrane in a tonotopic, or basal-to-apical, manner [14]. IHCs are aligned in a single row, whereas outer hair cells are arranged in three rows. IHCs are the sensory cells responsible for mechanotransduction of sound waves to neural inputs, while OHCs amplify sound vibrations for increased cochlear efficiency [15].

Each hair cell contains a bundle of ~100 stereocilia, actin-filled modified microvilli, extending from their apical surface [10, 16, 17]. Hair cell stereocilia are arranged in rows according to height [18]. The stereocilia bundles of each hair cell are bathed in the endolymph of the scala media and gently graze the base of the tectorial membrane. As the basilar membrane bows in response to movement of the endolymph and vibrations from the oval window, the stereocilia bundles are displaced, causing the opening and closing of transduction channels of the hair cell [16, 19].

At resting states, hair cells possess low levels of K^+ and Ca^{2+} . Ionic concentrations in hair cells are maintained by selective mechanically-gated ion

channels located on the apex of the cells. Once shearing and mechanical force from the tectorial membrane is exerted on the stereocilia, the ion channels open, allowing an influx of K^+ and Ca^{2+} from the endolymph to enter the hair cell [18-21]. The influx of K^+ and Ca^{2+} depolarizes the hair cells, causing a change in hair cell membrane potential and triggering the release of the neurotransmitters, mainly glutamate, from the presynaptic terminal at the bases of the IHCs [10, 16, 19]. These neurotransmitters bind to the postsynaptic terminal endings, including glutamate receptors, on the innervating nerve fibers of the auditory nerve, eliciting an action potential, electrical signals that are propagated along the nerve to the ascending auditory pathway [10, 15, 16].

A.6 SPIRAL GANGLION NEURONS- TRANSMITTERS OF NEURAL INFORMATION

Spiral ganglion neurons (SGNs) are specialized neurons that encode acoustic stimuli, including frequency, intensity. SGNs also encode information regarding temporal properties, such as action potential spike timing and phase locking, for rapid transmission to the brain. The auditory nerve is comprised of two SGN populations: Type I, which make up ~90% of all neurons, and Type II, which makes up ~5-10% [22, 23]. SGNs are bipolar neurons housed within the bony channel of Rosenthal's canal. Peripheral axons of SGNs extend to the sensory epithelium via the osseous spiral lamina, a bony ridge that anchors the basilar membrane. Type I SGNs send a single peripheral fiber to innervate a single IHC. In rodents, a single IHC can be innervated by axons from 10-30

different SGNs [15]. Type I SGNs are large and ensheathed by myelinating glial cells. Contrarily, Type II SGNs are much smaller and are covered by non-myelinating glial cells. These SGNs exclusively extend multiple axonal projections to several OHCs in the organ of Corti.

Like hair cells along the basilar membrane, the position of SGNs along the tonotopic axis of the coiled cochlea correlates with the frequencies they are most sensitive to. Hence, SGNs in the apex of the cochlea facilitate low-frequency transmission while SGNs of the base conduct high-frequency transmission [24]. Differences in sensitivity to signal frequency displayed by SGNs is due, in part, to the differential distribution of K^+ and Na^{2+} channels between SGNs and the extrinsic effect of neurotrophic factor gradients [25-27].

The establishment and survival of SGNs is dependent on the secretion of neurotrophic factors, such as brain-derived neurotrophic factor (BDNF) and neurotrophin-3 (NT3). Both BDNF and NT3 play an essential role in SGN development and survival [28, 29]. Mice deficient in BDNF and NT3 demonstrate a loss in SGNs during embryogenesis [29, 30]. BDNF is expressed in high levels in the basal regions of the auditory nerve, while NT3 levels are lower in this region. This is mirrored in the apex, which possesses high levels of NT3 and lower levels⁶ of BDNF [25, 28, 31, 32]. This gradient in neurotrophic factors demonstrates that neurotrophic factors not only promote the survival of SGNs but also regulate SGN localization and frequency discrimination.

A.7 AUDITORY GLIAL CELLS AND MYELINATION

Neural crest cells (NCCs) generate glial cells, which make up the majority of neural cells in the auditory nerve [33]. Glial cells within the peripheral auditory nerve include Schwann cells, which ensheath SGN axons, and satellite cells, another type of glial cell that cover ganglia [34]. The capacity of auditory glial cells to produce myelin is largely dependent on whether the glial cells are associated with Type I or II SGNs. The cell bodies and axons of Type I SGNs are ensheathed by myelinating glial cells while non-myelinating glial cells wrap Type II SGN somas and axons (Figure 1-3).

In developing peripheral nerves, glial precursors cells migrate alongside the neurons and axons they will envelop. Differentiation of progenitor cells to Schwann cell progenitors is dependent on paracrine signals secreted by neurons and axons [35-40]. Following differentiation, immature glial cells switch to autocrine signaling to maintain survival and to secrete factors that contribute to neuronal maintenance [40]. In rodents, peripheral glial cells are differentiated by embryonic day (E) 18 and start to produce myelin sheaths by postnatal day (P) 2 [41, 42]. Myelin is made from multiple layers of glial cell plasma membranes ensheathing neuron cell bodies or axons. Myelination of neurons is essential for saltatory conduction, or the rapid transmission, of neural impulses from sensory cells to the brain [39, 43, 44]. In rodents, the majority of myelination of SGNs in the auditory nerve occurs between P4 and P8, with myelination of neuron axons occurring before the myelination ganglia [45]. Around P7-8, before the onset of hearing, the initial action potentials are evoked [46].

One signal that is important for glial cell development is neuregulin, a cell adhesion molecule that interacts with ErbB receptors [38, 39, 47, 48]. Neuregulin drives NCCs toward glial cell fates. Neuregulin is secreted by axons and is a chemoattractant to prevent glial cell apoptosis and to increase glial cell migration into axon-rich areas [42, 47, 49]. Neuregulin deficient mice demonstrate significantly smaller axon caliber in sensory nerves, thinner myelin sheaths surrounding axons and shorter intermodal length along the nodes of Ranvier, resulting in decreased conduction velocity and defects in response to stimuli [50, 51].

Sox10 is also expressed in migrating NCCs and persists in terminally differentiated glial cells [37, 38]. Sox10 also regulates the production of myelin and the transcription of myelin-associated genes [52, 53]. Mice with mutated Sox10 demonstrate absent satellite cells, while neuron numbers remain the same, indicating that Sox10 is required for glial cell production but not needed for the control of neuronal number [37, 54, 55].

Sox10-positive glial cells are located in the auditory nerve [56]. In the auditory nerves of Sox10 deficient mice, SGNs overshoot their hair cell targets, sending axonal projections into the cochlear lateral wall [55]. The auditory nerve of Sox10 deficient mice also demonstrate signs of myelin dysfunction [55]. This suggests that Sox10 associated glial cell regulation contributes to SGN innervation and nerve refinement.

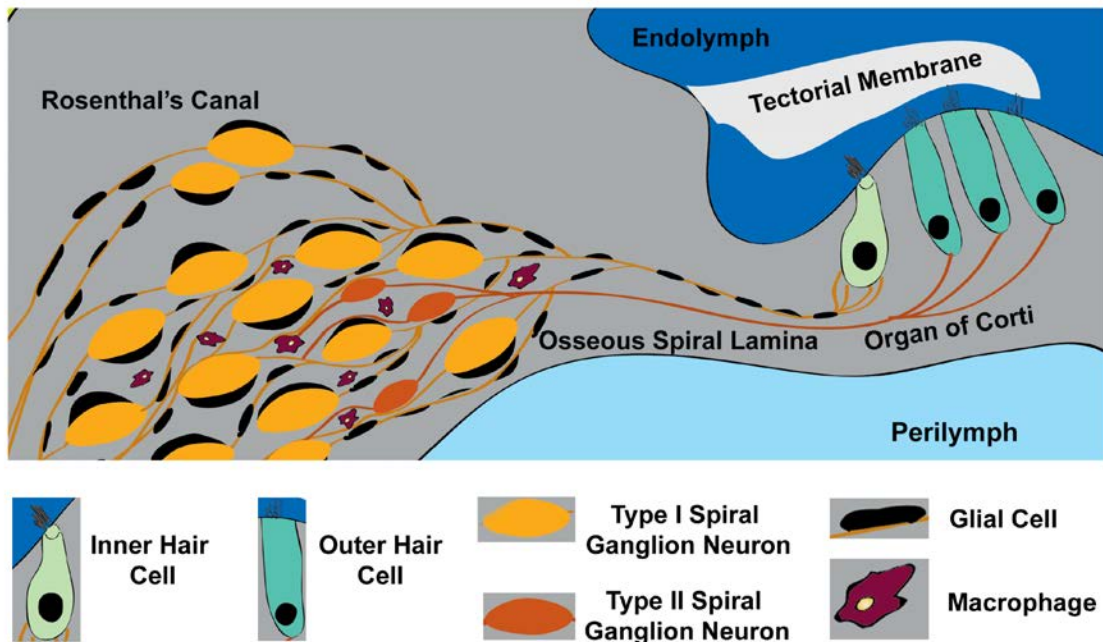


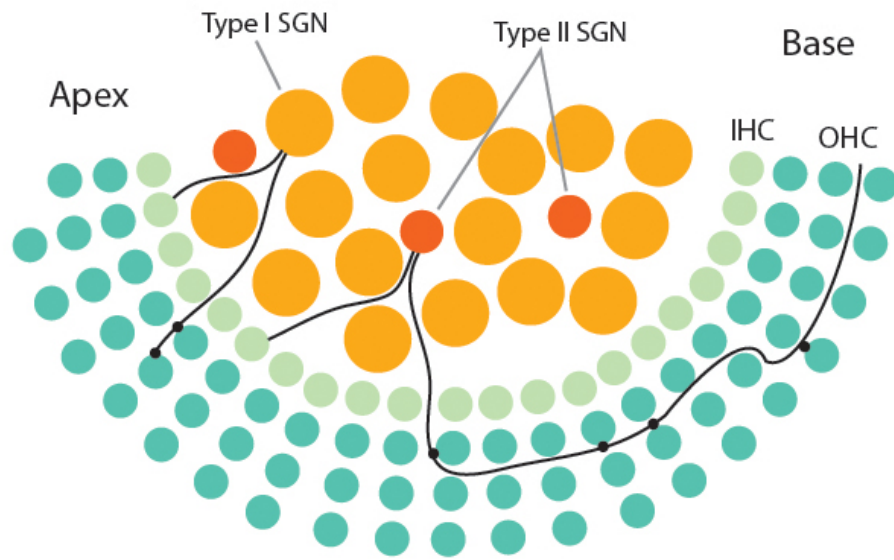
Figure 1-3. Microenvironment of the auditory nerve. This graphic schematic of a cochlear turn focuses on the cells of the auditory nerve and organ of Corti. The auditory nerve is made of SGNs and glial cells, together with macrophages and other non-neural cell types. Type I SGNs connect to IHCs while Type II SGNs connect to the OHCs. The SGN cell bodies are located in Rosenthal's Canal. The SGN fibers extend through the bony tunnel of the osseous spiral lamina. SGN cell bodies and axons are covered by glial cells. Macrophages are found throughout the auditory nerve. HCs and OHCs are located in the organ of Corti. Above the hair cells of the organ of Corti is the tectorial membrane. The organ of Corti is bathed in the endolymph of the scala media. Below the organ of Corti is the perilymph of the scala tympani. A key of the different cell types is located at the bottom of this graphic.

CHAPTER ONE: INTRODUCTION
B. AUDITORY NERVE REFINEMENT

B.1 SGN INNERVATION PATTERNS OF THE COCHLEA

Innervation between SGNs and hair cells is critical for auditory processing and hearing function. Formation of peripheral circuitry requires axonal outgrowth, guidance of axons to hair cells and the maturation of functional synapses. In mice, peripheral axons from the SGNs extend from the neuron bodies toward the sensory cells of the organ of Corti by E14 [32, 57]. By E15.5, Type I SGNs establish connections to IHC targets [57]. At E17.5, SGN axons develop branches and form multiple connections with hair cells. Later, in the postnatal cochlea, excessive branches are retracted and misguided axons are eliminated away from their hair cell targets [58, 59]. Additionally, extra cells that were generated undergo apoptosis [60]. By P12, SGN axons acquire their final circuitry patterns, allowing the auditory nerve to become fully functional (Figure 1-4). This occurs before the onset of hearing, between P12-14 [32, 58, 61, 62].

A Postnatal Cochlea



B Adult Cochlea

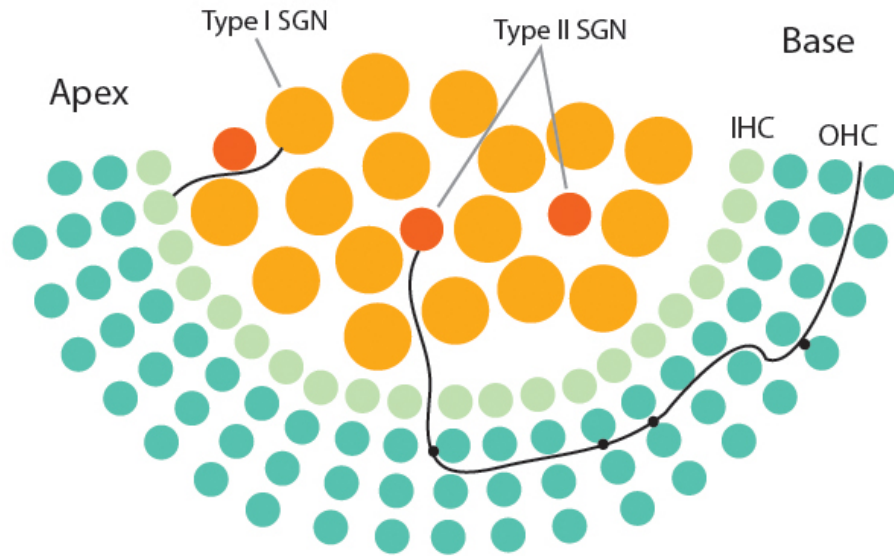


Figure 1-4. Innervation in the developing and adult cochlea. This graphic representation demonstrates the nerve refinement that occurs in the developing auditory nerve. **A.** During postnatal development, Type I SGNs (orange) innervate IHC (light green) form erroneous connections with OHCs (dark green). Type II SGNs (dark orange) also demonstrate incorrect innervations, sending nerve fibers to innervate IHCs within the organ of Corti. **B.** In the adult cochlea, Type I SGNs connect to only one IHC whereas Type II SGNs send out fibers that only innervate multiple OHCs.

B.2 MECHANISMS OF AUDITORY NERVE REFINEMENT

It has been proposed that the amount of activity produced by neurons controls which axons will be retained and which are eliminated [63]. Neurons that produce high levels of spontaneous activity and that are most responsive during sensory experience are labeled as “strong” and maintained, while “weakened” or excessive neurons and their axons are eliminated in a process referred to as “pruning” or “refinement” [64-66]. This selective elimination, referred to as activity-dependent plasticity, can be seen in the dorsal cochlear nucleus and auditory brainstem [67, 68]. Activity-dependent plasticity can also be seen in other regions of the nervous system, such as the retinogeniculate pathway, neuromuscular junction and the somatosensory cortex [63, 66, 69-71].

Molecular mechanisms contributing to the refinement of afferent wiring in the cochlea have not been fully characterized. A recent study investigating the gene profile of developing SGNs identified several gene pathways that are upregulated during embryonic and postnatal development of the auditory nerve [72]. Several immune-related gene groups demonstrated an increase in their mRNA expression during SGN development and axon extension. These immune-related pathways include the antigen presentation pathway and complement signaling. These findings suggest that immune signals or immune-specific cells play a critical role in the establishment of auditory nerve circuitry.

CHAPTER ONE: INTRODUCTION
C. MACROPHAGES AND COMPLEMENT SIGNALING

C.1 COCHLEAR MACROPHAGES

Macrophages are resident immune cells of the auditory nerve. Macrophages are polyfunctional cells that maintain and restore tissue homeostasis and integrity by surveying the microenvironment and recognizing debris or pathogens. Pathogens or damaged cells release chemoattractive signals that initiate the immune response, leading to the activation and infiltration of immune cells [73]. During this response, resident macrophages also release chemoattractants and cytokines for promoting bone marrow derived monocytes to infiltrate into the damaged tissue. Resident macrophages proliferate and infiltrating monocytes differentiate on site, and together, phagocytose and eliminate pathogens and cell debris [74, 75].

Tissue resident macrophages are derived from the yolk sac or from bone-marrow monocytes [75, 76]. During embryonic development, macrophages emerge from progenitor cells and migrate to their final tissue destinations by E8.5 [75]. Macrophages in the developing cochlea have not been characterized. However, resident macrophages are found in the adult cochlea. These macrophages demonstrate positive expression of CD45, CD168, F4/80, CD11b and IBA1 [77-79].

The detrimental or beneficial roles of immune cells in neural pathologies continues to be debated. Immune cells have long been implicated in the induction or progression of neural pathologies. However, recent studies have found that immune cells may also promote the cessation of neural diseases and the regeneration of injured tissue.

C.2 MACROPHAGES IN THE INJURED COCHLEA

Macrophage numbers significantly increase in the injured cochlea [78, 80-85]. Applications of ototoxic drugs, such as ouabain or amikaci, to the round window of mice result in the infiltration of macrophages into the injured cochlea [83, 85]. Further, hair cell ablation results in the migration of macrophages into the sensory epithelium, under the areas with robust hair cell loss [78, 80]. Concurrently, infiltration of macrophages into the spiral ganglion occurs after exposure to excessive noise or following SGN degeneration [82, 86]. Interestingly when macrophages are depleted, there is a subsequent decrease in SGN survival after ototoxic injury or following selective hair cell lesion [78, 80, 87], suggesting a beneficial role for macrophages in the injured cochlea.

The infiltration of macrophages often results in the increased expression of antigen-presentation and immune response genes. In the adult cochlea, cells express low levels of antigen-presentation genes, such as major histocompatibility class (MHC) II genes [88]. Following acoustic trauma, MHC class II genes are upregulated on the surface of cochlear cells and are also present on the surface of infiltrating macrophages [88, 89]. This increase in antigen-presentation abilities may contribute to the competency of cochlear cells to propagate immune responses and inflammation after injury. Nuclear factor- κ B is an important immune-response gene that stimulates the recruitment of immune cells. Nuclear factor- κ B deficient mice displayed accelerated age-related hearing loss, increased sensitivity to noise insults and decreased expression of inflammatory factors after noise exposure [90, 91]. This suggests that nuclear

factor- κ B-associated immune processes are required for protection from noise-induced hearing impairments. In a recent study, next generation RNA-sequencing of noise-exposed auditory nerves revealed a significant increase in inflammatory genes following noise exposure [92]. Among the genes upregulated in the noise-exposed cochleae were a large subset of complement component genes.

C.3 IMMUNE CELLS IN NERVE REFINEMENT

Investigations of the developing mouse hippocampus and retina has demonstrated that microglia are heavily involved in the deletion of excessive axons, synapses and neural precursors [69, 93-99]. Microglia-mediated deletion of synapses is regulated by the activity produced by neurons. This has been demonstrated in the developing mouse eye and hippocampus. These previous studies revealed that microglia preferred to engulf synaptic inputs with reduced neuronal activity [69, 93].

The critical role for microglia in nerve refinement is further emphasized when microglial cells are depleted. Microglia express the receptor (CX3CR1) for the chemokine, fractalkine. Fractalkine, or CX3CL1, is expressed by neurons and regulates chemoattraction of monocytes in the immune system [100, 101]. Mice deficient in the fractalkine receptor, CX3CR1^{-/-} mice, produce severely diminished numbers of mature immune cells [101]. CX3CR1^{-/-} mice also produce neuronal defects, including the overproduction and maintenance of excessive dendrites thalamocortical axons, immature synapses in the hippocampus and reduced

pruning of excitatory synapses in the cortex [93, 99, 102, 103]. Interestingly, mice deficient in complement signaling show reduced synaptic pruning, similar to that demonstrated by CX3CR1^{-/-} mice.

C.4 COMPLEMENT SIGNALING

The complement system is comprised of over 40 proteins, including soluble and membrane-bound proteins. Complement can be activated via three distinct routes: the classical pathway, lectin pathway and alternative pathway (Figure 1-5). Initiation of the three complement pathways converges on the cleavage of complement component 3 (C3), the most abundant complement protein [104, 105]. When cleaved, C3b fragments covalently bind to the receptors on the cell surface of foreign bodies and apoptotic cells, signaling phagocytes to engulf the opsonized targets. Additionally, the generation of C3b complexes begins the formation of a complement component 5 (C5) convertase, which initializes the membrane attack complex (MAC), a process where pores are punched through the cell surface, leading to cell lysis [105, 106].

The classical pathway is initiated by the cleavage of complement component 1 into 3 molecules: C1q, C1s and C1r. This then starts the cleavage of C4 and C2 to form the C3 convertase, C4bC2a, and initiates the generation of the MAC complex [105]. Similarly, the lectin pathway is initiated when mannose binding lectin (MBL) binds to the surface of foreign cells, causing a conformational change in this protein and the generation of MBL-associated

protein 2. Like C1q, MBL-associated protein 2 cleaves C4 and C2 to form C4bC2a, initiating C3 cleavage and the activation of the MAC pathway [105].

Unlike the classical and lectin pathways, the alternative pathway does not require the presence of pathogens or immune complexes. Instead, through this pathway, complement is continuously activated to assist with the rapid and acute response to pathogens [104, 107]. Activation of complement via the alternative pathway involves the spontaneous hydrolysis of C3 and formation of a C3bB complex with complement Factor B (fB). C3bB is then cleaved by complement Factor D to form a C3bBb convertase, initiating the activation of the MAC pathway [104, 105]. Complement activation results in the recognition and elimination of pathogens by phagocytic cells of the innate immune system.

Multiple cell types can synthesize complement proteins. The majority of soluble complement is generated in the liver by hepatocytes. However, extrahepatic complement synthesis occurs in several other tissues, including nervous tissue [108]. In nervous tissue, surface-bound complement proteins and soluble complement proteins are expressed by microglia/macrophages, neurons and glial cells [109]. Interestingly, high levels of classical complement components are secreted by developing retinal ganglion neurons, during the peak of synaptic refinement [96], demonstrating the key role complement signaling in nerve refinement.

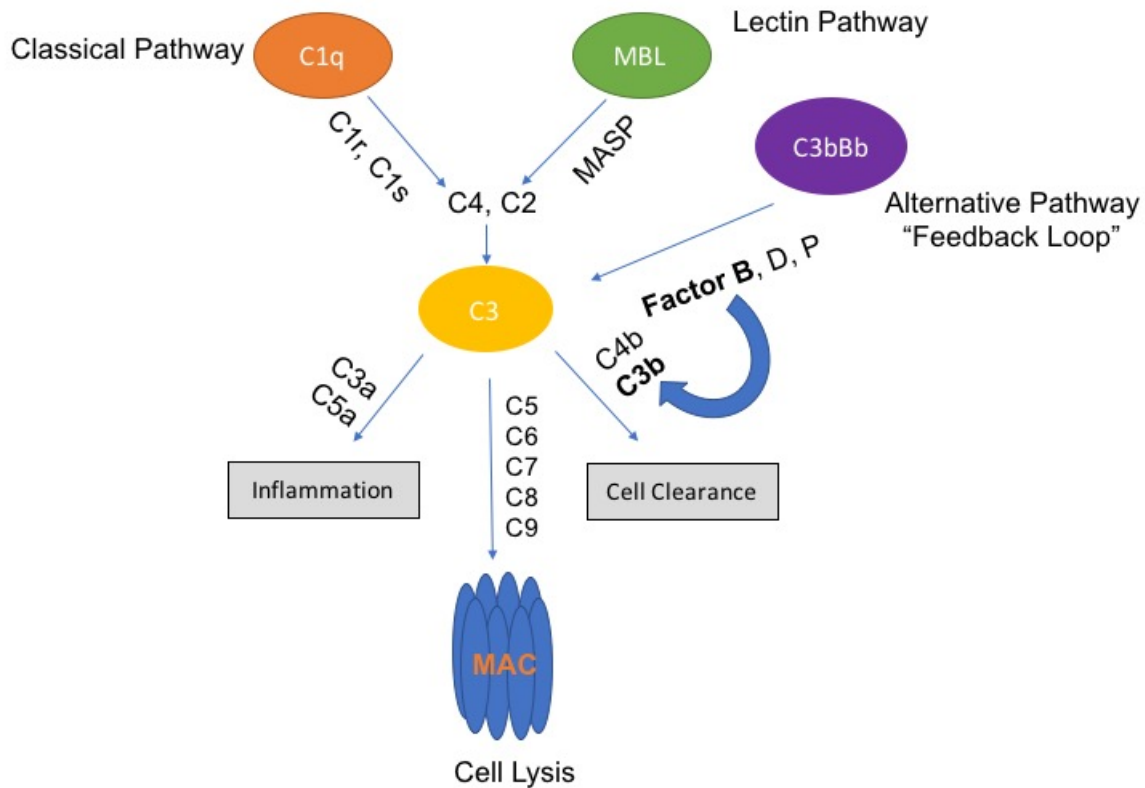


Figure 1-5. The three pathways of complement activation. This schematic of complement signaling demonstrates how the three pathways of complement activation converge on C3 activation. The classical and lectin pathways include the cleavage of C4 and C2 to make a C3 convertase. Activation of C3 induces the production of the cleavage products C3a and C5a, which promote inflammation. C3 activation also leads to the formation of C4b and C3b products, which promote cell clearance. The alternative pathway can spontaneously act on C3b through the Factor B component, a process known as a “Feedback Loop”. Activation of C3 and the terminal pathway ultimately leads to the activation of MAC (membrane attack complex) and cell lysis.

C.5 COMPLEMENT SIGNALING AND NERVE REFINEMENT

Complement activation by neural cells has been implicated in several neurological processes, including the promotion of neuroinflammation in injured tissue, the advancement of synapse loss in neurodegeneration and developmental nerve refinement. Most investigations elucidating the role of complement in nerve refinement focus on microglia/macrophage-mediated processes. In the central nervous system (CNS), microglia/macrophages are the dominant source of complement proteins and possess the receptors for C3 and C1q on their surfaces [110, 111]. C3 receptors are also expressed on the surface of axons and oligodendrocytes/Schwann cells [109, 112]. C3 knockout mice ($C3^{-/-}$) display defects in synapse elimination, evidenced by retained axons and synapse numbers in the retina [96]. Further, macrophages and microglia from $C3^{-/-}$ and C1q knockout ($C1q^{-/-}$) mice demonstrate reduced capacity to infiltrate damaged tissue and eliminate myelin and axonal debris [69, 95, 96].

CHAPTER ONE: INTRODUCTION

D. RATIONALE, SIGNIFICANCE AND SPECIFIC AIMS

D.1 RATIONAL & SIGNIFICANCE

Sound transduction requires a precise organization of the axonal connections between SGNs and hair cells [113]. In the adult cochlea, Type I SGNs exclusively innervate IHCs, while type II SGNs only innervate OHCs. However, cross-innervations to IHCs and OHCs by both populations of SGNs can be seen in the developing cochlea [59]. During development of the auditory nerve, mistargeted axonal projections are retracted or eliminated and excessive neural cells undergo apoptosis to obtain the specific neural circuitry seen in the mature cochlea [58-60]. However, the mechanisms underlying these developmental changes remain unclear.

Studies in other regions of the nervous system have shown that pruning and refinement of developing nerves is dependent on the activity of microglia/macrophages and the expression of immune-related signaling pathways [69, 93, 95]. Investigations of mice deficient in the chemokine CX3C receptor (CX3CR1^{-/-}), a receptor essential for microglia/macrophage migration and activity, revealed decreased nerve refinement of the hippocampus [93, 99, 102, 103]. Additionally, mice deficient in complement proteins, including C1q and C3, demonstrate decreased refinement in the retinogeniculate system [69, 95, 114]. Thus, the immune system may play an essential role in the refinement of the auditory nerve.

In this study, we investigated the contributions of the immune system, including macrophages and complement signaling, to auditory nerve refinement and development. The proposed study will provide critical insight into the how

neural cells and mistargeted nerve fibers are eliminated during auditory nerve development. Further, this study will characterize cochlear macrophages in the developing auditory nerve and will determine how the complement pathway is important for auditory nerve maturation. Further understanding of macrophage-mediated mechanisms underlying SGN innervation will provide significant information about the development of the peripheral auditory nerve.

D.2 SPECIFIC AIMS

The goals of this project are: 1) to examine the role of macrophages in elimination of excessive neural cells during postnatal development of the auditory nerve; and 2) to determine the potential role of alternative complement signaling in the developing auditory nerve.

Hypothesis: Alternative complement signaling promotes auditory nerve development by stimulating cochlear macrophages to eliminate excessive auditory glia and nerve fibers.

Specific Aim 1:

To test the hypothesis that the elimination of supernumerary fibers and auditory glial by macrophages is necessary for hearing onset in the postnatal cochlea.

Specific Aim 2:

To test the hypothesis that alternative complement deficient impairs auditory function and structural integrity.

CHAPTER TWO: MATERIALS AND METHODS

Animals: Adult CBA/CaJ and CD11b^{DTR/EGFP} breeding pairs were purchased from The Jackson Laboratory (Bar Harbor, ME, USA). CBA/CaJ mice are a standard experimental mouse strain used for auditory research [115, 116]. CD11b^{DTR/EGFP} mice have a transgene insert containing the diphtheria toxin receptor (DTR) and green fluorescent protein under the control of the *ITGAM* promoter [117]. Factor B knockout (fB^{-/-}) mice were generously provided by Dr. Carl Atkinson. As described in Matsumoto et al (1997), fB^{-/-} mice were generated by targeted gene homologous recombination in murine embryonic stem cells. fB^{-/-} are vital and show no difference in gross phenotype when compared to WT mice (Figure 2-1) [118, 119].

Mice were bred in-house in a low-noise environment at the Animal Research Facility of the Medical University of South Carolina (MUSC; Charleston, SC, USA). All aspects of animal research were conducted in accordance with the guidelines of the Institutional Animal Care and Use Committee of MUSC. All mice received food and water *ad libitum*, and were maintained on a 12-hr light/dark cycle. For postnatal mouse cochlear collections, the day of birth was referred to as postnatal day 0 (P0). For postnatal studies, postnatal pups aged P0-P14, mice of either sex were used. For complement-related studies, young adult mice of either sex were used in this study.

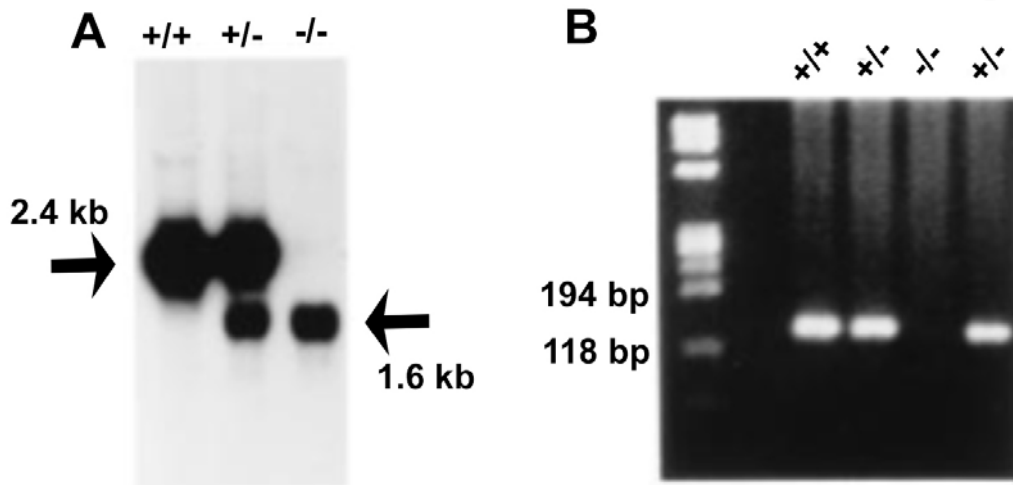


Figure 2-1. Characterization of Factor B^{-/-} mice. **A.** Southern blot of DNA from WT (+/+), heterozygous (+/-) and knockout (-/-) mice demonstrates that fB mRNA is truncated due to excision of fB exon 6. **B.** PCR screening for fB exon 6. Samples from FB^{-/-} mice do not express 6, whereas samples from WT and heterozygous express the gene. This figure was modified from Matsumoto et al [118].

Diphtheria toxin administration: P4-5 CD11b^{DTR/EGFP} mice received intraperitoneal injections (IP) of diphtheria toxin (DTX; 20-25 ng/g of body weight; Sigma-Aldrich) reconstituted in double distilled H₂O (ddH₂O). Injections were given to mice at P4 (Figure 2-2). It has been reported that vehicle-treated CD11b^{DTR/EGFP} mice and DTX-treated non-transgenic mice of the same background do not demonstrate auditory functional differences [120]. To assure age-matching between mice, CD11b^{DTR/EGFP} littermates injected with vehicle solutions and were used as controls.

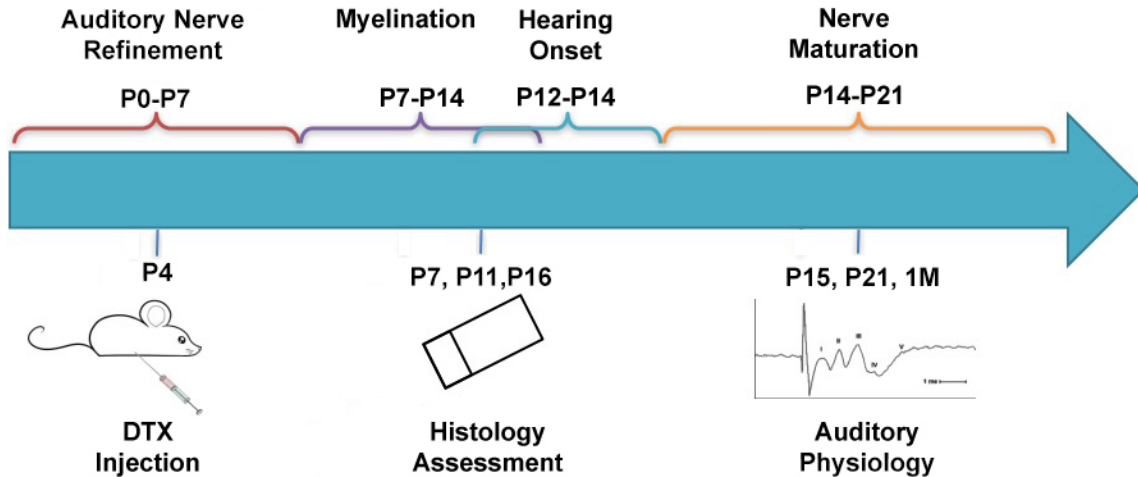


Figure 2-2. Diphtheria toxin administration to CD11b mice via intraperitoneal injection. The time course of experiments using CD11b^{DTR/EGFP} mice is illustrated. Experimentations (depicted below timeline) were performed at times of key developmental milestones (depicted above timeline). Injections of DTX were performed in CD11b mice at P4, during auditory nerve refinement. Histology alterations were assessed at P7, P11 and P16, when the auditory nerve is myelinated and hearing function commences. Auditory physiology of DTX-injected mice was assessed at P15, P21, and 1 month old.

BrdU postnatal injections: Neonatal CBA/CaJ mice were administered daily (IP) doses of bromodeoxyuridine (BrdU, 100 mg/kg, Sigma-Aldrich) for three consecutive days starting at P0. BrdU incorporation analysis was measured at P3, P7, P14, and P21 (see details in the immunohistochemistry section below).

Immunohistochemistry: Cochleae were fixed with 4% paraformaldehyde solution for 1-2 hours at room temperature (RT), decalcified with 0.12M ethylenediamine tetra acetic acid (EDTA) at RT with stirring, and cryopreserved with 30% sucrose for 30 minutes. The tissues were then embedded in Tissue-Tek OCT Compound (VWR, Radnor, PA, USA) and stained as whole-mount preparations or sectioned at 10 µm thickness. The primary antibodies used in this study include: rabbit anti-Iba1 (Wako Chemicals USA Inc., Richmond, VA USA (1:250)), rat anti-CD11b (Serotec, Oxford, UK (1:150)), mouse anti-CD68 (Abcam, Cambridge, MA, USA (1:100)), rabbit anti-F4/80 (Abcam (1:200)), mouse anti-Neurofilament 200 (Sigma-Aldrich (1:200)), rabbit anti-Myosin VIIa (Proteus BioSciences, Ramona, CA, USA (1:200)), mouse anti-C terminal binding protein 2 (BD Biosciences, San Jose, CA, USA (1:200)) goat anti-Sox10 (Santa Cruz Biotechnology, Santa Cruz, CA, USA (1:80)), rabbit anti-Kir4.1 (Alomone, Jerusalem, Israel (1:200)).

Secondary antibodies were biotinylated and binding was detected by labeling with fluorescein (FITC)-conjugated avidin D, Texas Red-conjugated avidin D (Vector Labs, Burlingame, CA, USA) or Alexa Fluor Dyes (ThermoFisher Scientific, Walham, MA, USA). Nuclei were counterstained with propidium iodide (PI) or 4',6-diamidino-2-phenylindole (DAPI).

The mouse monoclonal anti-BrdU was produced by clone BU33 and raised against BrdU incorporated into DNA, or coupled to a protein carrier. It recognized proliferative cells in the nuclei of frozen sections of animals treated with an *in vivo* administration of BrdU. In addition to the immunohistochemistry steps described

above, BrdU-labeled sections were treated with 2 moles of hydrogen chloride for 30 minutes and 0.1 moles of sodium borate buffer for 5 minutes prior to biotinylation.

Sections were examined on a Zeiss LSM5 Pascal (Carl Zeiss Inc., Jena, DE) confocal microscope, a Zeiss LSM 880 NLO or Leica TCS SP5 (Leica Microsystems, Allendale, NJ, USA) confocal microscope. FITC and Texas Red signals were detected by excitation with the 488 nm and 543 nm lines, respectively. Images were scanned at image scales of 225.0 μm (x) x 225.0 μm (y), 144.72 μm (x) x 144.72 (y) and 450.0 μm (x) x 450.0 μm (y). Captured images were processed using Zen 2012 Blue acquisition software (Zeiss Inc.), Leica Application Suite X software (Version 3.0.2.16120) and Adobe Photoshop CS6 (Adobe Systems Inc., San Jose, CA, USA).

Histology quantification: Quantitative analysis of macrophages, glial cells, and proliferative cell numbers were determined using AxioVision 4.8 (Carl Zeiss, Inc.) software. Regions of interests were determined by outlining intact RC and OSL, defined as boundaries from the habenular opening to a proximal site near the spiral ganglia, areas using the software outline tool. Similar tonotopic region sizes were examined between different cochlear samples. Within each region of interest, total cell numbers were determined by counting PI or DAPI counterstained cell nuclei using the measurement tool. Measurements of macrophages, glial cells, neurons and proliferative cells were determined by

counting cells immunolabeled for Iba1⁺, Sox10⁺, NF200⁺ or BrdU⁺, respectively, in each region of interest. At least 3 slides from each ear from each postnatal age were used for data collection and processed using statistical analysis described below.

Hair cell and synapse quantification: Whole mount preparations of cochleae from P7 and 1 month DTX-treated and control CD11b^{DTR/EGFP} mice were stained with Myosin VIIa to identify IHCs and OHCs. Hair cell numbers were counted manually using whole mount preparations from 1 month DTX-treated and control CD11b^{DTR/EGFP} mice (3 animals per group). Ribbon synapses under IHC were immunostained with CtBP2. CtBP2⁺ ribbons were measured manually from at least 10 IHCs in the apex, middle or base (3 animals per group). Confocal All images were taken with a Zeiss LSM 880 NLO using a 63x oil-immersion lens and acquired at 0.25 μm step size in the Z-axis in non-overlapping regions. Maximum projection images from confocal z-stacks were acquired with the same parameters described above. Care was taken to minimize pixel saturation while imaging each z-stack.

Tissue collection and total RNA isolation: Postnatal CBA/CaJ mice were euthanized and their cochleae were promptly collected. Microdissection was performed to remove the outer bony cochlear shell, cochlear lateral wall, and the majority of the sensory epithelium, preserving the modiolus portion of the cochlea. For RNA isolations, the left and right ear cochlea preparations from a

single mouse were pooled for individual samples. Total RNA was purified from cochlea preparations using the miRNeasy Mini Kit (Qiagen Inc, Germantown, MD, USA) according to the manufacturer's instructions.

Microarray data analysis: A microarray dataset of mouse auditory nerve development from our group (NCBI Gene Expression Omnibus accession GSE5417) [121] was used for comparative analysis. The dataset contains expression data for auditory nerve samples collected at P0, P3, P7, P10, P14, and P21 analyzed by Mouse 430 2.0 GeneChip (Affymetrix, Santa Clara, CA, USA). Raw hybridization data was normalized independently by both Robust Multi-Array Average and MicroArray Suite 5.0 algorithms using Expression Console Software (Affymetrix). Differential expression was defined as absolute signal log ratio >0.5 , $\geq 50\%$ present gene detection scores and $p \leq 0.05$ (Student's t-test, unpaired) for P7 vs. P0 (identifying 2391 probe sets). False discovery rate was estimated at 1.7% based on iterative comparisons involving randomized sample group assignments. Among the 2391 probe sets, 1878 analysis-ready genes were found. Functional analysis and canonical function identification was assessed with Ingenuity Pathway Analysis Software version (IPA®; QIAGEN, Redwood City, CA).

A representative heatmap image of complement-related genes was generated using the microarray dataset using expression data from P0, P7 and P21 auditory nerves. Complement-related genes were identified based on the

inclusion in the Gene Ontology Database annotation terms including: complement activation (GO: 0006956) regulation of complement activation (GO: 0030449), complement activation, classical pathway (GO: 0006958), complement activation, alternative pathway (GO: 0006957) and complement activation, lectin pathway (GO: 0001867). Only probesets with presence gene detection calls were included.

Quantitative PCR (qPCR): Reverse transcription of total RNA was performed with the QuantiTect Reverse Transcription Kit (Qiagen) according to the manufacturer's protocol. Briefly, genomic DNA was eliminated from RNA samples by incubation with gDNA Wipeout Buffer for 2 min at 42°C. Reverse transcription was performed with 50 ng of total RNA and Quantiscript Reverse Transcriptase in 20 µl reaction volumes incubated at 42°C for 15 min and 95°C for 3 min. The following gene-specific amplification reagents were purchased from Qiagen: H2D1 (QT01657761), H2K1 (QT01743700) C1qa (QT01057770), C3ar (QT00251216), Ppfibp2 (QT00098161), Runx1 (QT00100380) and fB (QT00101920). Quantitative PCR reactions were performed with the QuantiFast SYBR Green PCR Kit (Qiagen) using 1 µl of cDNA and a LightCycler 480 (Roche Diagnostics, IN, USA). Negative controls included reactions lacking cDNA template and reverse transcriptase. All reactions were performed in technical triplicate. Cycling parameters for PCR were: 50°C for 2 min, activation at 95°C for 5 min, and 40 cycles of 95°C for 10 sec and 60°C for 30 sec. Analysis of quantitative PCR data was conducted with the aid of LightCycler 480 software

(version 1.5.0.39). Amplification efficiency of each target was determined according to the equation $E = 10^{-1/S}$, where S is the slope of the standard curve generated from 10-fold serial dilutions of the DNA preparations. Relative expression levels were calculated using the $\Delta\Delta C_T$ method that involved calculated amplification efficiencies and then normalized to reference genes Hprt and 18S.

Transmission electron microscopy: For animals aged P7, cochleae were collected and perfused through the oval window with 0.5 ml of a fixative mixture comprised of 4% paraformaldehyde and 2% glutaraldehyde in 0.1 M phosphate buffer, pH 7.4. For collection of animals aged P11 and P16, anesthetized animals were perfused via cardiac catheter with 10 mL of normal saline containing 0.1% sodium nitrite followed by 15 ml of a mixture of 4% paraformaldehyde and 2% glutaraldehyde in 0.1 M phosphate buffer, pH 7.4. After removing the stapes and opening the oval and round windows, 0.5 ml of the same fixative described above was perfused gently into the scala vestibuli through the oval window. Inner ears were dissected and immersed in fixative overnight at 4°C. Decalcification for P16 cochleae was completed by immersion in 40 ml of 120 mM solution of EDTA, pH 7.0, with gentle stirring at room temperature for 2-3 days with daily changes of the EDTA solution. Cochlear tissues were postfixed with 1% osmium tetroxide-1.5% ferrocyanide for 2 hours in the dark, then dehydrated and embedded in Epon LX 112 resin. Ultrathin sections (70 nm thick) were stained with uranyl acetate and

lead citrate and examined and imaged using a JEOL JEM-1010 transmission electron microscope (JEOL USA, Inc., Peabody, MA, USA).

Toluidine Blue staining: Two-month-old WT and $fB^{-/-}$ mice were anesthetized, perfused, fixated, decalcified and embedded in Epon LX 112 resin as described for transmission electron microscopy. Semi-thin sections approximately 1 μm thick were cut and stained with 10% toluidine blue for 1 minute. Sections were rinsed in H₂O and allowed to air dry overnight before imaging.

Auditory brainstem response analysis: Auditory brainstem responses (ABRs) were measured as previously described [121, 122]. Mice were anesthetized by intraperitoneal injection of xylazine (20 mg/kg) and ketamine (100 mg/kg) and placed in a sound-isolation room. The acoustic stimuli were generated using Tucker Davis Technologies equipment System III (Tucker-Davis Technologies, Gainesville, FL, USA) and a SigGen software package (Version 4.4.1).

Calibration was completed using an Integrated Circuit Piezoelectric Sensor® Microphone System (PCB Piezotronics, Inc, Depew, NY, USA) in a probe tube clipped to the pinna. The signals were delivered into the animal ear canal through a 3-5 mm diameter plastic tube. ABRs were evoked at half octave frequencies from 4 to 45.2 kHz with 5 ms duration tone pips with \cos^2 rise/fall times of 0.5 ms delivered at 31 times/s. Sound levels were reduced in 5 dB steps from 90 dB SPL to 10 dB SPL to determine thresholds.

Distortion product otoacoustic emission analysis: Distortion product otoacoustic emission analysis testing was performed in mice under general anesthesia as previously described [123]. Briefly, DPOAEs were measured using a Tucker Davis Technologies equipment RZ6 system (Tucker Davis Technologies, Gainesville, FL, USA) and SigGen software using an ER-10B+ Lo Noise™ Microphone System (Etymotic Research, Inc, Grove Village, IL, USA). The acoustic assembly was tightly enclosed in the ear. Primary tones were swept from $f_2 = 5.6$ to 45.2 kHz with f_1/f_2 ratio of 1.2. DPOAE amplitudes of each mouse were analyzed for individual frequencies, and mean amplitudes were calculated for each frequency, including 5.6, 8.0, 11.3, 16, 20, 22.6, 32, 40 and 45.2 kHz.

Experimental design and statistical analyses: For postnatal experiments, biological sample sizes were determined based on similar experiments from previous studies conducted by our laboratory (Jyothi et al., 2010; Lang et al., 2016; Lang et al., 2015) and other labs [85, 121, 124-126] with the goal of achieving stringent and accurate measures of difference between control and DTX-treated animals, namely statistical power of $\geq 80\%$ and significance level of ≤ 0.05 . Statistical analyses were performed using GraphPad Prism 7 software (GraphPad Software, Inc. La Jolla, CA) for Windows. Quantitative data are expressed as mean \pm SEM, unless otherwise specified. Sample size is indicated for each figure. Differences across groups with multiple comparisons were analyzed with One-way ANOVA with *post hoc* Bonferroni Multiple Comparison

tests. Differences for single pairwise comparisons were analyzed using two-tailed, unpaired Student's *t* tests. Statistical significance was defined as a *p* value of ≤ 0.05 ; all significance values are indicated.

Core Facilities and Resources: Collaborations were conducted with the MUSC Proteogenomics Facility, supported by NIH-NIGMS South Carolina COBRE for Cardiovascular Disease (GM103342), NIH-NIGMS South Carolina IDeA Networks of Biomedical Research Excellence (INBRE; GM103499) and the Office of the Vice President for Research at the Medical University of South Carolina. Additionally, the services of the Morphology, Imaging and Instrumentation Core, supported by NIH-NIGMS P30 GM103342 to the South Carolina COBRE for Developmentally Based Cardiovascular Disease, were used. Also, this research was supported in part by the Cell & Molecular Imaging Shared Resource, Hollings Cancer Center, Medical University of South Carolina (P30 CA138313) and the Shared Instrumentation Grant S10 OD018113.

CHAPTER THREE: MACROPHAGE-MEDIATED GLIAL CELL ELIMINATION IN THE POSTNATAL MOUSE COCHLEA

***Note: This chapter has been published:**

Brown LN, Xing Y, Noble KV, Barth JL, Panganiban CH, Smythe NM, Bridges MC, Zhu J and Lang H. (2017) Macrophage-Mediated Glial Cell Elimination in the Postnatal Mouse Cochlea. *Front. Mol. Neurosci.* 10:407.doi: 10.3389/fnmol.2017.00407[127].

INTRODUCTION

The auditory nerve is the conduit for transmission of sound in the mammalian ear. Axonal projections of bipolar SGNs connect sensory hair cells (HCs) to central auditory processes in the brain. Two subpopulations of SGNs exist: type I, which account for 90-95% of total SGNs, and type II, which comprise the remaining 5-10% of SGNs. The cell bodies of both neuron types are housed within Rosenthal's canal (RC) and extend peripheral axons through the osseous spiral lamina (OSL) to form connections with HCs in the organ of Corti. Type I SGNs extend a single axon to a single IHC and type II SGNs innervate multiple OHC with numerous axonal projections [128]. SGNs begin to innervate cochlear HCs in a tonotopic pattern as early as embryonic day (E) 15.5 [57]. At this time, multiple type I SGNs extend axons past the IHC region, forming erroneous connections with OHCs. Similarly, type II SGN axons form mistargeted connections with IHCs [58, 59, 129]. Between E17.5 and the first postnatal week in rodents, excessive type I and II axons are eliminated by retraction or pruning to produce mature innervation patterns [59, 60, 124, 129, 130]. This refinement process occurs prior to hearing onset, which commences between P12-P14 [46].

SGNs and auditory nerve fibers are wrapped by neural crest-derived auditory glial cells [54, 131]. Type I SGN somas are covered by myelinating satellite cells and their axons are ensheathed by myelinating Schwann cells. Conversely, type II SGNs are enveloped by non-myelinating satellite and

Schwann cells. Recent studies have demonstrated that migration, maturity and survival of SGNs is largely dependent on surrounding glial cells [121, 122, 131-133]. Additionally, conditional deletion of Sox10, a transcription factor regulating glial cell differentiation, results in reduced glial numbers, abnormal SGN distribution, decreased SGN migration, and the appearance of nerve fibers that overshoot the organ of Corti and extend into the cochlear lateral wall, revealing the important role glial cells play in proper SGN innervation [55]. However, it is still unknown how glial cell numbers are regulated as the auditory nerve matures.

Immune cells such as macrophages and microglia contribute to nerve refinement in the central nervous system [69, 93, 97, 134]. Macrophages, monocyte-derived phagocytes, are members of the innate immune system and respond to various cytokine/chemokine signals to remove pathogens and apoptotic cells [135-137]. Macrophages have also been detected in the adult cochlea following cochlear insult [78, 80, 82, 86]. Damaged SGNs, auditory glial cells and fibrocytes secrete pro-inflammatory signals that promote the infiltration of macrophages [138, 139]. Recent studies have shown that immune-related gene expression increases in the developing auditory nerve, [72, 140, 141]. However, the role of macrophages in auditory development has not been characterized.

In this chapter, we characterized the spatiotemporal and activation profile of cochlear macrophages in the developing auditory nerve. Our investigations also focused on the interactions between cochlear

macrophages and auditory glial cells during postnatal development using a transient macrophage depletion mouse model. Finally, we investigated how macrophages contributed to auditory function and nerve maturation using the macrophage-depletion mouse model.

RESULTS

Glial cell numbers decrease after the second postnatal week.

SGNs undergo a rigorous course of refinement and retraction during postnatal development. Glial cells are in tight junction with SGNs. To determine changes in glial cell numbers during auditory nerve development we collected postnatal spiral ganglia at the ages of P0, P3, P7, P14, and P21 and calculated the density of Sox10⁺ cells. Sox10 transcription factor is a key developmental regulator expressed in both immature and differentiated glial cells of the auditory nerve [38, 52, 54]. Quantitative analyses of Sox10⁺ cells revealed that the highest density of glial cells in the OSL and RC occurred around P3-P7 (Figure 3-1A-D). After the first postnatal week, glial cell densities decreased. This temporal profile of glial cell numbers is in agreement with previous findings that the auditory nerve achieves a mature innervation pattern by the end of the first postnatal week in rodent models [58, 59, 125, 130].

To determine the proliferative ability of glial cells we utilized the BrdU assay. Cochlear samples were collected for analysis 3 days after BrdU injection. Double-labeling for BrdU and Sox10 revealed the presence of proliferative glial cells in the postnatal auditory nerve (Figure 3-1E-E'). Quantitative analysis of Sox10⁺/BrdU⁺ double-labeled cells revealed that the highest occurrence of glial cell proliferation occurred at P3-P7. Glial cell proliferation significantly decreased after the second postnatal week, after mature auditory nerve circuitry is established and SGNs are myelinated (Figure 3-1F, G).

The early phase of apoptosis is a rapid event necessary for the development of neural tissues and is often characterized by the cleavage of Caspase-3 [142-144]. To determine if the temporal alterations in glial cells were due to apoptosis we examined cochlear samples from mice aged P3 through P14 for the presence of Sox10/Cleaved-Caspase 3 positive cells. Very few Cleaved-Caspase 3⁺ glial cells were identified in P3 and P7 cochleae (Figure 3-1H, I, arrowheads). Interestingly, one Sox10⁻ cell stained positive for Cleaved-Caspase 3 in the P3 cochlea. The morphology of this apoptotic cell suggested it to be a SGN (Figure 3-1H, arrow), supporting previous research that found the highest incidences of SGN apoptosis in P4-6 rodent auditory nerves [60].

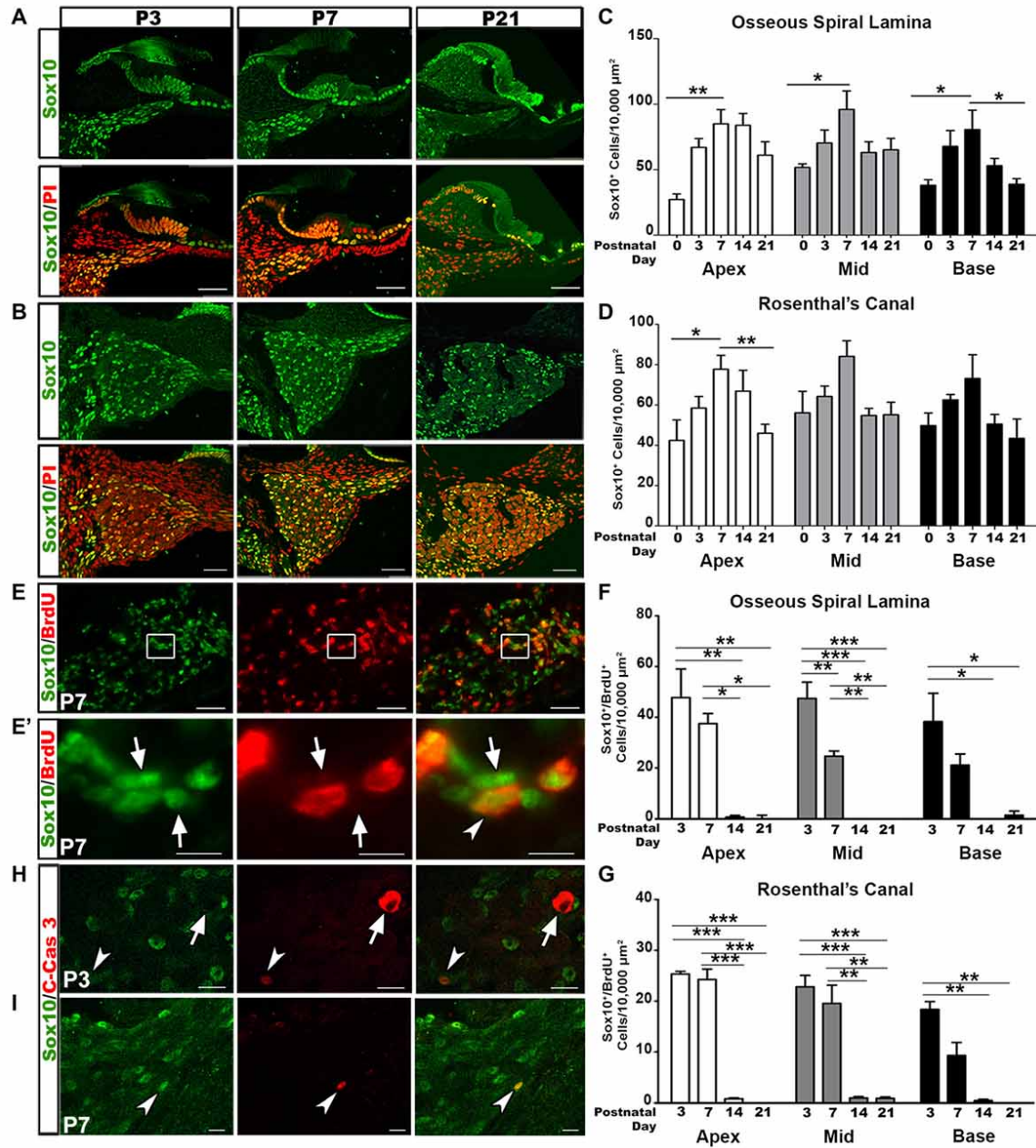


Figure 3-1. Increased glial cell numbers and proliferation correlate with auditory nerve refinement in postnatal mouse cochleae. (A,B) Confocal imaging of glial cell distribution in the postnatal cochlea. Sox10⁺ glia (green) and propidium iodide (PI; red) counterstained nuclei appeared in the osseous spiral lamina (OSL) **(A)** and Rosenthal's canal (RC) **(B)** of P3, 7 and 21 mouse cochleae. Scale bars = 50 μm. **(C,D)** Quantitative analysis for Sox10⁺ cells in the

OSL (**C**) and RC (**D**) in P0, 3, 7, 14 and 21 cochleae. Data bars represent mean density and error bars represent SEM. Two-tailed, unpaired Student's t-tests were used to compare densities at P7 to the other time points for each turn (* $p < 0.05$; ** $p < 0.01$; *** $p < 0.001$; $n = 4-7$ ears). The three cochlear turns are displayed: apical (white bars), middle (gray bars), and basal (black bars). (**E**) Dual-immunolabeling for Sox10 (green) and BrdU (red) identifies proliferative glial cells in the P7 RC. Cochlear samples were from mice that received a single intraperitoneal (IP) administration of BrdU at P0, P1 and P2. Scale Bars = 50 μm . (**E'**) Higher magnification of inset from (**E**) shows proliferative glia (arrows) and non-proliferative glia (arrowheads). Scale bar = 20 μm . (**F,G**) Quantitative analysis of Sox10⁺/BrdU⁺ cells in the OSL (**F**) and RC (**G**) for P3, 7, 14 and 21. One-way ANOVA followed by Bonferroni Multiple Comparison tests were used to compare densities between time points (* $p < 0.05$; ** $p < 0.01$; $n = 3-5$ cochlear samples). Quantifications for the different cochlear turns are demonstrated: apical (white bars), middle (gray bars) and basal (black bars). Data bars represent mean density and error bars represent SEM. (**H,I**) Dual-immunolabeling for Sox10 (green) and C-Cas3 (Cleaved-Caspase 3; red) reveals apoptotic glial cells (arrowheads) and apoptotic non-glial cells (arrow) in P3 (top) and P7 (bottom) cochleae. Scale Bars = 20 μm in (**H**), Scale Bars = 20 μm in (**I**). Apex: apical turn; Mid: middle turn; Base: basal turn.

Immune-related and axon guidance gene expression correlate with auditory nerve maturation

We utilized our published microarray dataset of developing mouse auditory nerves (NCBI GEO:GSE5417; [121]) to identify molecular regulators and pathways involved in postnatal nerve development. We performed a comparison analysis of approximately 45,000 gene probe sets to identify genes that were differentially expressed between P0 and P7 (absolute signal log ratio >0.5; $\geq 50\%$ present gene detection scores, Student's unpaired *t*-test $p \leq 0.05$). This analysis yielded 2391 probe sets with up- and down-regulated expression values and an estimated false discovery rate of 1.7% (Figure 3-2A). Functional enrichment analysis was conducted using 1878 analysis-ready genes found among the 2391 probe sets. Pathway enrichment analysis detected 30 unique signaling pathways that were significantly enriched (Table 1), including Axonal Guidance Signaling, which is expected given that auditory nerve maturation occurs during the first postnatal week. Interestingly, several immune response pathways, including GADD45 Signaling and Complement System, were also significantly enriched, suggesting that immune-related activities are critical during auditory nerve development.

We performed qPCR to validate the temporal expression patterns of two key regulatory genes associated with axon guidance cues, *Ppfibp2* and *Runx1*, which were identified as differentially expressed in our analysis. *Ppfibp2* is a gene that encodes liprin beta-1 protein, a positive regulator of axonal extension and synapse formation [145, 146]. *Runx1* is a transcription factor that negatively

regulates axonal projections and neuron maintenance [147, 148]. Although not significant, *Ppfbp2* showed a trend for increased gene expression from P0 to P7 and decreased by P21, in agreement with the microarray results (Figure 3-2B). We also found that *Runx1* expression significantly decreased at P7, when compared to P0 and P21 (Figure 3-2B), supporting the microarray results. Together, expression profiles of these genes indicate that P7 is a critical time point in auditory nerve maturation in the mouse cochlea.

The antigen presentation pathway includes MHC class I genes, which signal for the targeting of nerves for elimination during synaptic pruning in spinal motoneurons [149]. We performed qPCR to validate the expression of two MHC Class I genes, H2-D1 and H2-K1, which were identified as differentially expressed in our microarray analysis. Gene expression of H2-D1 and H2-K1 was upregulated in P7 auditory nerves, compared to P0 and P21 nerves, validating the expression values represented in the microarray dataset (Figure 3-2C).

Complement signaling also mediates synaptic pruning and axon elimination in central and peripheral nerves [69, 95, 150]. The complement system was identified as significant based on the differentially expressed genes identified by our microarray analysis (Table 1). We investigated the expression of two complement-related components identified as upregulated in our microarray dataset, complement component C1q, the molecular initiator of the classical complement pathway, and C3a receptor (C3aR), a receptor for the central complement component for all complement pathways. qPCR confirmed that gene

expression of C1q and C3aR was upregulated in the P0-P7 auditory nerve (Figure 3-2D).

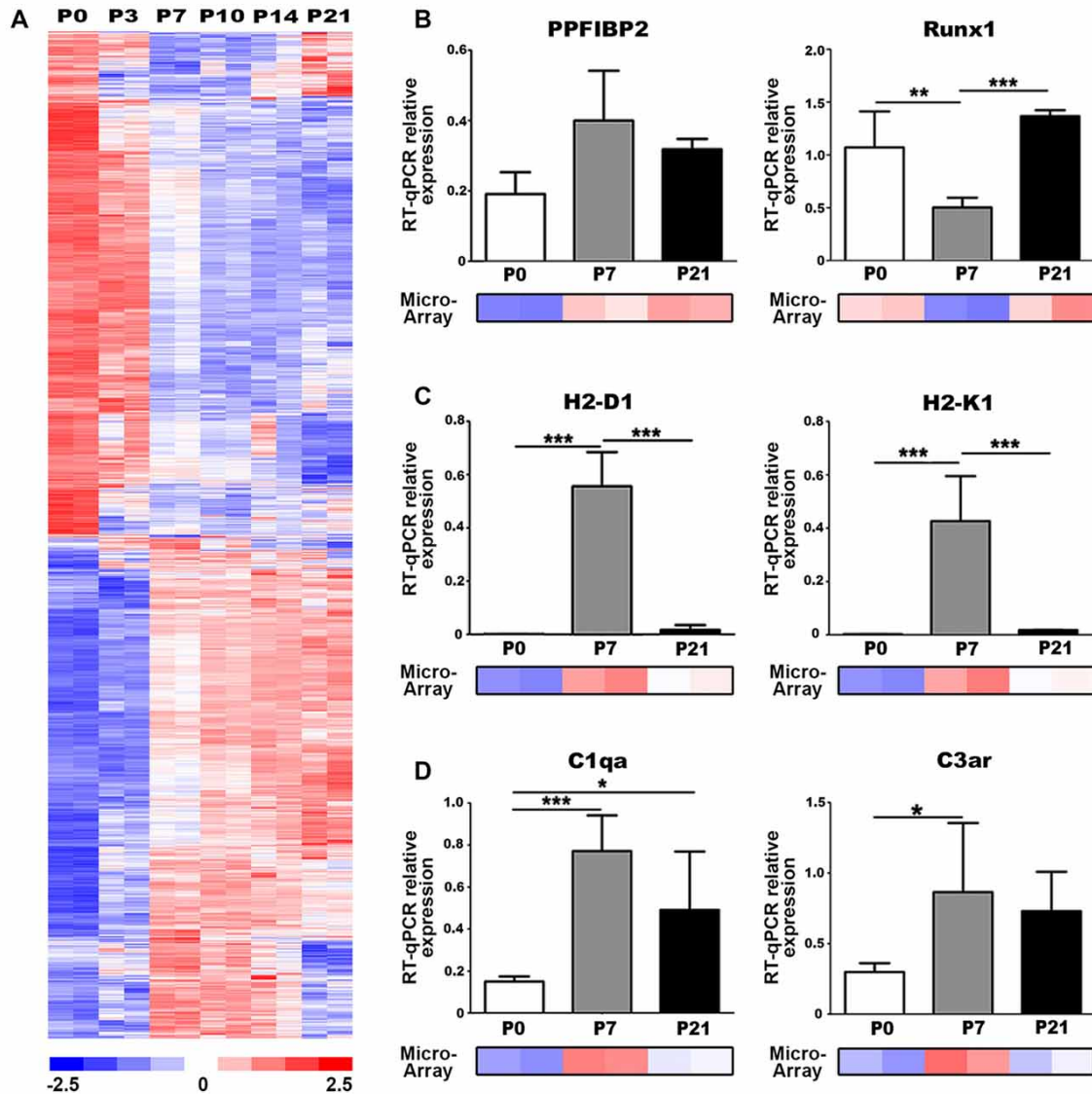


Figure 3-2. Genes associated with axonal guidance and immune responses are differentially expressed in the postnatal auditory nerve. (A) Expression profiles of genes differentially expressed between P0 and P7 in postnatal auditory nerves collected at P0, P3, P7, P10, P14 and P21. A total of 2391 probe sets, corresponding to 1878 genes, were identified comparing expression at P0 vs. P7 with absolute signal log ratio >0.5, $\geq 50\%$ present gene detection scores and $p \leq 0.05$ (Student's t-test). Colorimetric scaling (Z-standardization) for the heatmap is shown at the bottom. **(B–D)** Quantitative PCR (qPCR) validation for

gene expression of **(B)** axonal guidance genes **(C)**, major histocompatibility class (MHC) II genes, and **(D)** complement pathway genes at P0 (black), P7 (gray) and P21 (white) is displayed. Microarray expression data at P0, P7 and P21 are demonstrated for each gene. One-way ANOVA with post hoc Bonferroni Multiple Comparison tests were used to compare gene expression between the postnatal days. Data bars represent average mean of experiments run in triplicate; error bars represent SEM; * $p < 0.05$; ** $p < 0.01$, *** $p < 0.001$; $n = 3$.

Canonical pathway	p-value
Cell Cycle: G2/M DNA Damage Checkpoint Regulation	1.74E-04
Axonal Guidance Signaling	6.17E-04
GADD45 Signaling	3.02E-03
Cell Cycle Control of Chromosomal Replication	3.55E-03
Superpathway of Serine and Glycine Biosynthesis I	3.98E-03
dTMP <i>De Novo</i> Biosynthesis	4.90E-03
Melatonin Degradation II	4.90E-03
Estrogen-mediated S-phase Entry	5.50E-03
Osteoarthritis Pathway	8.51E-03
Adipogenesis pathway	9.77E-03
Serine Biosynthesis	1.15E-02
Glycine Degradation (Creatine Biosynthesis)	1.23E-02
Triacylglycerol Biosynthesis	1.41E-02
Hereditary Breast Cancer Signaling	1.66E-02
Phospholipases	2.04E-02
Pyrimidine Deoxyribonucleotides <i>De Novo</i> Biosynthesis I	2.29E-02
Antioxidant Action of Vitamin C	2.75E-02
Role of BRCA1 in DNA Damage Response	2.82E-02
Bladder Cancer Signaling	3.09E-02
Virus Entry via Endocytic Pathways	3.31E-02
Sphingomyelin Metabolism	3.39E-02
Sphingosine-1-phosphate Signaling	3.39E-02
Fatty Acid Activation	3.55E-02
Wnt/ β -catenin Signaling	3.72E-02
Cell Cycle: G1/S Checkpoint Regulation	4.17E-02
Cholesterol Biosynthesis I	4.68E-02
Cholesterol Biosynthesis II (via 24,25-dihydrolanosterol)	4.68E-02
Cholesterol Biosynthesis III (via Desmosterol)	4.68E-02
ATM Signaling	4.79E-02
Complement System	4.90E-02

Table 1. Ingenuity pathway analysis of canonical pathways identified by differentially expressed genes.

Macrophage numbers increase during auditory nerve maturation

We further addressed the hypothesis that immune activities contribute to auditory nerve refinement by examining macrophage activity in the postnatal auditory nerve. Iba1, a highly conserved cytoplasmic protein, is specific to cells of monocytic lineage [151, 152]. Analysis of Iba1⁺ cells revealed gradual increases in macrophage numbers in RC and the OSL from P0 to P3, reaching peak numbers at P7, and decreasing after P14 and P21 (Figure 3-3A-D). This increase in macrophage numbers coincides temporally with auditory nerve maturation and is subsequent to the glial cell increase.

To determine if the increase in macrophage density was due to the proliferation of resident macrophages, we injected BrdU into P0 pups and assessed macrophage proliferation. Dual labeling of Iba1⁺/BrdU⁺ cells demonstrated that the highest numbers of proliferative macrophages are seen during the first postnatal week (Figure 3-3E-G). Fewer proliferative macrophages were seen in the second and third postnatal weeks.

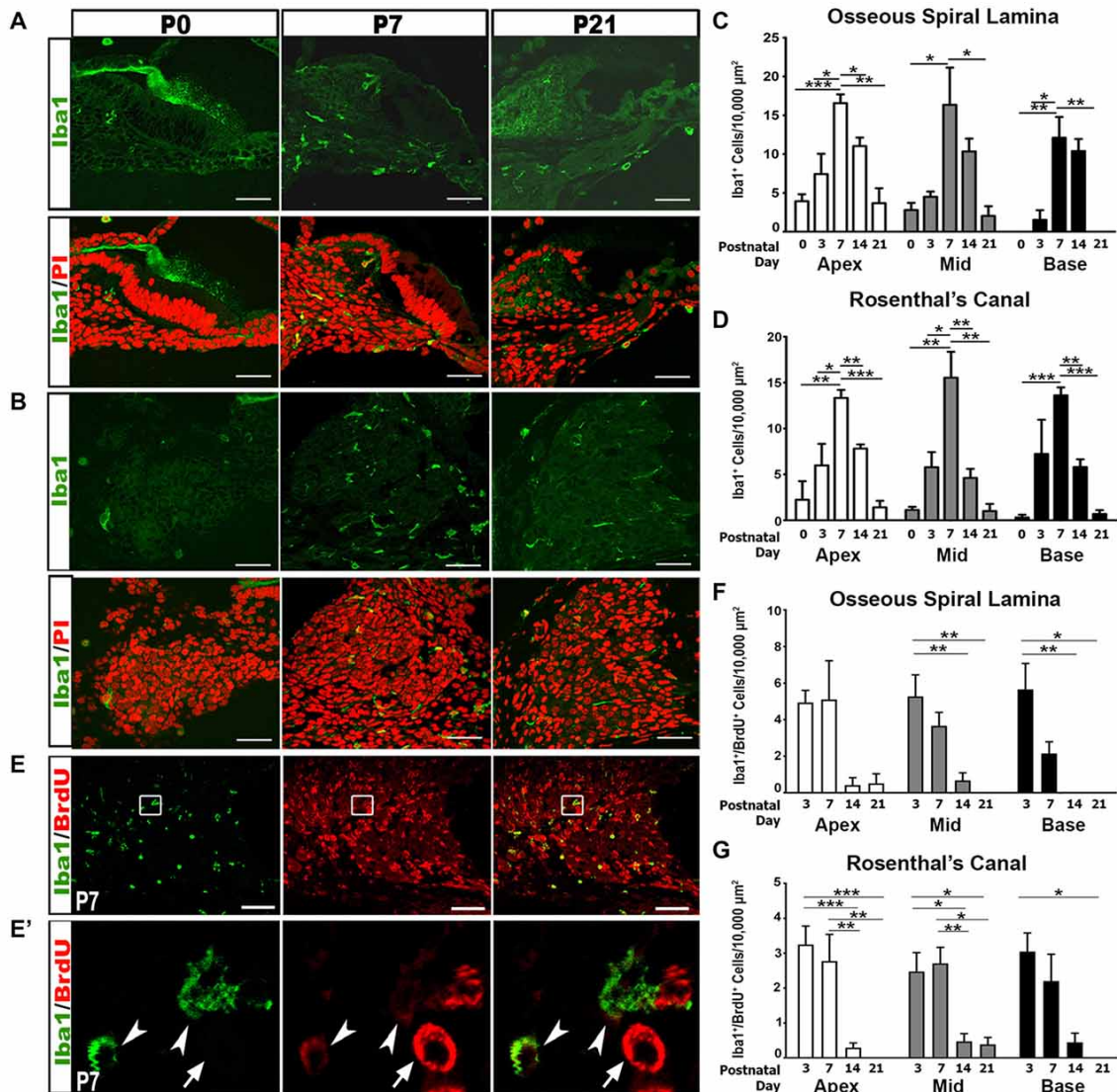


Figure 3-3. Iba1⁺ macrophage numbers and proliferation peak in the first postnatal week. (A,B) Confocal images show the temporal distribution of Iba1⁺ (green) macrophage cells in the OS (A) and RC (B) of P0, P7 and P21 cochleae. Scale bars = 50 μm . **(C,D)** Quantitative analyses of Iba1⁺ macrophage densities in the OS (C) and RC (D) of postnatal cochleae aged P0–P21 reveal an increase in macrophage numbers during nerve refinement. Quantifications for the different cochlear turns are displayed: apical (white bars), middle (gray bars) and basal (black bars). Data bars represent mean density and error bars

represent SEM. Two-tailed, unpaired Student's t-tests were used to compare Iba1⁺ macrophage densities at P7 to other postnatal time points in each turn (*p < 0.05; **p < 0.01; ***p < 0.001; n = 3–7 ears). **(E–G)** Confocal images show proliferating macrophages in the auditory nerve of a P7 cochlea. Macrophages are labeled with Iba1 (green) and proliferating cells are labeled with BrdU (red). Cochlear samples were from mice that received a single IP administration of BrdU at P0, P1 and P2. Scale bars = 50 μm. **(E')** A high magnification image from enclosed area shown in **(E)** identifies proliferative macrophages (arrowheads) and a proliferative non-macrophage cell (arrow). **(F,G)** Quantitative analysis of BrdU/Iba1⁺ macrophage densities in the OSL **(F)** and RC **(G)** of postnatal cochleae aged P3–P21 reveals that most macrophage proliferation occurs during the first postnatal week (P3–7). One-way ANOVA with post hoc Bonferroni Multiple Comparison tests were used to compare densities between time points (*p < 0.05; **p < 0.01; ***p < 0.001 n = 3–7 ears). Quantifications for the different cochlear turns: apical (white bars), middle (gray bars) and basal (black bars). Data bars represent mean density and error bars represent SEM. Apex: apical turn; Mid: middle turn; Base: basal turn.

Postnatal macrophages display activated phenotypes

We performed immunohistochemical analysis of Iba1⁺ macrophages in postnatal tissue using cochlear whole mount preparation from P7 mice. This allowed visualization of entire cell morphologies. Macrophages exist in several distinct morphological states that are related to their functional roles. Ramified appearance indicates surveillance function, while rounded or amoeboid shapes suggest phagocytic functions [153, 154]. Iba1⁺ macrophages were present in multiple locations of the cochlea including RC, the OSL, along the outskirts of and within the organ of Corti and in the cochlear lateral wall (Figure 3-4A). Investigation of macrophage morphology revealed that some macrophages were ramified (Figure 3-4Ai) while others were amoeboid (Figure 3-4Aii-iii).

To further characterize the macrophage phenotype the postnatal auditory nerve, we probed for a panel of lysosomal and surface protein markers that are expressed by mature monocytes and during immune cell activation. We first performed immunostaining for F4/80, a marker for glycoprotein presented on the surface of mature monocytes [155, 156]. Over 80% of Iba1⁺ cells in the P7 cochlea stained positive for F4/80, confirming the differentiated phenotype and mature identity of the Iba1⁺ cells in the auditory nerve (Figure 3-4B, E). Next, we assessed the activation and phagocytic profile of the immune cells in P3-7 auditory nerves by probing for immunoreactivity of CD11b, a cell surface integrin indicative of macrophage/microglia activation, and CD68, a lysosomal protein expressed during debris degradation [157-159]. The presence of Iba1⁺/CD11b⁺

and Iba1⁺/CD68⁺ cells suggested that a portion of macrophages engulfed particles and were actively degrading debris and cell fragments (Figure 3-4C-E).

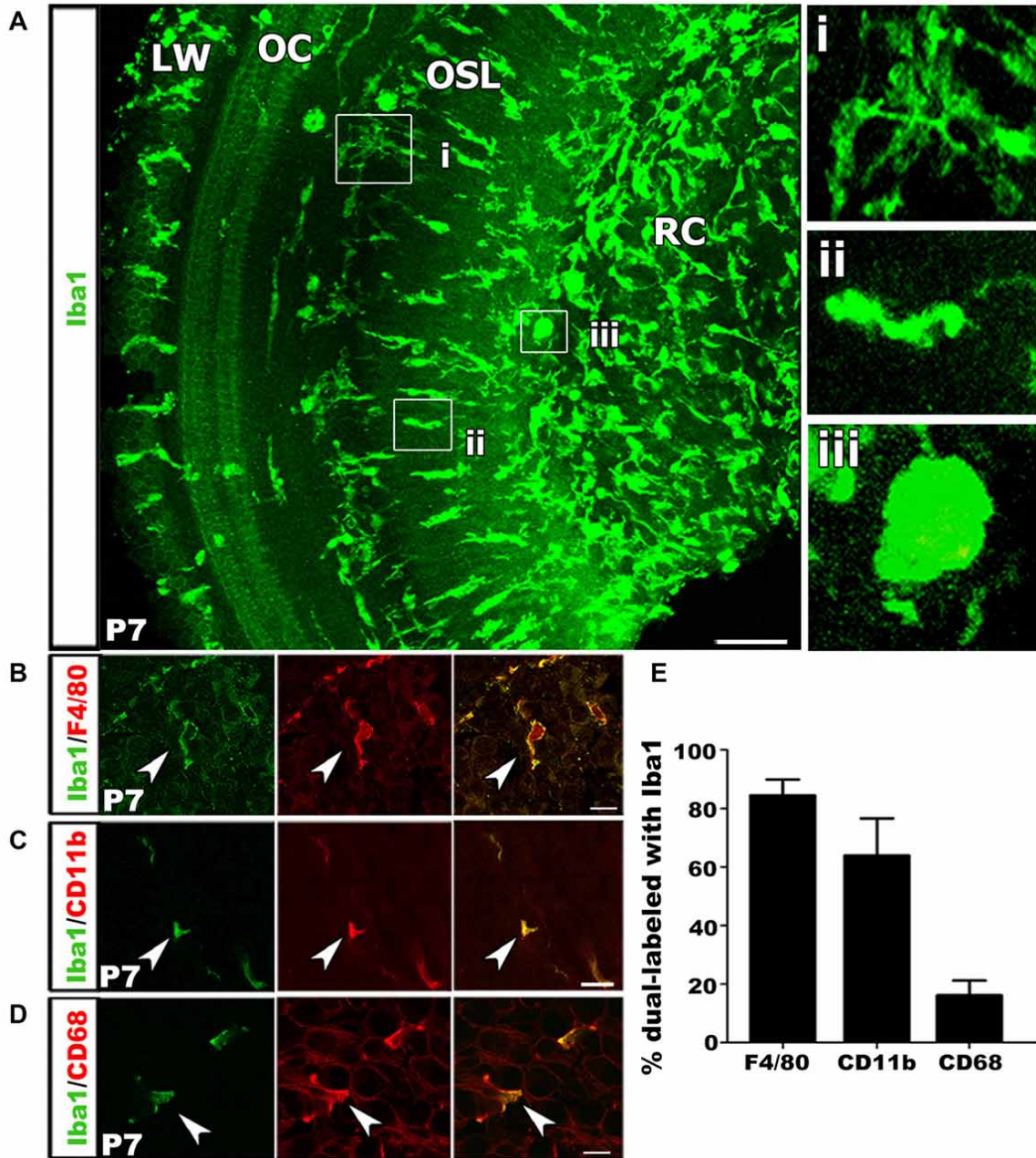


Figure 3-4. Macrophage activation occurs in the developing auditory nerve. (A) Confocal z-stack 3D rendering in mid-apical portion of a P7 mouse cochlea immunolabeled with Iba1 (green). Numerous Iba1⁺ macrophages are present in the OSL and RC with an amoeboid shape, suggesting these Iba1⁺ cells are the activated macrophages. High magnification images

from **(A)** shows a ramified macrophage **(i)** and an amoeboid macrophage in the OSL **(ii)** and RC **(iii)**. LW, lateral wall; OC, organ of Corti; OSL, osseous spiral lamina; RC, Rosenthal's canal. Scale bar = 50 μm . **(B)** Macrophages co-labeled with Iba1 (green) and F4/80 (red) antibodies (arrowhead). **(C)** An image of co-labeled macrophage cells with Iba1 (green) and CD11b (red), reveal macrophages at P7 are mature leukocytes (arrowhead). **(D)** Co-localization of Iba1 (green) and CD68 (red), a lysosomal glycoprotein marker, reveals phagocytic activity of cochlear macrophages (arrowhead). (A–D) Scale bars = 10 μm . **(E)** Bar graph depicting the percentage of Iba1⁺ cells that co-label with F4/80, CD11b and CD68. Percentages calculated from three to four mouse samples for each probe.

Macrophages phagocytose glial cells and axonal fragments

To further investigate the physical interaction between auditory glial cells and macrophages, 3D confocal microscopy was employed. We chose to examine the auditory nerve at P7, when cochlear macrophage numbers were the highest. Dual immunostaining for Sox10⁺ glia and Iba1⁺ macrophages in RC revealed that macrophages were in close proximity to glial cells (Figure 3-5A-B'''). Upon closer examination, it was apparent that Sox10⁺ glial cell nuclei were engulfed within the cytoplasm of macrophages (Figure 3-5A'). Internalization of glia by macrophages was confirmed by maximum projection analysis and 3D reconstructions of sections stained for Sox10 and Iba1 (Figure 3-5B'''). We then examined macrophage-axon relationships in the P7 auditory nerve. We assessed neurofilament 200⁺ (NF200) nerve fibers that extend through the OSL to reach their hair cell targets. Dual immunostaining of Iba1 and NF200 revealed that macrophages directly contact SGN axons in P7 cochleae (Figure 3-5C-C'''). Maximum projection images and 3D reconstruction confirmed that macrophages phagocytose and digest axonal fragments (Figure 3-5C''').

Using electron microscopy, we investigated the ultrastructure of different macrophage phenotypes in the auditory nerve of P7 cochleae. As expected, macrophages showed an active phenotype, including densely-packed cytoplasm filled with multiple lysosomes, abundant rough endoplasmic reticulum, electron-dense lipid bodies and phagoliposomes (Figure 3-6A-C). We also detected several glial cells that were not enclosing nerve fibers or neuron cell bodies (Figure 3-6D, asterisks). Interestingly, these free-floating, or supernumerary, glial

cells were in close proximity to macrophages demonstrating activated morphologies (Figure 3-6D'). These observations correspond with the findings of glia-macrophage interactions identified by immunostaining and 3D reconstruction.

The ultrastructural analysis also detected SGN axons that were undergoing degeneration (Figure 3-6E, arrows). In some cases, a single glial cell ensheathed several degenerating axons (Figure 3-6E'). Active macrophages were seen encroaching on these degenerating SGN axons (Figure 3-6E'). There were also several macrophages that surrounded glia-wrapped degenerating axons (Figure 3-6F, G). Both myelinated and unmyelinated degenerating axons were engulfed by macrophages. These macrophages possessed myelin-like debris within their cytoplasm (Figure 3-6F, arrowheads), indicating that both glial cells and damaged or degenerative axons are phagocytosed by cochlear macrophages.

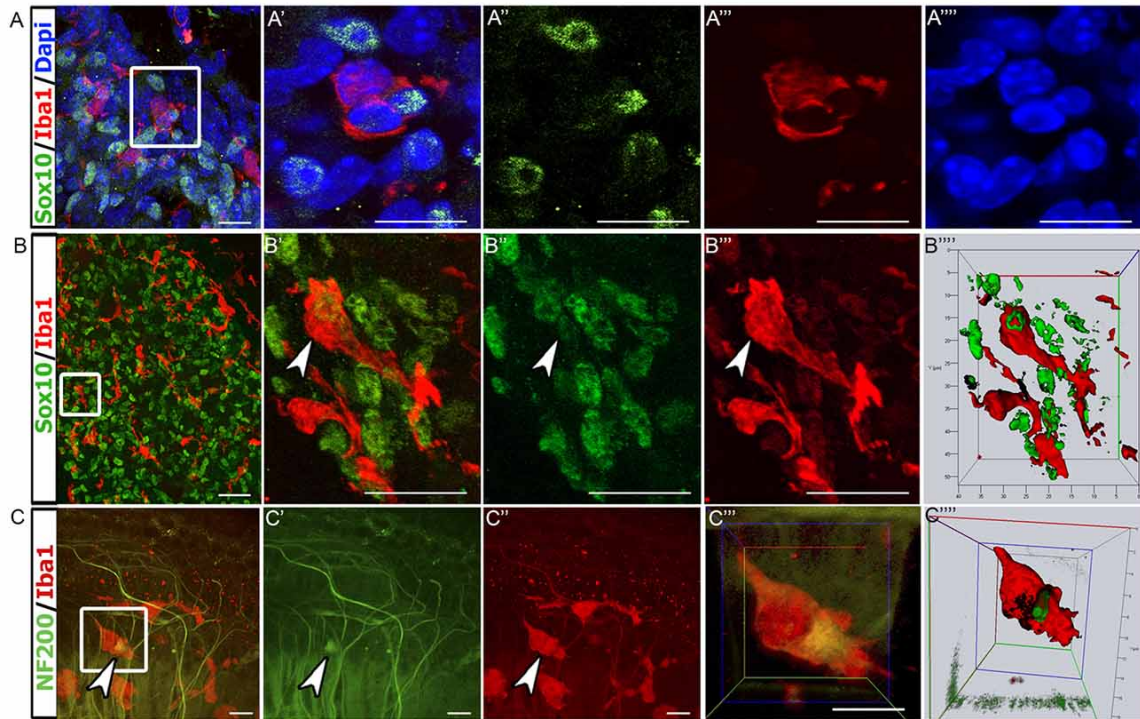


Figure 3-5. Macrophages engulf glial cells and the fragments of auditory nerve fibers. (A–A''') Confocal images of Sox10⁺ glial cells (green) and Iba1⁺ macrophages (red) in the P7 auditory nerve. Macrophages are in close proximity of glial cells. 4',6-diamidino-2-phenylindole (DAPI; blue) was used to counterstain cell nuclei. Panel (A') shows enlarged image from enclosed area. (A–A''') Scale bars = 10 μ m. **(B–B''')** Another confocal image of Sox10⁺ cells (green) and Iba1⁺ macrophages (red) from a thick section of P7 auditory nerve. Panel (B''') shows stacking and 3D rendering of the enclosed area reveals an Iba1⁺ macrophage (red) engulfing a Sox10⁺ glial cell (green; arrowhead). (B–B''') Scale bars = 15 μ m. **(C–C''')** Confocal imaging of a P7 whole-mount cochlear preparation stained with Iba1 (red) and NF200 (green). Panel (C''') shows stacking and 3D rendering of enclosed area shows an Iba1⁺

macrophage phagocytosing a NF200⁺ nerve fiber fragment (arrowhead). (C–
C'') Scale bars = 50 μm.

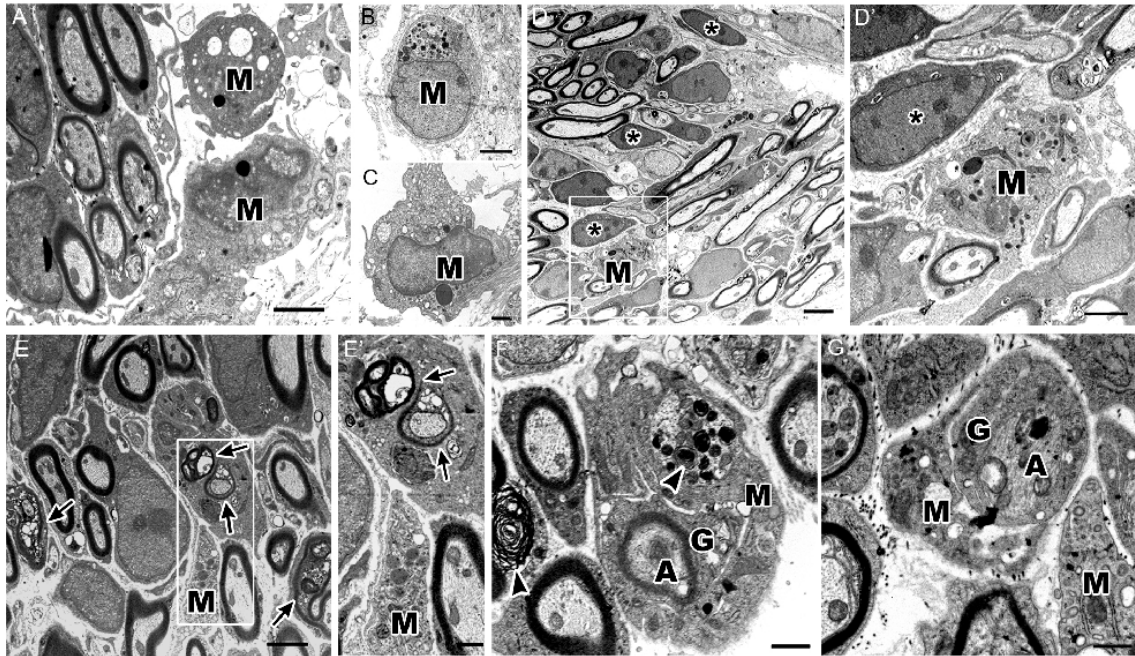


Figure 3-6. Ultrastructure of cochlea shows macrophages engulf degenerating axons and glial cells. (A–C) Micrographs of the P7 auditory nerve reveals cochlear macrophages (M) with activated morphologies including densely packed cytoplasm filled with multiple lysosomes, abundant rough endoplasmic reticulum, electron dense lipid bodies and phagoliposomes. **(A,B)** Scale bars = 2 μ m, **(C)** Scale bar = 800 nm. **(D)** Electron micrograph shows myelinated axons in the OSL of a P7 mouse. Scale bar = 4 μ m. Asterisks demonstrate supernumerary glial cells that are not juxtaposed to nerve fibers. **(D')** Enclosed area highlights an activated macrophage (M) approaching a supernumerary glial cell (asterisk). Scale bar = 800 nm. **(E)** Micrograph of axons undergoing development-related degeneration (arrows). Scale bar = 2 μ m. **(E')** Enclosed area shows a macrophage (M) encroaching a glial cell with several degenerating axons within the cytoplasm

(arrows). Scale bar = 800 nm. **(F)** The ultrastructure of the OSL area in another P7 mouse cochlea shows a macrophage (M) phagocytosing a glial cell (G) wrapping a myelinated, degenerative axon (A). Arrowheads highlight myelin blebs along degenerating axons and within the active macrophage. Scale bar = 800 nm. **(G)** Micrograph of a macrophage (M) engulfing a non-myelinating glial cell (G) and associated, degenerating axon (A). Scale bar = 600 nm. All images were composed from analysis of at least three mouse cochleae.

Transient depletion of postnatal macrophages increases glial cell numbers

To determine if macrophages are required to remove postnatal glial cells, we employed the $CD11b^{DTR/EGFP}$ mouse model to transiently deplete active macrophages in the developing auditory nerve. Murine cells have low binding affinity for diphtheria toxin (DTX). $CD11b^{DTR/EGFP}$ mice express DTX receptors under the *CD11b* promoter. Administration of DTX to $CD11b^{DTR/EGFP}$ mice results in a temporary depletion of only $CD11b^+$ cells, with reductions lasting for 3-5 days [99, 117, 160]. To transiently deplete $CD11b^+$ macrophages before the completion of auditory nerve maturation, DTX was administered to $CD11b^{DTR/EGFP}$ pups at P4-5. Comparison of $Iba1^+$ macrophage numbers in DTX-treated and control mice at P7 revealed significantly reduced macrophage numbers (Figure 3-7A-C). This corresponded with earlier results that demonstrated that a majority of $Iba1^+$ cells also stained positive for $CD11b$ (Figure 3-7C). Consequences on glial cell numbers were assessed by immunostaining with Sox10 in the OSL and RC (Figure 14D). We found that glial cells in the auditory nerve of DTX-treated mice were significantly increased compared to controls (Figure 3-7E, F). These results support the hypothesis that active macrophages regulate glial cell numbers during auditory nerve maturation.

During the first postnatal week, specifically between P4-6, SGNs undergo a reduction in cell numbers due to an increase in apoptosis [60]. To ensure that DTX treatment did not alter the SGN population, we probed for NF200 in DTX-treated and control auditory nerves. There was no apparent difference in SGN distribution in DTX-treated and control auditory nerves (Figure 3-8A, D). This

suggests that the mechanism of glial cell maintenance in macrophage-depleted nerves is not SGN-dependent. Whole mount preparations immunolabeled with MyosinVIIa were analyzed to investigate possible HC disruptions following DTX treatment. We found no detectable differences in the IHC or OHC numbers when comparing DTX-treated and control adult auditory nerves (Figure 3-8B, F, G). To investigate the effect of macrophage depletion on final afferent synapse distribution patterns, we immunostained whole-mount preparations of basilar membranes with anti-C-terminal binding protein (CtBP2) in adult CD11b^{DTR/EGFP} mice. Immunostaining of CtBP2 revealed no apparent difference in synapse distribution after DTX treatment (Figure 3-8C, E).

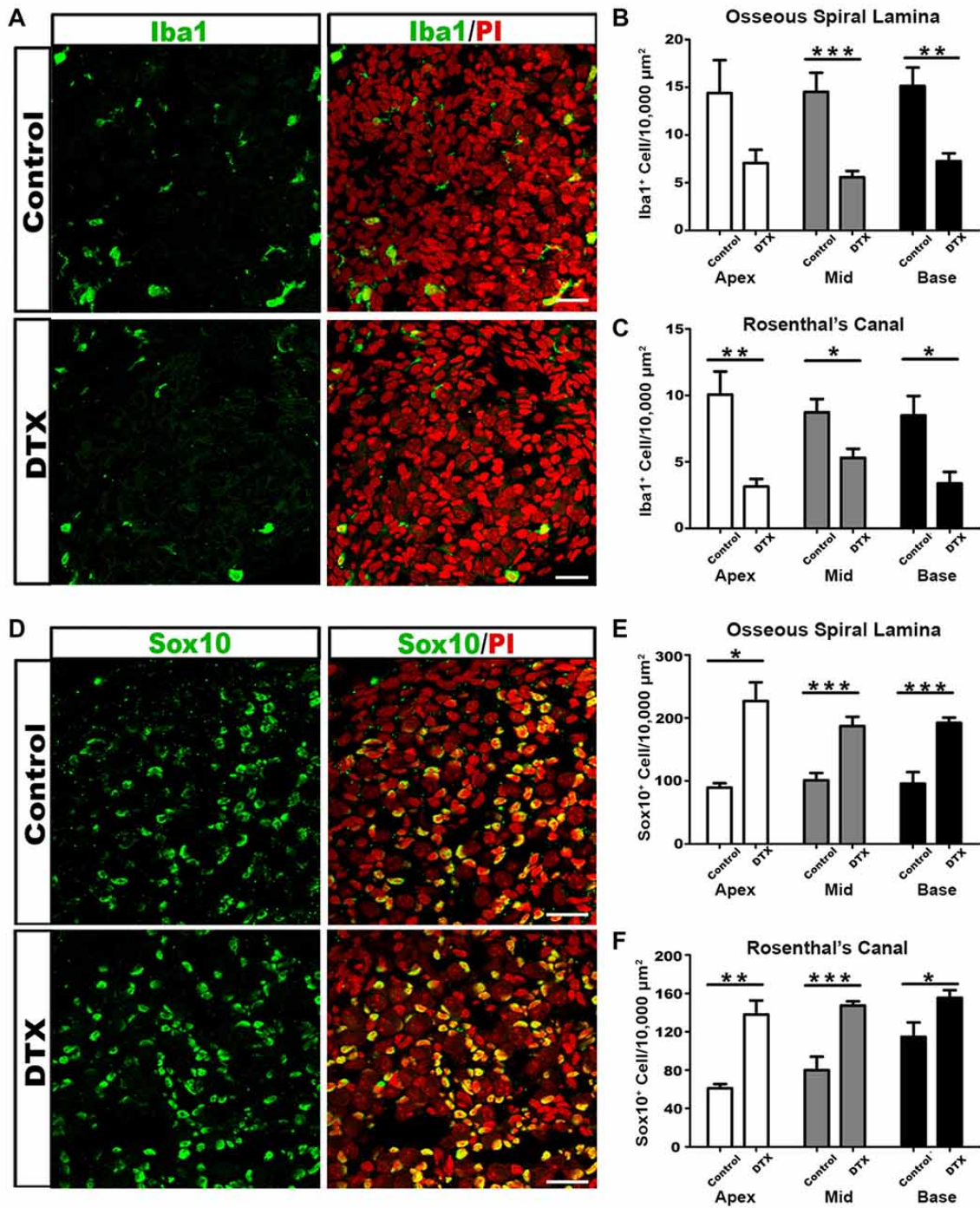


Figure 3-7. DTX treatment results in decreased macrophages and increased glial cells in the auditory nerve of postnatal $CD11b^{DTR/EGFP}$ mice. (A) Confocal images of Iba1⁺ macrophages (green) and cell nuclei (PI-red) in middle turn RC of control (top panel) and DTX-treated (bottom

panel) P7 cochleae. Scale bar = 25 μm . **(B,C)** Quantification of Iba1+ cells reveals fewer macrophages in DTX-treated OSL **(B)** and RC **(C)**, in comparison to controls. **(D)** Confocal images of Sox10⁺ glial cells in middle turn RC of control (top panel) and DTX-treated (bottom panel) P7 cochleae. Scale bars = 25 μm . **(E,F)** Quantification of Sox10⁺ glial cells reveal more glia in DTX-treated OSL **(E)** and RC **(F)**, in comparison to controls. Two-tailed, unpaired Student's t-tests were used for statistical analyses (*p < 0.05; **p < 0.01; ***p < 0.001; n = 3–7 cochleae per treatment). Bars represent mean density and error bars represent SEM. DTX, diphtheria toxin; Apex, apical turn; Mid, middle turn; Base, basal turn.

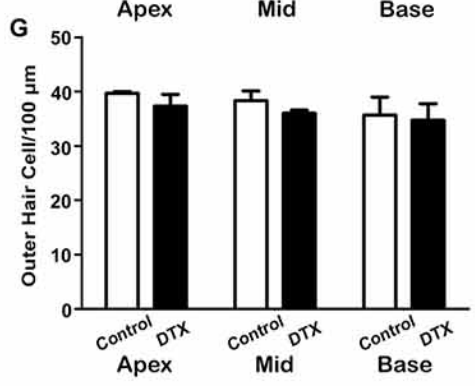
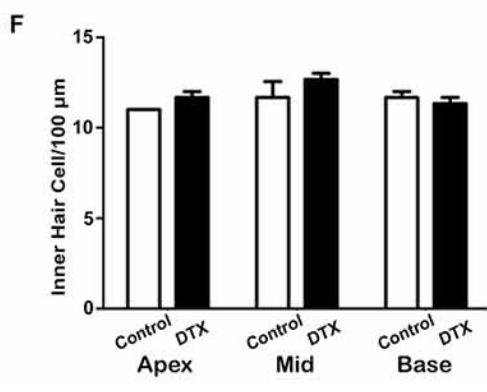
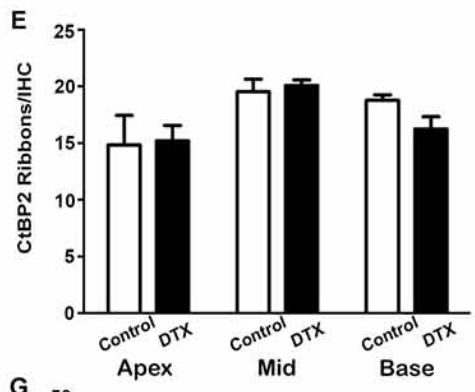
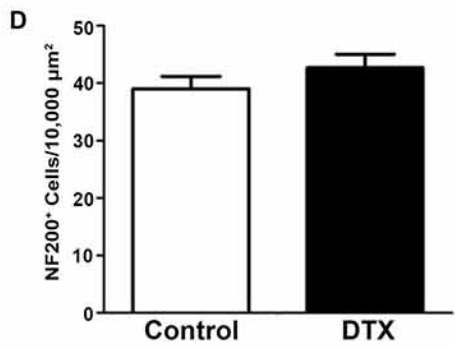
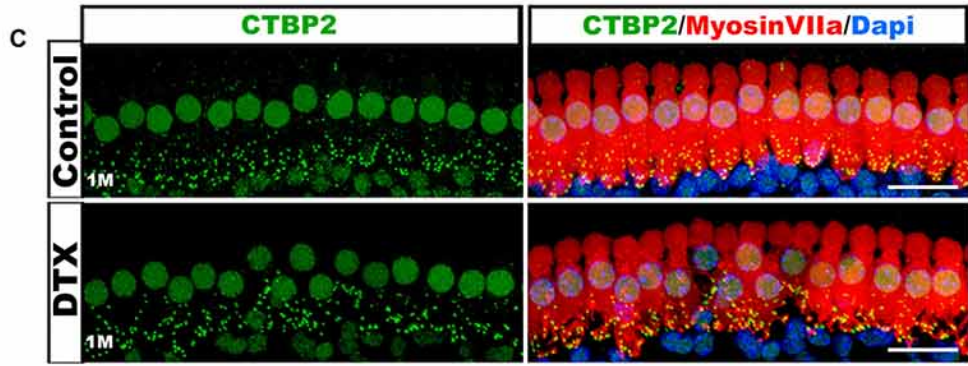
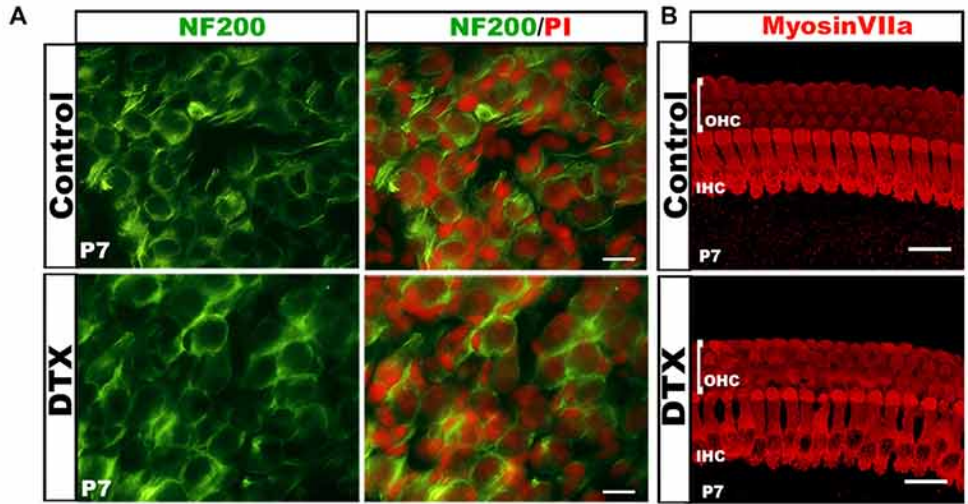


Figure 3-8. DTX-treated mice have relatively normal neuronal cells, hair cells (HCs) and afferent synapses. (A) NF200 (green) stained P7 cochlea show no difference between neurons of control and DTX-treated mice. PI (red) was used to counterstain nuclei. Scale bar = 25 μ m. **(B)** Confocal imaging of Myosin VIIa+ HCs in the OC of P7 control and DTX-treated mice. The intact three rows of outer hair cells (OHCs) and one row of inner hair cells (IHCs) were presented in both treatment conditions. Scale bar = 20 μ m. **(C)** Immunostaining of Myosin VIIa (red) and CtBP2 (green) revealed no significant loss of afferent synapses under IHCs in 1 month old DTX-treated mice compared to controls. DAPI (blue) was used to counterstain cell nuclei. Scale bar = 20 μ m. **(D)** Quantification of NF200⁺ neurons in P7 mice reveal no significant difference in spiral ganglion neuron (SGN) numbers in DTX-treated and control auditory nerves. **(E–G)** Quantitative analysis of Myosin VIIa and CtBP2 immunostaining in 1 month auditory nerves reveals no significant differences in IHC **(F)**, OHC **(G)** or ribbon synapse **(E)** numbers of DTX-treated and control mice. Two-tailed, unpaired Student's t-tests were used for statistical analyses. No statistical significance was determined. n = 3 mice per group. Bars represent mean density and error bars represent SEM. Apex: apical turn; Mid: middle turn; Base: basal turn.

Transient depletion of macrophages results in dysfunction of myelinating glial cells.

The production and compaction of myelin around SGN cell bodies and axons is a main function of auditory glial cells. Since myelin becomes more compact and mature between P10-P12 in rodent cochleae [161] we investigated the ultrastructure of the auditory nerves in P11 $CD11b^{DTR/EGFP}$ mice. As expected, myelinated axons were seen in both control and DTX-treated auditory nerves (Figure 3-9A, B). DTX-treated nerves contained supernumerary glial cells that were not associated with nerve fibers or neuron cell bodies (Figure 3-9B). Myelinated SGNs were also seen in both control and DTX-treated nerves (Figure 3-9C, D); however, the myelin sheath surrounding SGNs of DTX-treated nerves showed modest alterations, including vacuolation and alveolated interruptions (Figure 3-8D; arrowheads). Nodes of Ranvier of DTX-treated nerves also demonstrated abnormalities, evidenced by robust myelin blebbing and folding in the paranodal regions (Figure 3-9E, F). Additionally, a group of myelinated axons were ensheathed by several Schwann cells (Figure 3-9G). High magnification revealed distinct cell boundaries were between the Schwann cells, indicating that supernumerary glial cells intermingle with and enwrap other myelinating Schwann cells (Figure 3-9G'). We investigated the auditory nerves of $CD11b^{DTR/EGFP}$ mice at P16, a time after myelination is complete and after hearing onset. In P16 DTX-treated nerves, myelin appeared to recover and was comparable to that of control auditory nerves (Figure 3-9H, I). However, there were occasional cases of blebbing in the myelin surrounding neurons in DTX-

treated nerves (Figure 3-9J). Additionally, few glial cells appeared to enwrap degenerating axons (Figure 3-9K).

CD11b⁺ cells have been found to reside in the cochlear lateral wall of the adult cochlea. These cells, termed perivascular-resident macrophage-like melanocytes, remain tightly bound to lateral wall blood vessels to control permeability within the intrastrial space of the cochlear lateral wall [120, 162]. We investigated the ultrastructure of the cochlear lateral wall to determine if DTX-treatment altered lateral wall cells (Figure 3-9L, M). Although marginal cells were maintained, losses of the interdigital processes of both marginal cells and intermediate cells with enlarged intrastrial space appeared in stria vascularis, indicating edema of the cochlear lateral wall of P11 DTX-treated cochleae (Figure 3-9M). Endothelial cells surrounding blood vessels in DTX-treated lateral walls also showed ruffling in their cell membranes (Figure 3-9M'). This was not seen in endothelial cells of P11 control cochleae (Figure 3-9L'). Interestingly, examination of P16 DTX-treated and control cochleae revealed that edema of the stria vascularis was no longer present and endothelial cells surrounding lateral wall blood vessels were comparable to those present in control cochleae (Figure 3-9N-O'). Our analysis of macrophage-depleted cochleae agrees with recent studies that reported recovery/self-repairing capability of the cochlear lateral wall following damage [163-165].

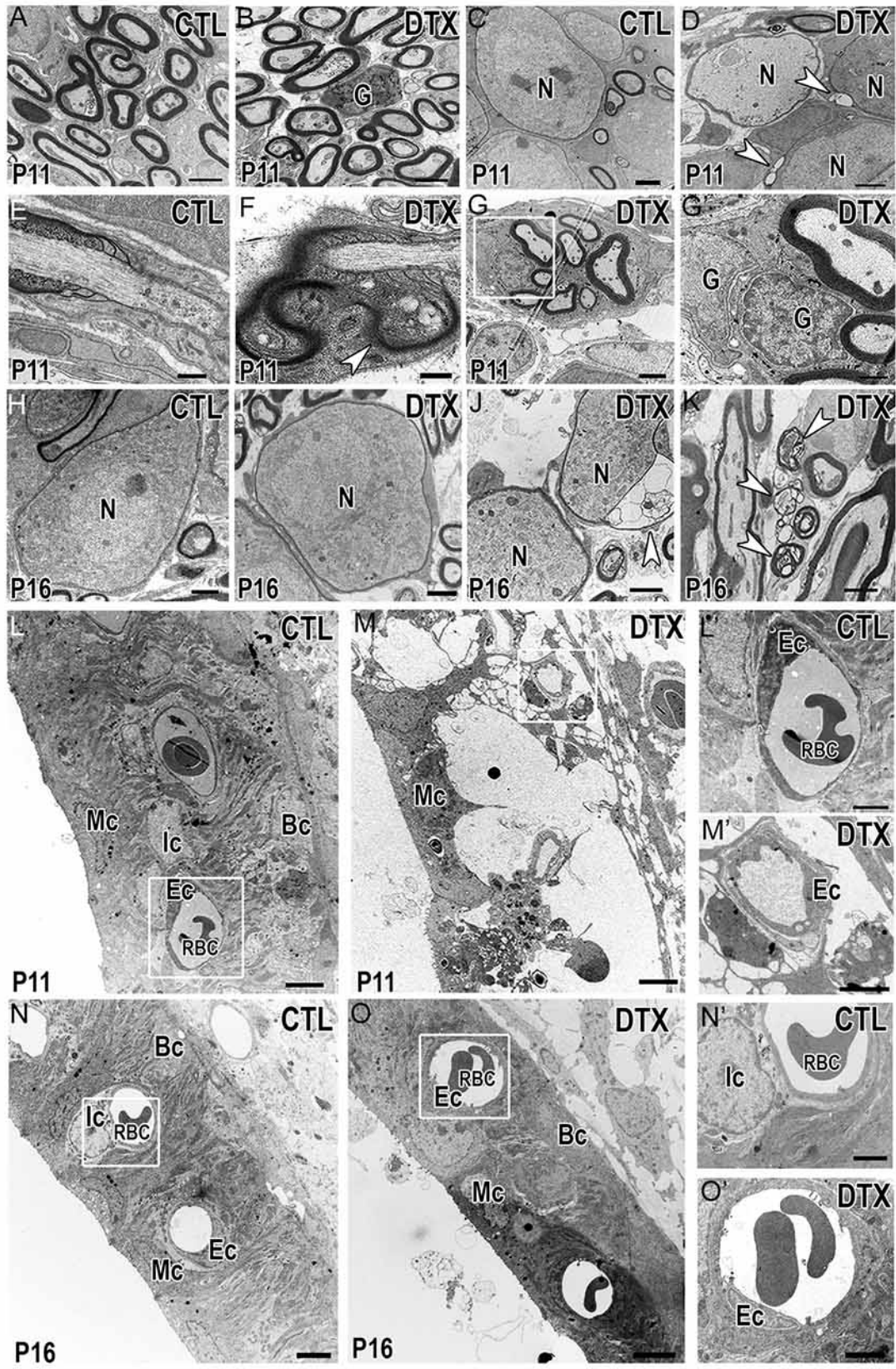


Figure 3-9. Depletion of macrophages results in transient myelin and LW-related abnormalities. (A,B) Electron micrographs demonstrate myelinated axons in control (CTL) **(A)** and DTX-treated (DTX) **(B)** auditory nerves of P11 CD11b^{DTR/EGFP} mice. A supernumerary glial cell can be found in the DTX-treated cochlea. Scale bars = 2 μ m. **(C,D)** Micrograph illustrates myelinated neurons in control **(C)** and DTX-treated **(D)** auditory nerves. Arrowheads highlight vacuolations within the myelin of two neurons in the DTX-treated samples. Scale bars = 1 μ m. **(E,F)** Micrographs of nodes of Ranvier in control **(E)** and DTX-treated **(F)** samples. Arrowhead shows thickened Schwann cell microvilli and myelin folding in the paranodal loops. Scale bars = 400 nm **(G)** Cluster of myelinated auditory nerve fibers in the OSL of P18 DTX-treated auditory nerves. Scale bars = 2 μ m. **(G')** High magnification of the enclosed area in **(G)** reveals supernumerary glial cells wrapping other glial cells. Scale bar = 800 nm. **(H–J)** Electron micrographs of neurons found in control **(H)** and DTX treated **(I)** auditory nerves of P16 CD11b^{DTR/EGFP} mice. **(J)** Arrowhead highlights blebbing in the myelin surround a neuron in the DTX-treated cochlea. Scale bars = 2 μ m. **(K)** Glial cell containing several degenerative axons in the cytoplasm (arrowheads). Scale bar = 2 μ m. **(L, M)** Micrographs of cochlear LWs from control **(L)** and DTX-treated **(M)** P11 CD11bDTR/EGFP mice. Scale bars = 4 μ m. **(L', M')** High magnification of the enclosed areas in L-M reveal blood vessel and endothelial cell morphology in control **(L')** and DTX-treated **(M')** cochleae. Scale bars = 2 μ m. **(N, O)** Micrographs of cochlear LWs from control **(N)** and DTX-treated **(O)** P16 CD11bDTR/EGFP mice reveals DTX-treated LWs are able

to recover. Scale bars = 4 μm . (**N'**, **O'**) High magnifications of the enclosed areas in (**N,O**) reveal blood vessel and endothelial cells in control (**N'**) and DTX-treated (**O'**) cochleae. Scale bars = 2 μm . G, glial cell; N, spiral ganglion neuron; Mc, marginal cell; Ic, intermediate cell; Bc, basal cell; Ec, endothelial cell; RBC, red blood cell.

Macrophage depletion impairs auditory function of postnatal and young adult mice

We next investigated how macrophage depletion affected auditory function. Auditory brainstem response (ABR) tests were performed at P15, after the onset of hearing, and at P21 and 1 month, when auditory nerve function is more mature. At P15, ABR thresholds of DTX-treated mice were higher than controls (Figure 3-10A). Although ABR responses improved by P21, DTX-treated mice continued to display elevated thresholds when compared to control mice (Figure 3-10B). Representative ABR waveforms produced in response to tone bursts at 8 kHz in P21 control mice demonstrate characteristic waveforms, similar to those produced by adult mice, while DTX-treated mice produced dampened and wider peaks (Figure 3-10E, F). By 1 month DTX-treated and control mice demonstrated similar ABR thresholds, with the exception of thresholds produced at the high frequencies (Figure 3-10C). To determine if OHC loss or dysfunction was present in DTX-treated mice we measured the distortion product otoacoustic emissions (DPOAE) in the adult mice (Figure 3-10D). Nearly all frequencies tested, except a slight increase at 32kHz, showed no difference in DPOAE thresholds when comparing DTX-treated and control responses (Figure 3-10D).

ABR wave I amplitude input/output function measurements allow the examination of activities of the auditory nerve. ABR wave I latencies give insight into functional integrity of the myelin in the auditory nerve. In DTX-treated mice, ABR wave I amplitudes measured at 8 kHz were decreased compared with

controls when presented with stimuli at 90-50 dB SPL (Figure 3-10G). Wave I amplitudes give insight into the firing synchrony of the auditory nerve. Wave I amplitudes in response to 90dB stimuli, measured at 4-40 kHz, were significantly lower in DTX-treated mice compared to vehicle-treated mice (Figure 3-10H). Additionally, increased wave I latencies were observed in DTX-treated mice at 8 kHz when 60 to 70 dB SPL stimuli were given (Figure 3-10I). These results demonstrate that macrophage-depletion impairs auditory nerve function.

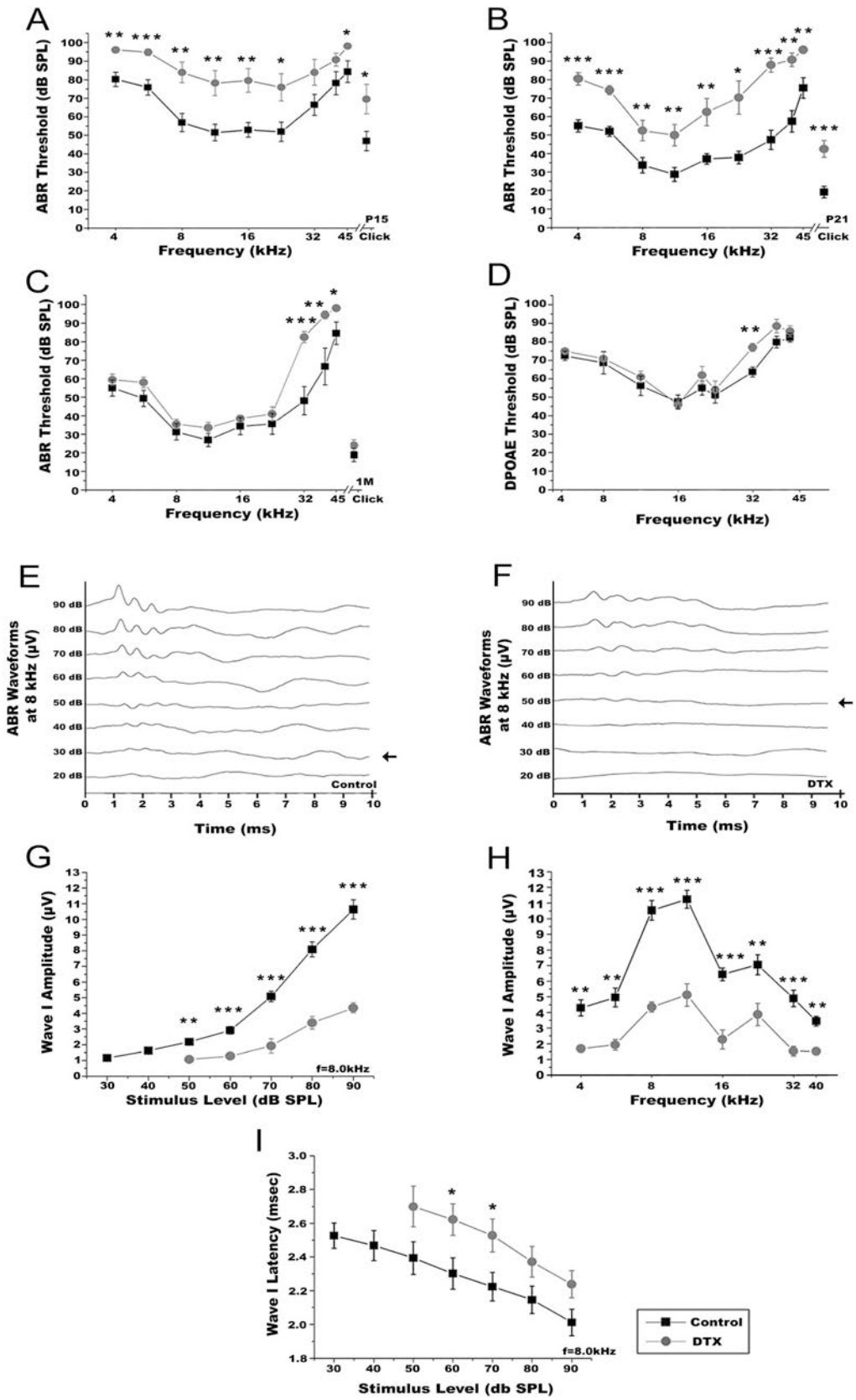


Figure 3-10. Macrophage depletion impairs auditory function in DT-treated CD11b^{DTR/EGFP} mice. (A–C) Auditory brainstem response (ABR) thresholds from P15 **(A)**, P21 **(B)** and 1 month **(C)** control (black) and DTX-treated (gray) CD11b^{DTR/EGFP} mice. ABRs were measured from 4.0 kHz to 42.5 kHz with sound pressure levels from 10 dB to 90 dB. Two-tailed, unpaired Student's t-tests were used to compare thresholds for each group at each frequency (*p < 0.05; **p < 0.01; ***p < 0.001; n = 11–13 ears). Error bars represent SEM. **(D)** Distortion product otoacoustic emission (DPOAE) thresholds of 1 month control and DTX-treated CD11b^{DTR/EGFP} mice. DPOAEs were measured from 5.6 kHz to 42.5 kHz with sound pressure levels from 10 dB to 90 dB. Two-tailed, unpaired Student's t-tests were used to compare thresholds for each group at each frequency (**p < 0.01; n = 8–10 ears). Error bars represent SEM. **(E,F)** Representative ABR recordings from P21 control **(E)** and DTX-treated **(F)** CD11b^{DTR/EGFP} mice with 8 kHz pure tone stimulus. Arrows indicate the lowest ABR thresholds at this frequency. **(G)** Average wave I amplitudes for P21 DTX-treated (gray, n = 4–7 ears) and control (black, n = 7–11 ears) CD11b^{DTR/EGFP} mice in response to 8.0 kHz stimulus. DTX-treated CD11b^{DTR/EGFP} mice displayed decreased wave I amplitude responses at 90, 80, 70, 60 and 50 dB SPL. Unpaired Student's t-test analyses were used to compare amplitudes for each group at each stimulus level tested (**p < 0.01; ***p < 0.001). Error bars represent SEM. **(H)** Average wave I amplitudes at 4.0–40 kHz for stimuli presented at 90 dB SPL for P21 control and DT treated (gray, n = 4–7 ears) and control (black, n = 11 ears) CD11b^{DTR/EGFP} mice. Responses are decreased in DTX-treated

CD11bDTR/EGFP mice at all frequencies in comparison to control mice.

Unpaired t-test analyses were used to compare thresholds for each group at each frequency (**p < 0.01; ***p < 0.001). Error bars represent SEM. **(I)** Average Wave I latencies for P21DTX-treated (gray, n = 3–8 ears) and control (black, n = 7–11 ears) CD11b^{DTR/EGFP} mice in response to 8.0 kHz stimulus. DTX-treated CD11b^{DTR/EGFP} mice displayed longer latency responses at 90, 80, 70, 60 and 50 dB SPL. Unpaired Student's t-test analyses were used to compare amplitudes for each group at each stimulus level tested (*p < 0.05). Error bars represent SEM.

DISCUSSION

The refinement of auditory nerve fibers during development has been extensively studied. However, it remains unclear how glial cells, which ensheath SGNs and peripheral axons, are affected during the refinement period. In this chapter, we identify the temporal distribution patterns of cochlear glial cells during auditory nerve refinement. We demonstrate that cochlear macrophages eliminate supernumerary glial cells in the developing auditory nerve. We also show that macrophage depletion in the auditory nerve results in elevated glial cell numbers, abnormal myelin sheath formation, and diminished hearing function. These data reveal a critical role that cochlear macrophages play in glial cell regulation and auditory nerve maturation and hearing onset.

Using immunohistochemical analyses, we found that postnatal glial cells undergo an increase in cell numbers between P3 and P7 (Figure 3-1A-D). Glial cell numbers significantly decrease after the first postnatal week, when mature auditory nerve circuitry is established. It is probable that extra glial cells, termed supernumerary glia in the context of this report, are temporarily produced to support processes important for proper nerve development. Glial cells, such as astrocytes and oligodendrocytes produce neurotrophic factors that are critical for the survival of neurons in the central nervous system [166, 167]. Glial cells from both the central and peripheral auditory nerve promote neuron survival and extension of SGN neurites *in vitro* [131, 133]. It is possible that supernumerary glial cells are produced to ensure abundant production of trophic factors for the survival of developing neurons. Since glial cells have been implicated as active

participants in nerve refinement, plasticity, and regeneration, it is also possible that supernumerary glial cells are produced to facilitate axonal and synaptic elimination during auditory nerve refinement. In mammalian neuromuscular junctions, glial cells facilitate synapse elimination and clear axonal debris during injury-induced nerve retraction [49, 168]. Further studies are required to future investigate the function of supernumerary glial cells in auditory nerve refinement. It is also important to determine why glial cell numbers decrease following refinement and nerve maturation.

Myelin production and integrity are essential for the proper function and survival of neurons. Complete myelination of SGNs and nerve fibers by glial cells is important for proper auditory signal conduction from the peripheral auditory nerve to central auditory processes [169]. Mouse models with abnormal myelination in the inner ear, including Connexin29-deficient mice and Saposin B-deficient mice, have been previously described [136, 137]. In the inner ear, the gap junction protein Connexin29 is highly expressed in myelinating glial cells that ensheath the somas and processes of SGNs. Connexin29-deficient mice demonstrate abnormal myelination of SGN somas, elevated ABR thresholds, and significantly delayed ABR wave I latencies [137]. Saposin B is a glycoprotein responsible for lipid transfer in myelin. Satellite cells in the auditory nerve of Saposin B-deficient mice display abnormal inclusion bodies in their myelin sheaths, leading to SGN degeneration and progressive nerve fiber loss [136]. These pathological alterations result in increased ABR thresholds and delayed wave I latencies [136].

Our transcriptomic analysis detected increased expression of immune response genes during the period of nerve refinement, including H2-K1, H2-D1, C1q, and C3aR (Figure 3-2). These results are consistent with a previous study [72], suggesting that immune signals play a role in auditory nerve refinement. Previous studies also have identified a role for complement and MHC class I signaling molecules in regulating microglia-mediated nerve pruning in the developing mammalian hippocampus, cerebellum, motor cortex, and optic nerve [69, 93-96, 170]. Interestingly, C1q deficient and H2-K/H2-D1 double knockout mice do not exhibit altered auditory nerve fiber or synapse numbers [140]. However, it remains to be determined whether these signaling molecules are involved in other components of auditory nerve development, such as glial cell maturation. It is possible that these molecules could play a role in glial cell maintenance. H2-K/H2-D1 double knockout mice demonstrate progressive hearing impairment, shown by elevated ABR thresholds, suggesting that these mice may possess morphologic abnormalities in the auditory nerve that remain to be identified [140]. Further exploration of the differentially expressed genes identified in our study may provide insight into molecular cues or gene networks that regulate auditory nerve maturation.

We found that macrophages engulf nerve fiber fragments during auditory nerve refinement. At the same time, macrophages seem to engulf glial cells (Figure 3-5,3-6). Similarly, several studies have shown that microglia or macrophages in the CNS regulate the number of synaptic outputs during development, as well as in adulthood, by engulfing synaptic elements that are

misconnected or redundant [69, 93, 98, 171, 172]. Our loss-of-function experiments found that activated macrophages are needed to eliminate supernumerary glial cells during refinement. Quantitative assessment of glial cells remaining in macrophage-depleted auditory nerves revealed a significant increase in glial cell numbers, when compared to controls (Figure 3-7D-F). It remains to be determined why supernumerary glial cells are targeted by macrophages for elimination. Our analysis of the ultrastructure in P7 CBA mice revealed that macrophages engulf both myelinating and non-myelinating glial cells as they enwrap degenerating axons. However, it is unknown how targeted glial cells are marked for macrophage phagocytosis. Recent studies have identified several signals that act as “find me” and “eat me” signals for macrophage phagocytosis of apoptotic cells [101, 173]. Identification of glial-related “eat me” signals will be important for further understanding the glia-macrophage relationship we have identified in the developing auditory nerve.

Here, CD11b^{DTR/EGFP} mice treated with DTX at P4/5 demonstrated myelin abnormalities and functional impairments similar to the Connexin29 and Saposin B mouse models mentioned above. DTX-treated CD11b^{DTR/EGFP} mice presented with abnormally high glial cell numbers, the presence of myelin blebbing, abnormal myelination at the paranodes of the nodes of Ranvier, and supernumerary glial cell clustering around SGN axons. However, DTX-treated mice did not demonstrate alterations in neuron numbers or HC innervation and afferent synapse patterns. Our ultrastructural investigation of auditory nerves following macrophage-depletion confirmed the presence of supernumerary glial

cells not directly enclosing SGNs or axons. In addition, pathological alterations of myelin sheaths in the auditory nerve suggest that macrophage depletion leads to abnormal glial cell function (Figure 3-9I-K). Moreover, cochleae of DTX-treated CD11b^{DTR/EGFP} mice exhibited impaired ABR wave I amplitudes and latencies, indicating that proper macrophage activities are critical for auditory nerve maturation and normal hearing function. Further studies will be necessary to determine how elevation of glial cell numbers following macrophage depletion contributes to the pathophysiological changes in the auditory nerve.

DTX-treated mice demonstrated auditory impairment at P15, after hearing function begins. DTX-treated mice continued to produce worsened ABR responses than control mice at P21. Additionally, DTX-treated mice demonstrated dampened wave I amplitudes and increased wave I latencies while DPOAE threshold responses remained comparable between DTX-treated mice and controls. By 1 month of age, control and DTX-treated animals presented similar ABR thresholds (Figure 3-10C), with significant differences only seen in the higher frequencies tested, suggesting that DTX-treated mice eventually employed compensatory mechanisms for auditory nerve maturation.

The stria vascularis maintains the homeostasis of the endolymph in the inner ear. Maintenance of the stria vascularis is essential for the production of the endocochlear potential, which is required for hearing function [174-176]. Within the stria vascularis are resident macrophages referred to as perivascular-resident macrophage-like melanocytes. These cells are positive for macrophage-specific markers including F4/80, CD68 and CD11b [177]. Previous studies demonstrated

that these macrophage-like cells contribute to the integrity of the stria vascularis in adult mice [177]. Additionally, disruption of CD11b+ cells in the cochlear LW causes leakage from capillaries of the stria compartment, leading to a significant reduction in endocochlear potential and auditory function decline [162, 177]. In this chapter, we observed strial edema in the LWs of P11 DTX-treated mice (Figure 3-9L-M'), suggesting that the perivascular-resident macrophage-like melanocytes may be affected by DTX treatment. However, edema was not found in the stria compartment of P16 DTX-treated mice (Figure 16N-O'), suggesting that the LW is capable of recovering from macrophage depletion. Since proper generation of endocochlear potential is critical for maintenance of auditory function, it is possible that the changes of LW function also contribute to the temporary hearing impairments seen in the DTX-treated mice. It will be important for future studies to investigate the role of macrophages in LW development and contributions to endocochlear potential of postnatal mice.

Recently, the Lang lab demonstrated that glial cell numbers are increased after auditory nerve injury and that auditory glial cells have the potential to differentiate into neural progenitor cells following acute nerve injury [121, 122]. Interestingly, macrophage numbers are increased following auditory injury and are required for SGN protection and the maintenance of SGN numbers after cochlear injury in the adult cochlea [77, 78, 80, 82, 85, 86]. Investigation of glial cell refinement and glia-macrophage relationships during development will lead to better understanding of the auditory nerve microenvironment. This will be vital

for identifying novel strategies that may promote auditory nerve repair or regeneration.

CHAPTER FOUR:
COCHLEAR PATHOPHYSIOLOGICAL ALTERATIONS IN COMPLEMENT
FACTOR B DEFICIENT MICE

INTRODUCTION

Complement signaling is comprised of over 40 fluid-phase and membrane-bound proteins that are important for activating the innate immune system [178]. The complement cascade can be activated by 3 pathways: classical, lectin and alternative pathways [178]. The 3 pathways all converge on the cleavage of the central complement component, C3. The classical complement pathway initiates with the cleavage of C1q to two subunits and requires the formation of antigen-antibody complexes. The lectin pathway initiates with the binding of mannose-binding lectin to pathogen surfaces. The alternative pathway can be triggered in the absence of an antibody through the spontaneous hydrolysis of C3. The alternative pathway also amplifies the activation of the classical and lectin pathway through the generation of C3b deposits. The alternative pathway is important for immune responses and the for opsonization of microbes and pathogens to be targeted for elimination.

Although complement is primarily produced by hepatocytes in the liver, complement can be produced and secreted by phagocytes and neural cells [109, 112]. In the central nervous system, microglia, the resident phagocytes, are the major source of complement production [110]. In the peripheral nervous system, immune cells, such as macrophages, are the dominant source of complement proteins.

The interplay between complement and immune cells is critical in developmental, injury and age-related inflammatory processes. Complement signaling and microglia/macrophage process have been found to be required and

beneficial for the structural development of several regions in the brain and for visual function maturation. In the developing brain and retina, microglia mediate synaptic pruning through complement signaling. Mice deficient in C1q and C3 display defects in synapse elimination in the retinogeniculate system and in the hippocampus [69, 95, 96]. Following injury, complement proteins rapidly bind to damaged/apoptotic cells and cellular debris, for elimination by circulating immune cells. Complement proteins also promote the infiltration and activation of immune cells as they invade damaged tissue [114, 179]. Mice deficient in complement signaling demonstrate decreased macrophage infiltration and reduced removal of synaptic terminals and apoptotic cells [94, 180-182]. Interestingly, complement deficient mice also demonstrate protection against age-related neurodegeneration, progressive synapse loss and plaque formation [107, 182-186]. This indicates that complement signaling exacerbates neurological diseases and can play detrimental roles for nerve maintenance.

Recent studies of the rodent cochlea have revealed a role of complement system in the auditory nerve. Whole transcriptome analysis of rat cochleae revealed that the expression of multiple complement components significantly increases following noise trauma [92]. Investigations of the developing mouse auditory nerve established that the expression of genes from several immune-related pathways, such as the complement pathway, are increased during auditory nerve refinement [72]. As described in Chapter 3, we have also demonstrated that the expressions of complement genes are increased in the developing auditory nerve (Figure 3-2D). Understanding of the contributions of

the complement activation pathways to nerve development is still very much in its infancy.

The auditory phenotype of classical complement molecule deficient mice, C1qa^{-/-} mice, has recently been characterized [140]. Calton et al (2014) found that mice deficient in C1qa signaling did not demonstrate a difference in cochlear synaptic refinement, when compared to WT mice. These researchers also found that C1qa^{-/-} mice did not demonstrate protection against age-related, progressive hearing loss [140]. Thus, we aimed to investigate the role of a different complement activation pathway, the alternative complement pathway, in auditory function.

In healthy conditions, alternative complement signaling is active at low levels due to the rapid hydrolysis of C3 [104]. Circulating C3b molecules undergo conformational changes, which allows the binding of complement factor B (fB) and the generation of a C3bB complex. C3bB is cleaved by complement factor D, resulting in the formation of the C3 convertase, C3bBb that can catalyze the generation of more C3b molecules, referred to as complement tickover [187].

In this chapter, we characterized the auditory nerve functional alterations and cochlear pathological changes in mice deficient in the alternative complement pathway. Since complement factor B (fB) is exclusive to the alternative pathway, we utilized fB^{-/-} mice (Figure 1-5). Using a combination of auditory brainstem response measurements, electron microscopy and immunohistochemical analyses, we addressed the hypothesis that alternative complement deficient impairs auditory function and structural integrity.

RESULTS

Complement gene expression in the auditory nerve

Finally, we performed microarray analysis to identify complement-related genes that are differentially expressed in the auditory nerve. We examined the expression of complement-related genes in the normal postnatal mouse auditory nerve. Using our published microarray dataset (NCBI GEO: GSE5417; [121]), found that a subset of complement genes are activated by P7 or P21 in CBA/CaJ mice (Figure 4-9A). To further assess the gene expression of fB in the cochlea, we performed RT-PCR using mRNA collected from P0, P7 and P21 auditory nerves. We found that fB expression increased from P0 to P7. fB expression was also measured in the P21 auditory nerve (Figure 4-9B).

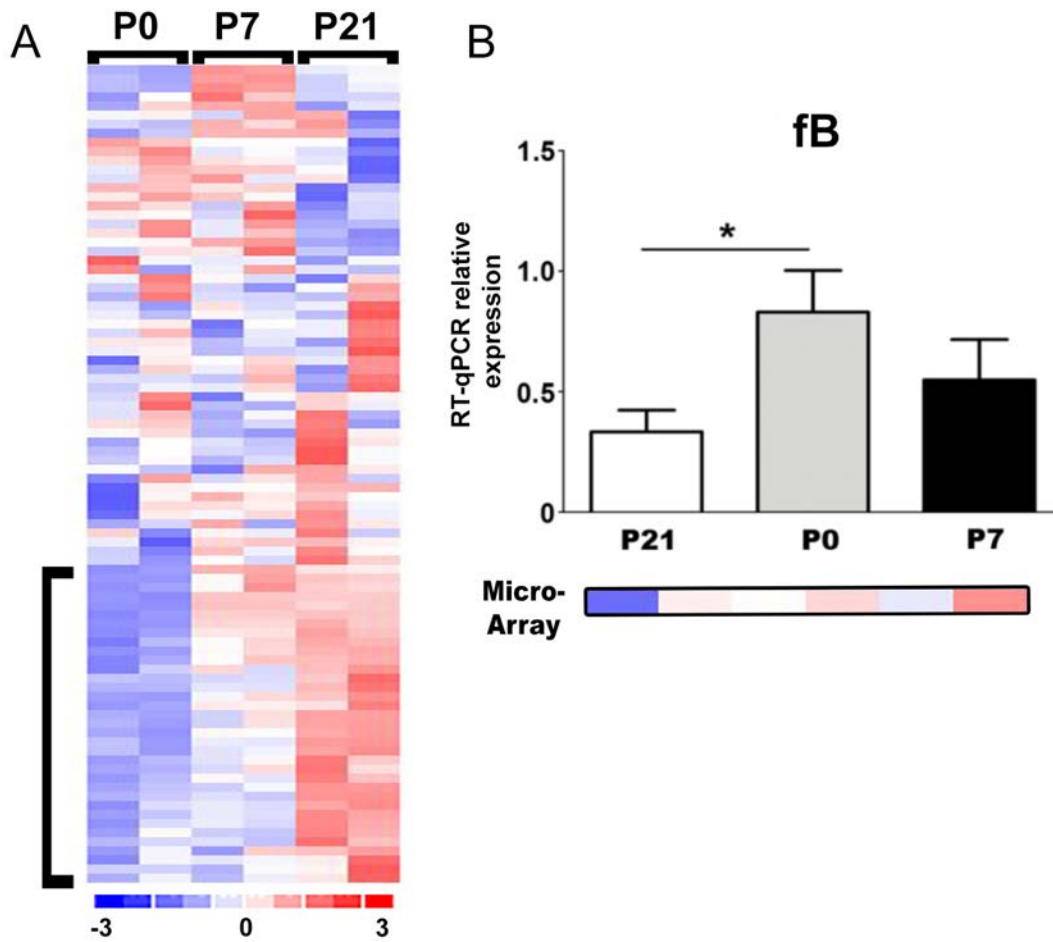


Figure 4-1. Complement gene expression in postnatal CBA/CaJ mouse auditory nerve. **A.** Expression profile of complement-related genes in postnatal auditory nerves at P0, P7 and P21. The two columns represent two biological replicates for microarray analysis. The expression of over 50 unique genes are represented. Colorimetric scaling (Z-standardization) for the heatmap is shown at the bottom. **B.** Quantitative PCR for the gene expression of fB in P0, P7 and P21 auditory nerves. Data bars represent average mean of experiments run in triplicate; error bars represent SEM. * $p < 0.05$; $n = 3$.

Mice deficient in fB signaling have impaired auditory function

The onset of hearing in mice is around P12-P14 [46]. We first investigated the effect of fB deficiency on hearing onset using ABR measurements in P14 fB^{-/-} mice. P14 fB^{-/-} mice showed significantly higher ABR thresholds at frequencies 16 and 22.6 kHz, in comparison to WT mice. (Figure 4-1A)

Next, we investigated the auditory function in adult fB deficient mice. ABR measurements revealed that fB^{-/-} mice aged 1.5 month had significantly elevated ABR thresholds, when compared to age-matched WT mice. Elevated ABR thresholds were measured at all frequencies tested (Figure 4-1B). This trend of severe hearing impairment was also seen in 4-month-old fB^{-/-} mice. Four-month-old fB^{-/-} mice had no response to stimuli at 90 dB SPL at 22.6, 32, 40, and 45.2 kHz (Figure 4-1C,D). Together, these data suggest that fB^{-/-} mice also show elevated age-related hearing loss.

The amplitude and latency of ABR wave I responses correlate with the synchronous firing of SGNs in response to acoustic stimuli. The degree of myelination of the peripheral auditory nerve has a major impact on the latency of ABR responses [188-190]. To further investigate auditory nerve function alterations in fB^{-/-} mice, we compared ABR wave I amplitude and latency measurements recorded at frequency 11.3 kHz in 1.5-month-old fB^{-/-} and WT mice. Mice deficient of fB demonstrated decreased ABR wave I amplitudes at frequency 11.3 kHz, when compared to WT mice (Figure 4-2A). The ABR wave I response measurement in fB^{-/-} mice also demonstrated delayed latencies in response to stimuli, when compared to WT mice (Figure 4-2B).

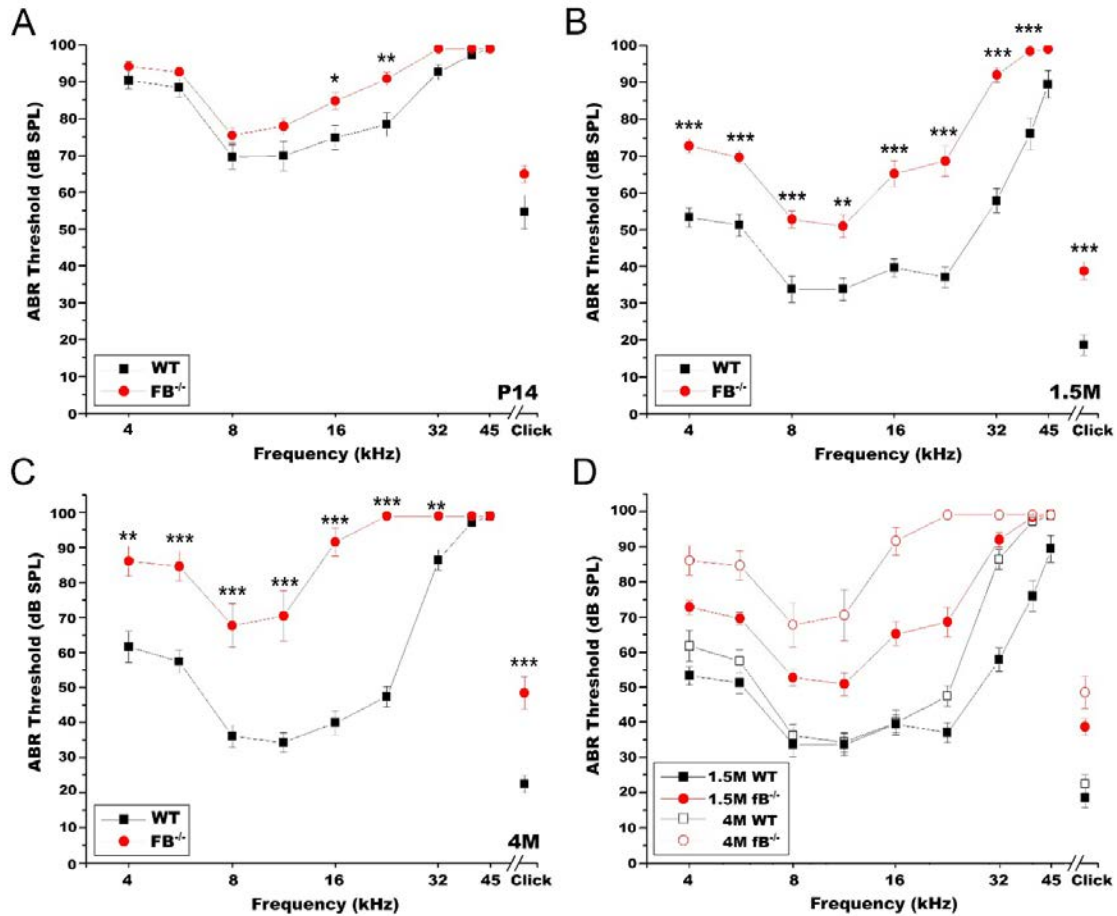


Figure 4-2. Auditory Brainstem Response (ABR) Measurements in fb deficient mice. A-C. ABR thresholds of P14 (A), 1.5-month (B) and 4-month-old (C) fb^{-/-} mice (red line) are significantly higher than age-matched WT mice (black line). **D.** Compilation of age-related ABR thresholds recorded in 1.5-month (closed symbols) and 4-month-old (open symbols) fb^{-/-} (red lines) mice and WT (black lines) mice. ABRs were measured from 4.0 kHz to 42.5 kHz with sound pressure levels from 10 dB to 90 dB. Two-tailed, unpaired Student's t-tests were used to compare thresholds for each group at each frequency (*p < 0.05; **p < 0.01; ***p < 0.001; n = 6–10 ears). Error bars represent SEM.

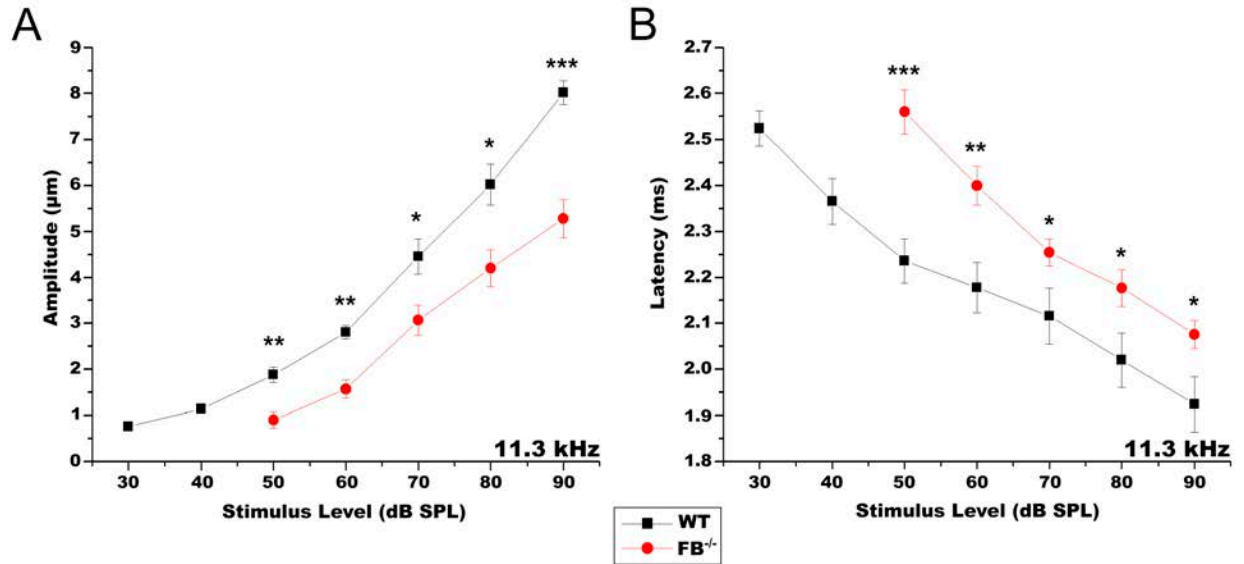


Figure 4-3. fB^{-/-} mice display decreased amplitudes and increased latencies of auditory nerve fibers. (A-B) Average wave I amplitudes (A) and latencies (B) for 1.5-month fB^{-/-} and WT mice in response to 11.3 kHz stimulus. Unpaired Student's t-test analyses were used to compare amplitudes for each group at each stimulus level tested (*p < 0.05, n=4-10). Error bars represent SEM.

Characterization of gross morphology of HCs and SGNs in $fB^{-/-}$ mice

To examine how the loss of fB function impacted cochlear structure, we assessed the cochlear morphology using light microscopy. Cochlear sections of young adult $fB^{-/-}$ mice were stained using toluidine blue. Compared to age-matched WT mice, $fB^{-/-}$ mice had normal IHCs and OHCs (Figure 4-3A, C). Quantitative analysis of immunostaining for the hair cell marker, Myosin VIIa, revealed there was no significant HC loss in $fB^{-/-}$ mice (Figure 4-3B, D).

Next, we examined the SGN numbers in mice deficient in fB signaling. To visualize the SGNs, we immunostained cochlear sections from 1-2-month-old mice for the expression of NF200, a marker that specifically binds to the filaments in neurons. NF200⁺ neurons were visualized in both mouse strains (Figure 4-4A,B). Quantitative analysis revealed that young adult $fB^{-/-}$ mice demonstrated a trend for fewer neurons than WT mice, although the difference was not statistically different (Figure 4-4C).

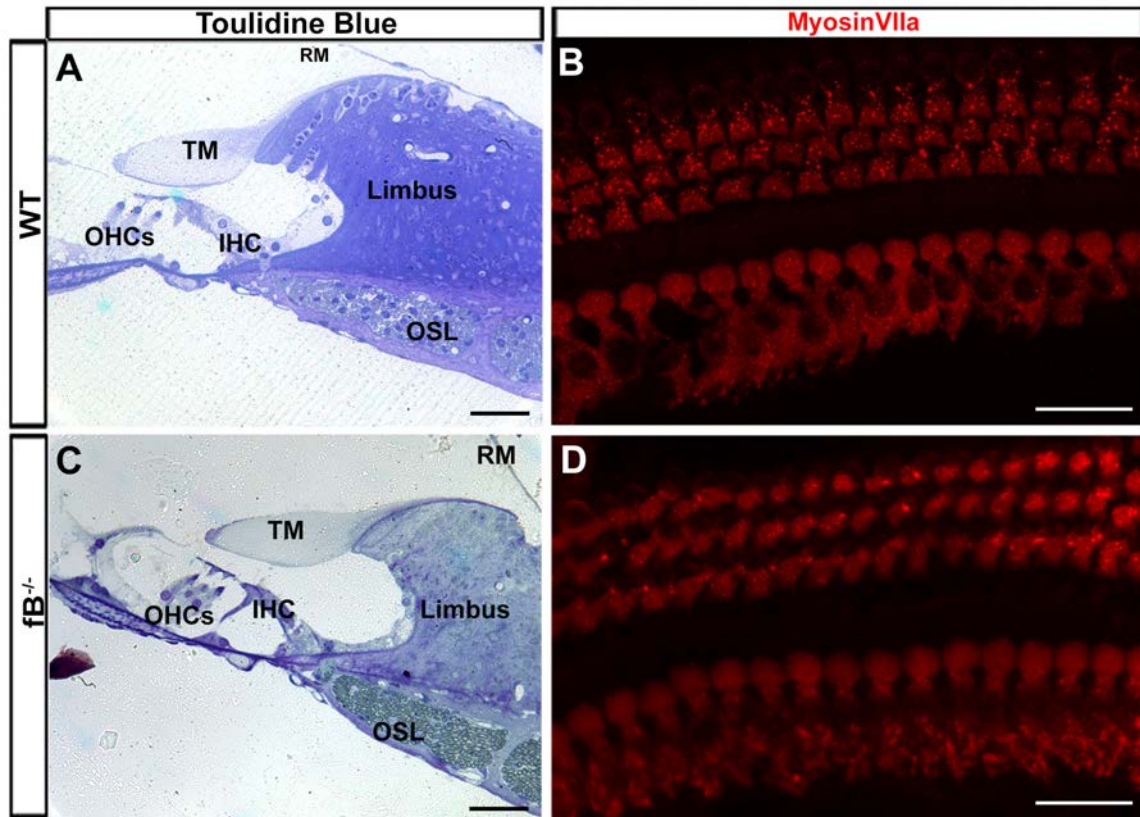


Figure 4-4. Organ of Corti is comparable in *fB*^{-/-} and WT mice. A,C. Light microscopy of toluidine blue-stained cochlear samples from 1-month WT and *fB*^{-/-} mice. Representative images of the organ of Corti of WT (top row) and *fB*^{-/-} (bottom row) mice. Scale bars = 200 μ m; RM: Reissner's Membrane, TM: tectorial membrane, OSL: osseous spiral lamina, OHC: outer hair cell, IHC: inner hair cell. Images in **A, C** represent analysis of n=4 samples for WT and *fB*^{-/-} mice. **B,D.** Confocal microscopy of MyosinVIIa⁺ hair cells in WT (**B**) and *fB*^{-/-} (**D**) cochleae. Hair cells are well preserved in both mouse strains. Scale bar = 25 μ m.

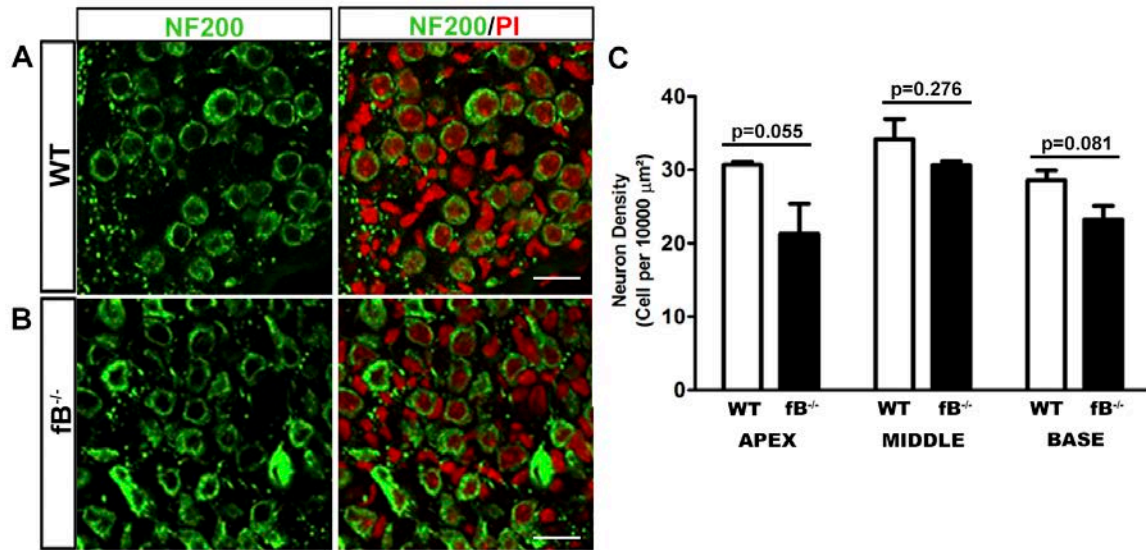


Figure 4-5. Neuron densities are not significantly altered in fB^{-/-} mouse cochleae. **A-B.** Confocal images of NF200⁺ neurons in middle turn RC of 1-month WT (**A**) and fB^{-/-} (**B**) mice. Propidium iodide (PI) was used to counterstain cell nuclei. Scale bar = 20 μm. **C.** Quantification of SGNs in WT and fB^{-/-} auditory nerves. P values for unpaired Student's t-tests comparing neuron counts in WT and fB^{-/-} mice are provided for each cochlear turn. Data bars represent mean density; error bars represent SEM. n= 3-4 cochlear samples.

fB^{-/-} mice display reduced glial cell numbers and potassium channel dysfunction

The increased ABR wave I latencies suggested that fB deficiency alters the myelination of the peripheral auditory nerve. Myelin for the peripheral auditory nerve is produced by two types of auditory glial cells: satellite and Schwann cells. Electron microscopy of fB^{-/-} mice revealed glial cell pathologies, including abnormal inclusions and enlarged space between satellite cells and the ensheathed SGNs (Figure 4-5A-B'). Additionally, examination of SGN cell bodies revealed the presence of myelin blebs and irregular myelin whorls were presented in the myelinated cells of fB^{-/-} mice, while satellite cells closely flanked the SGNs in WT auditory nerves (Figure 4-5B',F). We also investigated Schwann cells that ensheath SGN axons in WT and fB^{-/-} mice (Figure 4-5C, D). There were instances of Schwann cell abnormalities, including abnormally wide spacing between the Schwann cell cytoplasm and the adjacent SGN axon (Figure 4-5E). These glial cell-specific pathologies support the delayed ABR wave I latencies seen in fB^{-/-} mice.

We further explored the satellite cells of fB^{-/-} mice by immunostaining for Kir4.1 and Sox10. Kir4.1 is a K⁺ channel subunit expressed on the surface of glial cells and is required for myelination [191, 192]. Sox10 is a transcription factor essential for glial cell development and maintenance. Using quantitative immunohistochemistry, we found that the number of Sox10⁺ glial cells in fB^{-/-} mice is significantly increased when compared to age-matched WT mice. Significant increases in Sox10⁺ glial cell numbers were seen in all turns of the

OSL and in the apex RC of $fB^{-/-}$ mice (Figure 4-6A-B, E-F). Compared to WT mice, auditory glial cells in $fB^{-/-}$ mice also had diminished Kir4.1 expression (Figure 4-6C, D). Together with the results from our electron microscopy observations, our data suggests that fB signaling is required for proper auditory nerve myelination and the regulation of auditory glial cell numbers.

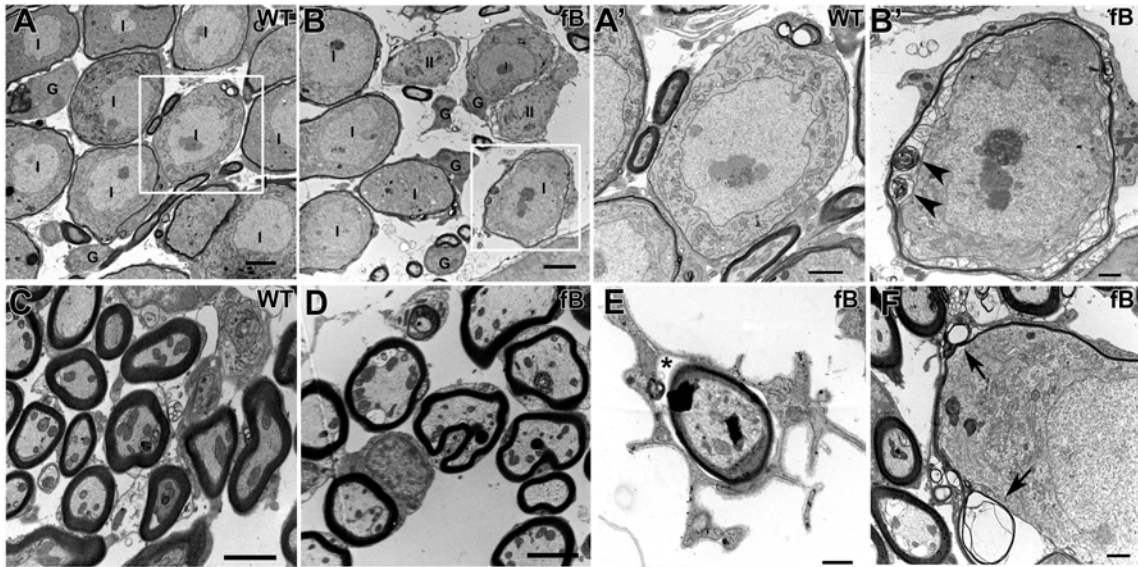


Figure 4-6. Ultrastructure analysis of $fB^{-/-}$ mouse cochleae reveal myelin pathologies. A,B. Electron micrographs of SGNs in RC of 1-month WT (**A**) and $fB^{-/-}$ (**B**) mice. Scale bars = 4 μ m. **A'-B'**. High magnification of the enclosed areas in the WT (**A'**) RC reveal tight associations between the myelin of satellite cells and SGNS. High magnification of the enclosed area in **B'** reveals enlarged spacing separating SGNs and satellite cells in $fB^{-/-}$ cochleae. Arrowheads point out myelin segments in the cytoplasm of a myelinated glial cell surrounding SGN of a $fB^{-/-}$ cochlea. A': scale bar = 2 μ m, B': scale bar = 1 μ m. **C,D.** Electron micrographs of axons in the OSL of WT (**C**) and $fB^{-/-}$ (**D**) mice. $fB^{-/-}$ cochleae appear to have fewer axons compared to WT cochleae. Scale bars = 2 μ m. **F,E.** Electron micrographs of $fB^{-/-}$ samples revealing examples of irregular spacing (asterisk) between the myelin of Schwann cells and Type I SGN axons (**E**) and abnormal myelin blebs (black arrows) in the myelin surrounding SGNs (**F**). Scale bars, 600 nm in E and 1 μ m in F.

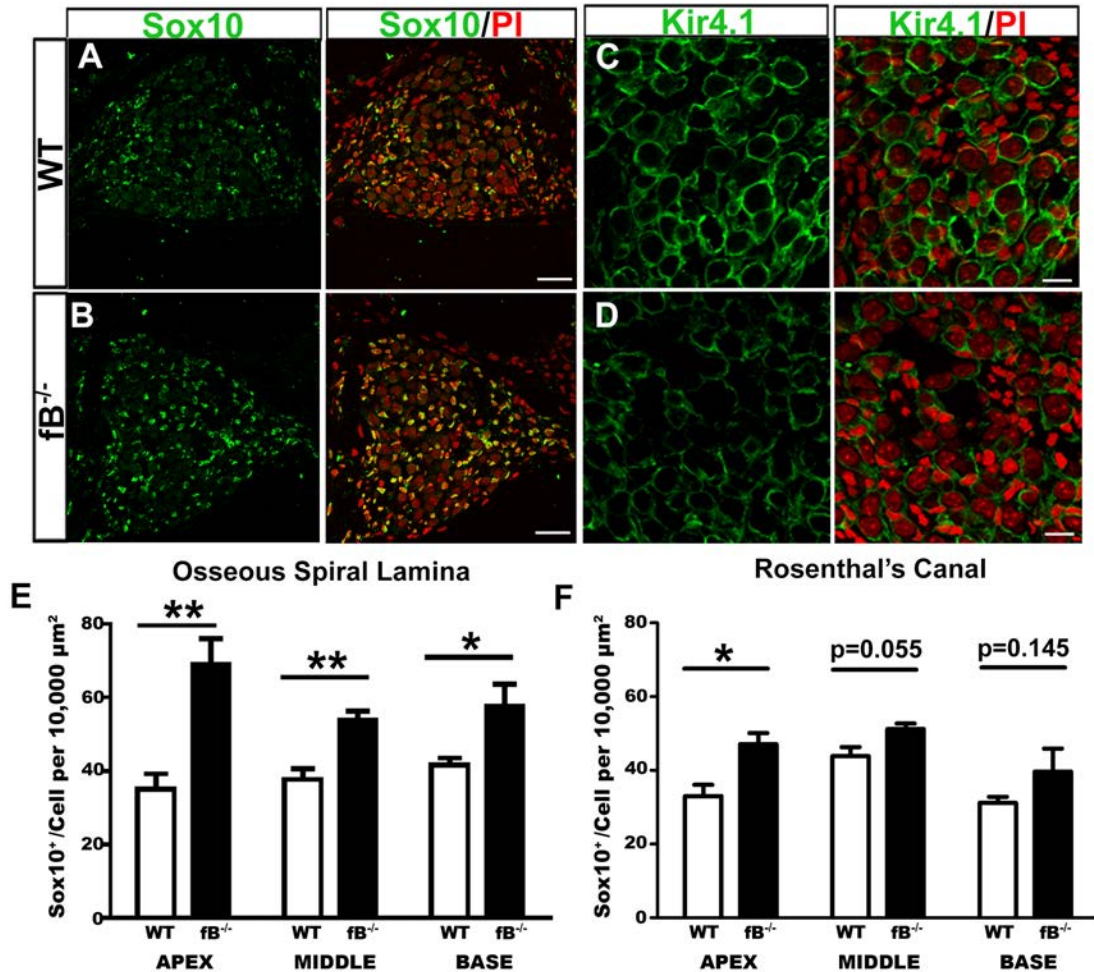


Figure 4-7. Glial cell numbers are increased in $fB^{-/-}$ mouse cochlear nerves and demonstrate potassium channel dysfunction. A,B. Confocal images of Sox10⁺ glial cells in the middle turn RC of 1-month WT (A) and $fB^{-/-}$ (B) mice. Cell nuclei were counterstained with propidium iodide (PI). Scale bars = 50 μm. C,D. Kir4.1 immunoreactivity was reduced in satellite glial cells surrounding SGNs in 1-month $fB^{-/-}$ (D) mice compared to WT (C) and. Confocal images were obtained using the same microscope acquisition settings. Diminished Kir4.1 immunoreactivity can be seen in $fB^{-/-}$ samples. Cell nuclei were counterstained with propidium iodide (PI). Scale bars = 10 μm. E,F. Quantification of Sox10⁺ glial

cells reveal more glial cells are found in the OSL (**E**) and RC (**F**) of $fB^{-/-}$ mice, in comparison to WT mice. Two-tailed, unpaired Student's t-tests were used for statistical analysis. $*p < 0.05$; $**p < 0.01$, $***p < 0.001$; P values for non-significant comparisons are provided for each cochlear turn. Data bars represent average mean; error bars represent SEM. $n = 4-5$ cochlear samples.

Macrophages are found in the auditory nerves of fB deficient mice

Complement signaling initiates the innate immune response by activating immune cells, such as macrophages [114, 178, 179]. Macrophages possess complement receptors on their cell surface and produce several complement-related genes. To investigate the impact of fB deficiency on immune cells in the auditory nerve, we investigated macrophage numbers in the adult fB^{-/-} mice. We identified macrophages in the adult auditory nerve of fB^{-/-} mice by examining the immunoreactivity of IBA1, a calcium binding protein expressed in the cytoplasm of microglia/macrophages [77, 151, 152]. IBA1⁺ macrophages were seen in the cochlea of fB^{-/-} mice (Figure 4-7A,B). Quantitative analysis revealed no significant difference in IBA1⁺ macrophage numbers in the auditory nerves of WT and fB^{-/-} mice (Figure 4-7C,D). However, further investigations of macrophage densities and numbers are required.

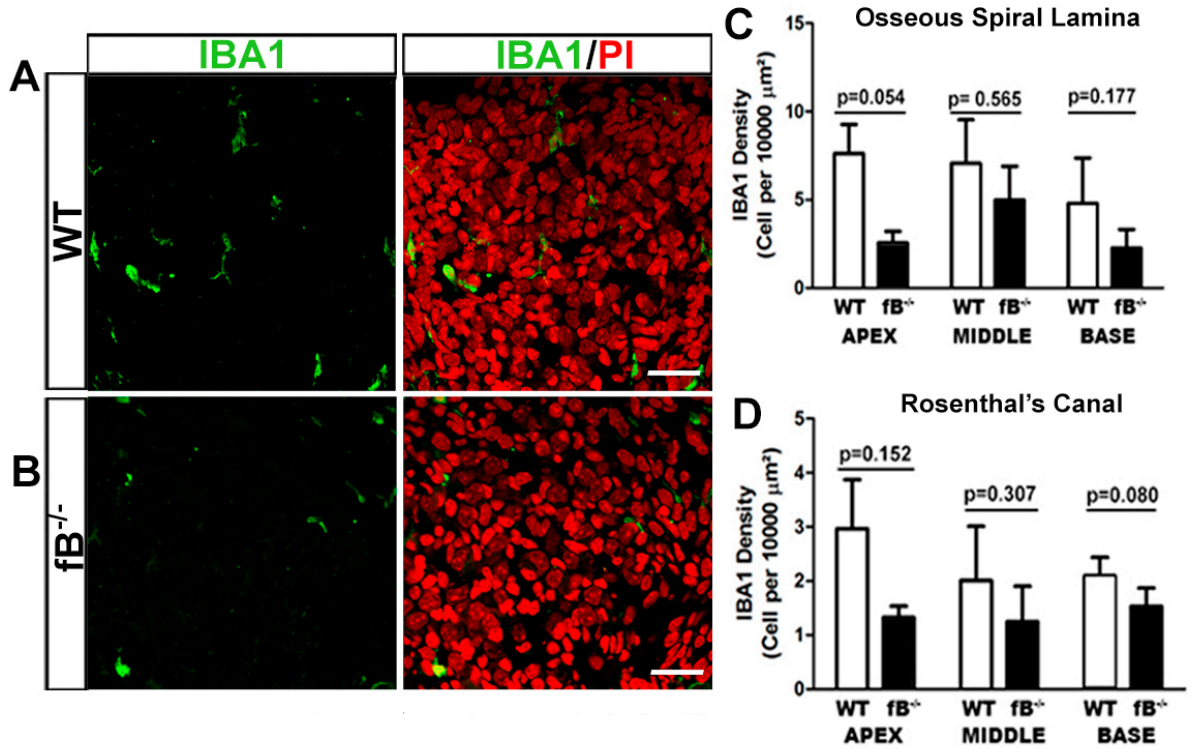


Figure 4-8. Macrophage densities in the auditory nerves of fB deficient mice. **A-B.** Confocal images of IBA1⁺ macrophages in the mid turn RC of WT (**A**) and fB^{-/-} (**B**) mice. Nuclei were counterstained with propidium iodide (PI). Scale bar = 20 μm . **C-D.** Quantifications of IBA1⁺ macrophages in the OSL (**C**) and RC (**D**) of WT and fB^{-/-} mice. P values for unpaired Student's t-tests comparing neuron counts in WT and fB^{-/-} mice are provided for each cochlear turn. Data bars represent average mean; error bars represent SEM. n= 3 cochlear samples.

A loss of cochlear lateral wall integrity in $fB^{-/-}$ mice

The cochlear LW maintains the ionic concentrations of the cochlear fluids and generates the endocochlear potential for proper auditory function [9, 165, 174, 175]. Using electron microscopy, we investigated the ultrastructural profile of the cochlear LW of WT and $fB^{-/-}$ mice (Figure 4-8A-B). $fB^{-/-}$ mice had a loss of interdigitation between the intermediate and marginal cells (Figure 4-8B, arrowheads). To confirm that the ion channels of cells in the cochlear LWs of $fB^{-/-}$ mice were disrupted, we probed for the immunoreactivity for the inwardly rectifying K^+ channel subunit, Kir4.1, in 1.5-month $fB^{-/-}$ mice. Compared to WT mice, the intensity of Kir4.1 immunostaining in $fB^{-/-}$ mice was diminished (Figure 4-8C-D). These data suggest that fB deficiency results in the disruption of structural integrity and ionic homeostasis in the cochlear LW.

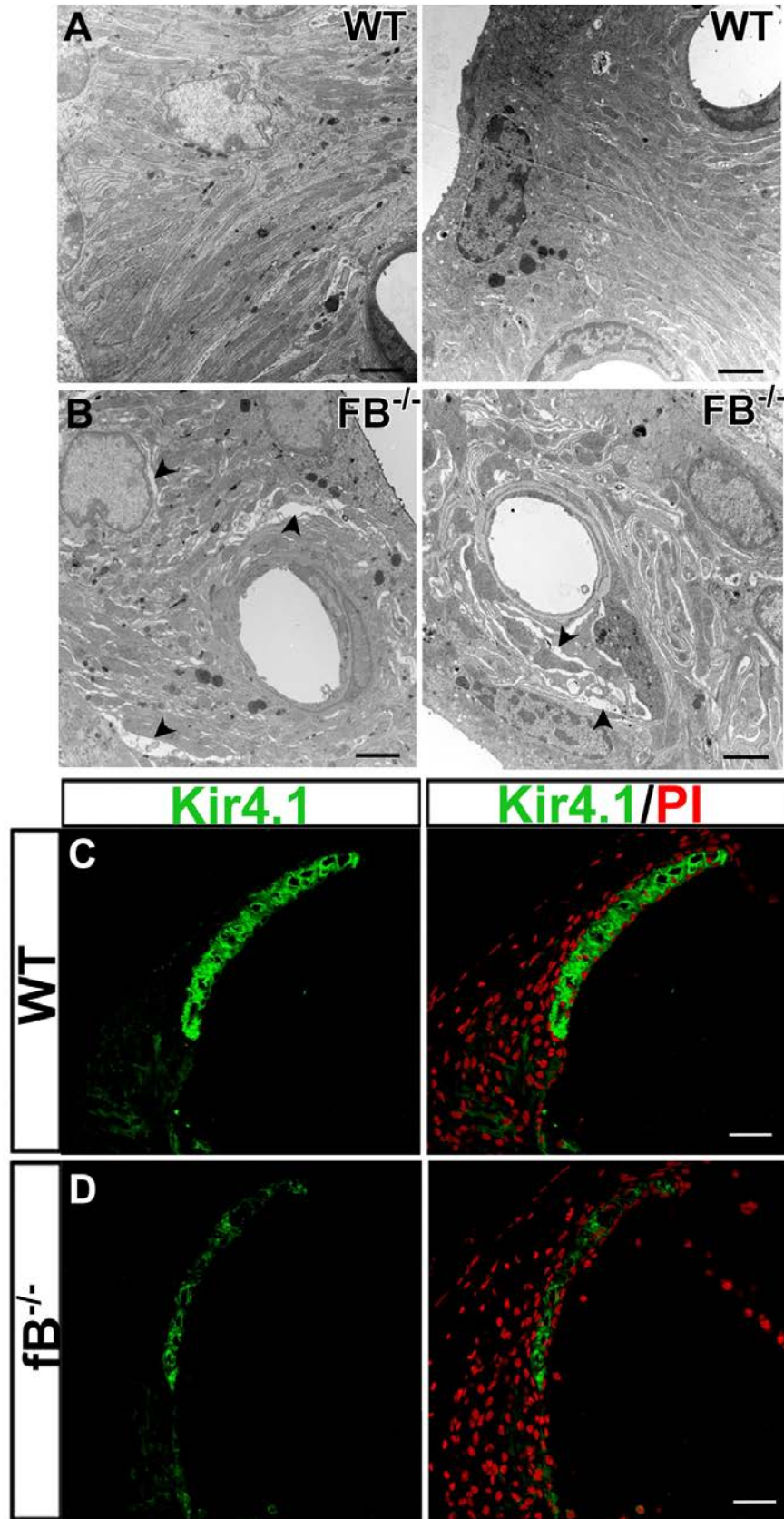


Figure 4-9. fB deficiency results in cochlear LW pathologies. A, B. Electron micrographs depict the intermediate cells of the cochlear LW of WT (**A**) and fB^{-/-} (**B**) mice. In fB^{-/-} samples, the integrity of the interdigitation between intermediate and marginal cells is lost. Arrowheads highlight areas of severe intermediate cell pathology. **C,D.** Confocal representations of Kir4.1 staining in the cochlear LWs of young adult WT (**C**) and fB^{-/-} (**D**) mice reveal diminished Kir4.1 immunoreactivity in fB^{-/-} mouse cochleae. Propidium iodide (PI) was used to counterstain cell nuclei. Confocal images were obtained using the same microscope acquisition settings. A,B: scale bars = 2 μm; C,D: scale bars = 50μm.

DISCUSSION

Using young adult $fb^{-/-}$ mice, we demonstrated that alternative complement signaling is required for proper hearing onset and the maintenance of auditory functions. Mice deficient in fb signaling had elevated ABR thresholds, decreased ABR wave I amplitudes and delayed ABR wave I latencies. Additionally, we found that adult $fb^{-/-}$ mice display multiple pathologies, including mild SGN loss, abnormal myelination, increased auditory glial cell numbers and loss of strial interdigitation in the cochlear LW.

The alternative complement pathway serves as a feedback mechanism to amplify complement signaling when C3b proteins are present. Deletion of alternative complement signaling results in decreased ability of the classical and lectin pathways to activate the complement cascade [193]. Thus, animals with depleted alternative complement components also demonstrate dampened complement activation via the classical and lectin pathways.

Alternative complement signaling has been widely implicated in injured or degenerating nervous tissue. For instance, $fb^{-/-}$ mice that have undergone cerebral ischemia-reperfusion injury demonstrate reduced neurological pathologies and display protection from demyelination [180]. Further, inhibition of the alternative complement pathway, via administration of neutralizing antibodies to fb or fb genetic deletion, results in decreased neuroinflammation and decreased neuron death in traumatic brain injury models [194, 195].

In this chapter, we found that adult $fb^{-/-}$ mice demonstrate progressive hearing loss (Figure 4-1). At P14 $fb^{-/-}$ mice displayed higher ABR thresholds than

age-matched WT counterparts. These hearing impairments were exacerbated in older $fB^{-/-}$ mice. By 4-months, $fB^{-/-}$ mice exhibited profound hearing deficits, a characteristic that is not demonstrated by WT mice of this strain until mice are 8-months [116]. Future investigations characterizing auditory function and cochlear pathological alterations in aged $fB^{-/-}$ mice would add critical knowledge regarding the role of alternative complement signaling in age-related hearing loss.

In Chapter 3, we demonstrated that transient depletion of macrophages during auditory nerve development resulted in the maintenance of supernumerary auditory glial cells, or glial cells not associated with SGN somas or axons (Figure 3-9B). Here, we found that adult $fB^{-/-}$ mice possess a significant increase in auditory glial cell numbers (Figure 4-6E,F). Further, our histological assessment of adult $fB^{-/-}$ mice revealed abnormal myelination in the satellite cells surrounding SGNs and the Schwann cells that surround axons (Figure 4-5). SGN degeneration and demyelination of the auditory nerve are central characteristics of age-related hearing loss [196]. It is probable that the hearing impairments exhibited by $fB^{-/-}$ mice are a result of SGN demyelination. Since $fB^{-/-}$ mice appear to have normal SGN numbers, it is not likely that the increased auditory glial cell densities are due to alterations in auditory nerve SGNs. Rather, the increase in glial cells seen in adult $fB^{-/-}$ mice may be due to the maintenance of supernumerary glial cells during postnatal glial cell development. Investigations of postnatal $fB^{-/-}$ mice will provide critical insight into how alternative complement signaling contributes to glial cell development and function.

Kir4.1 is expressed by glial cells in the auditory nerve and intermediate cells of the cochlear LW [197]. Kir4.1 is critical for the rectifying of K^+ by the cochlear LW for proper generation and maintenance of the endocochlear potential [198]. Also, Kir4.1 channels on the surface of glial cells play a critical role in siphoning extracellular K^+ released by neurons during activity [192, 199]. Mice lacking Kir4.1 signaling demonstrate profound hearing loss due to reduced endocochlear potential, decreased myelination and diminished ability of glial cells to expel SGN-released K^+ ions [9, 198, 199]. Using immunostaining, we found that Kir4.1 expression is diminished in glial cells and intermediate cells of the cochlear LW of $fB^{-/-}$ mice (Figure 4-6C,D; 4-8C,D). Also, our ultrastructural analysis of 1-month $fB^{-/-}$ mice revealed a loss of interdigitation between the strial intermediate and marginal cells of the LW. This suggests that alternative complement signaling may play a role in K^+ rectification and homeostasis in the cochlea. Additional physiological tests, including endocochlear potential measurements, are required to fully characterize auditory function alterations of $fB^{-/-}$ mice.

Here, we demonstrate that alternative complement deficient mice display severe hearing deficits. These deficits may be due, in part, to glial cell dysfunctions and cochlear lateral wall pathologies. Interestingly, results from recent studies have found that inhibition of the complement pathway ameliorates neuronal injury and functional defects [181, 194, 200, 201]. It will be important to examine how $fB^{-/-}$ mice respond to cochlear injury, such as noise or application of ototoxic drugs. Further investigations are required to fully understand the

contribution of alternative complement signaling to the auditory nerve
morphology and function.

CHAPTER FIVE: SUMMARY AND FUTURE DIRECTIONS

SUMMARY

We studied two aspects of how the immune system contributes to auditory nerve function. The major focus of this dissertation was to investigate the role of macrophages in the auditory nerve maturation. Our findings demonstrated that macrophages engulf glial cells during auditory nerve refinement. Transient depletion of macrophages resulted in increased glial cell numbers, myelin dysfunction, cochlear LW pathologies, and temporary hearing impairment. Together, these results demonstrate that macrophages act as more than “sentinels” in the auditory nerve microenvironment. Rather, macrophages play a role in several important processes required for hearing, including: 1) regulation of glial cell numbers, 2) proper formation of myelin, and 3) maintenance of cochlear LW integrity. Another focus of this dissertation was to elucidate the role of alternative complement signaling in the cochlea. Our results demonstrated that alternative complement signaling is important for several processes in the cochlea, including: 1) regulation of glial cell number and 2) conservancy of LW integrity. Further, complement factor B deficiency resulted in impaired auditory function, including elevated age-related hearing loss. Overall, these results suggest an important role for immune cells and immune-related pathways in auditory nerve maturation and function.

A critical finding from this study was the contributions of the immune system to auditory glial cell development and function. In the two mouse models we investigated, we found evidence of myelin pathologies, including myelin whorls, myelin blebs in the nodes of Ranvier and inclusion bodies in the myelin

sheath (Figures 3-9 and 4-5). In both animal models, we also found auditory function impairments, including decreased auditory thresholds and prolonged ABR wave I latencies (Figures 3-10, 4-2 and 4-3). A link between auditory nerve demyelination and hearing loss has recently been characterized [202]. Thus, it is likely that the physiological changes we found associated with the macrophage-depleted and $fB^{-/-}$ mice are due, in part, to myelin pathologies.

Interestingly, several demyelinating diseases of the central and peripheral nervous systems, including multiple sclerosis (MS) and Charcot-Marie-Tooth disease (CMT), also demonstrate similar myelin abnormalities that are driven by inflammatory processes. Further, these demyelinating diseases are characterized to have associated auditory impairments, including difficulties in speech perception and word discrimination [203-205]. Thus, investigations of the interactions between macrophages and glial cell in the auditory nerve will expand knowledge of the mechanisms governing auditory deficits associated with demyelinating conditions.

MS is a demyelinating disorder where the myelin sheaths in the brain and spinal cord undergo degenerative changes due to chronic neuroinflammation [206]. The characteristics of MS include the reduction of myelin proteins, dysfunction of myelinating oligodendrocytes and the loss of myelinating oligodendrocytes and Schwann cells and their precursors [206, 207]. These pathologies are primarily driven by inflammatory mechanisms, including the increased expression of pro-inflammatory cytokines and excessive macrophage/microglia activation [208, 209]. Similarly, we found that during

auditory nerve development macrophage numbers increase and immune-related molecular pathways are upregulated. Further, we identified a novel role of macrophages in eliminating excessive glial cells to regulate glial cell numbers. It is possible that the signaling interactions between macrophages and glial cells that is required for normal auditory nerve development is dysfunctional in patients suffering MS.

The results from this study raise several questions. It is unclear how glial cells are targeted for macrophage-mediated elimination. It will be important to determine if auditory glial cells are targeted by macrophages for elimination or if glial cells release “eat me” signals that macrophages respond to. It will also be essential to investigate whether glial cells participate in eliminating cells.

It will also be critical to examine how alternative complement deficiency effects auditory nerve development. This includes investigating how glial cell function is influenced by alternative complement signaling. Further, it is unclear which cell types are the major source of complement in the auditory nerve. It is crucial to identify which cells generate complement proteins in the auditory nerve.

FUTURE DIRECTIONS

Do glial cells participate in nerve refinement?

In chapter 3 we demonstrated that glial cells are phagocytosed by macrophages in the developing auditory nerve (Figure 3-6, 3-7). However, macrophages may not be the only phagocytes in the developing auditory nerve.

It is possible that glial cells are able to exhibit phagocytic functions [210, 211]. In the injured nerve, including injury related to Wallerian degeneration, glial cells participate in the clearance of dying cells, including the engulfment of other glial cells.

Wallerian degeneration is the process of nerve regrowth after axons have been cut or severed. During Wallerian degeneration, axons scale back toward the neuron cell body and ensheathing glial cells proliferate around the site of injury [212]. Glial cells also align to the uninjured portion of the axon to provide a scaffold and produce neurotropic factors for the regrowth of axons [213]. Interestingly, Schwann cells of peripheral nerves or oligodendrocytes of the CNS actively participate in the elimination of degraded axons and myelin sheath and phagocytosis of apoptotic glial cells [168, 211, 214]. The clearance of myelin debris and dead glial cells is required for axonal extension and remyelination of degenerating nerves.

Glial cells also promote the recruitment of immune cells [215]. Glial cells express multiple inflammatory mediators, including Toll-like receptors, inducible Nitric oxide synthase and tumor necrosis factor- alpha [210, 212]. However, in mouse models of Wallerian degeneration, Schwann cells are the major phagocytes until post injury day 3. Together, this demonstrates the potential phagocytic role of glial cells. It also suggests that auditory glial cells, and not only macrophages, may play a phagocytic role in the deletion of dying glial cells during auditory nerve development.

What signals contribute to macrophage-mediated cell elimination?

It remains unclear how glial cells are targeted for macrophage-mediated elimination and phagocytosis. It is possible that the molecular mechanisms underlying axon and synapse elimination during development are also at play in the clearance of glial cells. In Chapter 3 we demonstrated that transient depletion of macrophages resulted in an increase in glial cell numbers. This suggests that glial cell elimination involves immune signals.

Immune signals are required for activating macrophages. Macrophages phagocytose debris or cells when they recognize extracellular cues as harmful or foreign. Immune-related engulfment ligands, or “eat me signals” induce the selective clearance of cells by phagocytes. Additionally, the presence of “punishment” signals promote the clearance of cells. These “punishment” signals bind to weakened or asynchronously firing synapses to regulate refinement.

During synaptic refinement of the dorsal lateral geniculate nucleus (dLGN), the major “eat me” and “punishment” signals expressed by axons include the complement proteins, C1q and C3 [96]. C1q binds selectively to apoptotic cells and degenerating axons in severed motoneurons and in the developing optic nerves [94, 216, 217]. This activates this classical complement pathway and targets cells and axons for elimination. C1q and C3 proteins can be secreted by healthy axons to opsonize weaker neighboring axons [218]. Mice lacking C1q or C3 signaling exhibit decreased microglial-mediated synapse engulfment [69, 96]. Additionally, these mice have overlapping innervations

between left-right eye territories [96], demonstrating the important role of complement signals in nerve innervation and refinement.

A recent study investigating classical complement signaling in the mouse cochlea found that C1qa signaling was not critical for hearing onset and auditory function in the adult mouse [140]. Investigation of our previously published microarray data and other published microarray arrays revealed that several complement-related genes are expressed in the developing auditory nerve [72, 121]. Measurements of several complement-related genes, including C3a receptor, C1qa and fB revealed that complement gene expression is increased in the auditory nerve after P7. This suggests that complement signaling may contribute to auditory nerve development.

Further investigations of the complement expression profiles of cochlear macrophages and auditory glial cells will determine if macrophage-mediated glial cell elimination in the developing auditory nerve is complement-dependent. In Chapter 3 we found that transient macrophage-depleted mice had increased glial cell numbers during postnatal nerve development. Similarly, In Chapter 4 we observed that adult fB^{-/-} mice had increased glial cell densities. This suggests that alternative complement signaling is important for macrophage-mediated glial cell elimination required for auditory nerve development. However, it is unclear if the increase in glial cell numbers we observed in adult fB^{-/-} mice is due to decreased macrophage-mediated glial cell elimination during auditory nerve development, as described in Chapter 3, or caused by an imbalance of glial cell proliferation/apoptosis mechanisms.

How might cochlear macrophages use complement signaling to recognize target cells?

The binding or tagging of complement proteins to the cell surface is called opsonization. The most abundant complement protein that opsonize target cells is C3b [219]. C3b can bind directly to the surface of pathogens or viruses during injury response and to weakened nerve fibers and apoptotic cells during developmental processes [220-222]. Microglia are able to eliminate weakened axons and synapses during the pruning and refinement [221, 223]. Macrophages and microglia possess complement C3 receptors that bind the C3b ligand, initiating pathogen recognition and engulfment [219, 224].

A major source of free C3b is through the cleavage of C3 by the alternative complement convertase C3bB, which is generated upon the binding and conformational change of C3b and fB [104, 106]. Since fB deficient animals generate less C3b due to decreased spontaneous activation, it is likely that the reduction in free C3b in the serum results in reduced opsonization of cells that need to be recognized by phagocytes. It is possible that the increase in glial cell numbers demonstrated in the auditory nerves of fB^{-/-} mice (figure 4-6) is a result of decreased C3b to opsonize auditory glial cells, resulting in decreased recognition of target glial cells by macrophages. Our results further point to a contributing role for complement signaling in mediating macrophage-related processes during auditory nerve development.

How does alternative complement signaling impact glial cell function?

We found that adult $fB^{-/-}$ mice exhibited myelin abnormalities and impaired auditory function. In Chapter 4, we observed decreased ABR wave I amplitudes in $fB^{-/-}$ mice, when compared to WT mice (Figure 4-2). We also found that $fB^{-/-}$ mice demonstrated increased ABR wave I latencies and diminished expression of the potassium channel, Kir4.1, by auditory glial cells (Figure 4-2, 4-6). A decrease in ABR wave I amplitude and delay in ABR wave I latency suggests asynchronous firing patterns in SGN fibers. Glial cell expression of Kir4.1 is required for myelin synthesis, signal conduction and action potential propagation [191, 192, 225, 226]. It is likely that the poor signal conduction and auditory function impairments exhibited by $fB^{-/-}$ mice are due to dysfunction in myelin production by glial cells. Further, myelin dysfunction is likely a result of improper alternative complement signaling.

Examples of complement signals influencing glial cell function can be seen in multiple sclerosis. Multiple sclerosis is a chronic inflammatory disease characterized by demyelination and loss of nerve function. A recent study investigating the cerebellum of multiple sclerosis patients found that the terminal complement protein, C9, is activated in Kir4.1-rich glia cells [225]. Complement signals, including C1q, C3 and fB are also increased in degenerative neurons and glial cells in cortical brain regions during progressive multiple sclerosis [227]. These results suggest that complement signaling is required for stable glial cell function. More studies are required to understand the interplay between complement signaling and glial cell function in the auditory nerve.

What other immune pathways contribute to auditory nerve development?

Recently, MHC class I genes have been implicated in mediating synapse density of the dLGN and the mouse cortex [149, 170, 228, 229]. During development of the mouse cortex and dLGN, the expression of MHC class I is increased when exuberant synaptic connections are eliminated and when axonal projections are segregate to their targets [230]. Further, mice deficient in MHC class I α -chain molecules, H2-D1 and H2-K1, demonstrate defects in synaptic refinement, evidenced by the overproduction of pre-synaptic terminals in the retinogeniculate pathway, hippocampus and dLGN [149, 170, 228-230]. In our studies, we found that the expression of H2-D1 and H2-K1 are increased in the developing mouse auditory nerve (Figure 3-2). Specifically, expression of these two genes as upregulated at P7, corresponding to auditory nerve refinement [127]. These results are in agreement with studies from several other laboratories [62, 140].

MHC Class I proteins act as antigen presenting molecules to support recognition of pathogens and help to drive the homing of phagocytes [231]. During antigen presentation, MHC Class I proteins form a complex with antigens and are shuttled to the cell surface to increase the efficiency of recognition of self and non-self-cells by phagocytes [231-233]. Apoptotic cells release fragmented antigen-MHC Class I complexes, increasing recruitment and recognition by dendritic cells, including macrophages [231]. We found the presence of apoptotic glial cells in the auditory nerve during refinement (Figure 3-1). During this period of development, we also found that macrophage numbers increase in the

auditory nerve. It is possible that the presence of apoptotic glial cells recruit macrophages to the developing auditory nerve through MHC Class I-dependent mechanisms. Given the putative role of MHC Class I molecules in the synaptic refinement, it is possible that MHC Class I proteins contribute to macrophage recruitment and the homeostasis of the developing auditory nerve.

CONCLUSIONS

In this study, we investigated the contributions of the immune system to auditory nerve development and hearing function. We found that cochlear macrophages play a role in auditory nerve development by regulating glial cell numbers. A lack of macrophages during auditory nerve development resulted in several cochlear pathologies, including supernumerary glial cells, myelin dysfunction, transient cochlear LW abnormalities and temporary hearing impairment. We also investigated how alternative complement signaling influenced auditory function. Utilizing mice deficient in fB signaling, we found that alternative complement signaling is required for the maintenance of auditory function. fB deficient mice demonstrated myelin and cochlear LW abnormalities and progressive hearing impairments. Both macrophage-depleted and fB deficient mice demonstrated glial cell abnormalities, myelin dysfunction and hearing impairment. We conclude that immune-related processes contribute to cochlear maintenance and auditory function. Further investigations of how the immune system contributes to auditory function maintenance in adult cochlea will be critical in identifying therapeutics to address hearing impairments.

REFERENCES

1. Ryland, M.G., *The amazing ear: what happens before the brainstem auditory evoked response*. Am J Electroneurodiagnostic Technol, 2009. **49**(1): p. 1-13.
2. Ballachanda, B.B., *Theoretical and applied external ear acoustics*. J Am Acad Audiol, 1997. **8**(6): p. 411-20.
3. Cheng, J.T., et al., *The Effect of Ear Canal Orientation on Tympanic Membrane Motion and the Sound Field Near the Tympanic Membrane*. J Assoc Res Otolaryngol, 2015. **16**(4): p. 413-32.
4. Ravicz, M.E., J. Tao Cheng, and J.J. Rosowski, *Sound pressure distribution within natural and artificial human ear canals: Forward stimulation*. J Acoust Soc Am, 2014. **136**(6): p. 3132-46.
5. Purves D, A.G., Fitzpatrick D *The Middle Ear*, in *Neuroscience*]. 2001, Sinauer Associates;: Sunderland, MA.
6. Mason, M.J., *Structure and function of the mammalian middle ear. II: Inferring function from structure*. J Anat, 2016. **228**(2): p. 300-12.
7. Hemila, S., S. Nummela, and T. Reuter, *What middle ear parameters tell about impedance matching and high frequency hearing*. Hear Res, 1995. **85**(1-2): p. 31-44.
8. Hara, A., A.N. Salt, and R. Thalmann, *Perilymph composition in scala tympani of the cochlea: influence of cerebrospinal fluid*. Hear Res, 1989. **42**(2-3): p. 265-71.
9. Nin, F., et al., *The endocochlear potential depends on two K⁺ diffusion potentials and an electrical barrier in the stria vascularis of the inner ear*. Proc Natl Acad Sci U S A, 2008. **105**(5): p. 1751-6.
10. Reichenbach, T. and A.J. Hudspeth, *The physics of hearing: fluid mechanics and the active process of the inner ear*. Rep Prog Phys, 2014. **77**(7): p. 076601.
11. Chen, J. and A. Streit, *Induction of the inner ear: stepwise specification of otic fate from multipotent progenitors*. Hear Res, 2013. **297**: p. 3-12.
12. Fritsch, B., et al., *Inner ear development: building a spiral ganglion and an organ of Corti out of unspecified ectoderm*. Cell Tissue Res, 2015. **361**(1): p. 7-24.
13. Yost, W.A., *Fundamentals of Hearing: An Introduction*. 5th ed. 2007, Chicago, IL: Academic Press.
14. Mann, Z.F. and M.W. Kelley, *Development of tonotopy in the auditory periphery*. Hear Res, 2011. **276**(1-2): p. 2-15.
15. Raphael, Y. and R.A. Altschuler, *Structure and innervation of the cochlea*. Brain Res Bull, 2003. **60**(5-6): p. 397-422.

16. Gillespie, P.G. and U. Muller, *Mechanotransduction by hair cells: models, molecules, and mechanisms*. Cell, 2009. **139**(1): p. 33-44.
17. Hudspeth, A.J. and R. Jacobs, *Stereocilia mediate transduction in vertebrate hair cells (auditory system/cilium/vestibular system)*. Proc Natl Acad Sci U S A, 1979. **76**(3): p. 1506-9.
18. Ricci, A.J., A.C. Crawford, and R. Fettiplace, *Mechanisms of active hair bundle motion in auditory hair cells*. J Neurosci, 2002. **22**(1): p. 44-52.
19. Corns, L.F., et al., *Calcium entry into stereocilia drives adaptation of the mechano-electrical transducer current of mammalian cochlear hair cells*. Proc Natl Acad Sci U S A, 2014. **111**(41): p. 14918-23.
20. Wangemann, P., *Supporting sensory transduction: cochlear fluid homeostasis and the endocochlear potential*. J Physiol, 2006. **576**(Pt 1): p. 11-21.
21. Velez-Ortega, A.C., et al., *Mechanotransduction current is essential for stability of the transducing stereocilia in mammalian auditory hair cells*. Elife, 2017. **6**.
22. Nadol, J.B., Jr., *Comparative anatomy of the cochlea and auditory nerve in mammals*. Hear Res, 1988. **34**(3): p. 253-66.
23. Berglund, A.M. and D.K. Ryugo, *Hair cell innervation by spiral ganglion neurons in the mouse*. J Comp Neurol, 1987. **255**(4): p. 560-70.
24. Coate, T.M. and M.W. Kelley, *Making connections in the inner ear: recent insights into the development of spiral ganglion neurons and their connectivity with sensory hair cells*. Semin Cell Dev Biol, 2013. **24**(5): p. 460-9.
25. Adamson, C.L., M.A. Reid, and R.L. Davis, *Opposite actions of brain-derived neurotrophic factor and neurotrophin-3 on firing features and ion channel composition of murine spiral ganglion neurons*. J Neurosci, 2002. **22**(4): p. 1385-96.
26. Zhou, Z., Q. Liu, and R.L. Davis, *Complex regulation of spiral ganglion neuron firing patterns by neurotrophin-3*. J Neurosci, 2005. **25**(33): p. 7558-66.
27. Chen, W.C., et al., *Complex distribution patterns of voltage-gated calcium channel alpha-subunits in the spiral ganglion*. Hear Res, 2011. **278**(1-2): p. 52-68.
28. Mou, K., et al., *Synergistic effects of BDNF and NT-3 on postnatal spiral ganglion neurons*. J Comp Neurol, 1997. **386**(4): p. 529-39.
29. Ernfors, P., et al., *Complementary roles of BDNF and NT-3 in vestibular and auditory development*. Neuron, 1995. **14**(6): p. 1153-64.

30. Liebl, D.J., et al., *Absence of sensory neurons before target innervation in brain-derived neurotrophic factor-, neurotrophin 3-, and TrkC-deficient embryonic mice*. J Neurosci, 1997. **17**(23): p. 9113-21.
31. Agterberg, M.J.H., et al., *Enhanced Survival of Spiral Ganglion Cells After Cessation of Treatment with Brain-Derived Neurotrophic Factor in Deafened Guinea Pigs*. J Assoc Res Otolaryngol, 2009. **10**(3): p. 355-67.
32. Defourny, J., F. Lallemand, and B. Malgrange, *Structure and development of cochlear afferent innervation in mammals*. Am J Physiol Cell Physiol, 2011. **301**(4): p. C750-61.
33. Le Douarin, N.M. and E. Dupin, *Multipotentiality of the neural crest*. Curr Opin Genet Dev, 2003. **13**(5): p. 529-36.
34. Spoenclin, H., *Anatomy of cochlear innervation*. Am J Otolaryngol, 1985. **6**(6): p. 453-67.
35. Shah, N.M., et al., *Glial growth factor restricts mammalian neural crest stem cells to a glial fate*. Cell, 1994. **77**(3): p. 349-60.
36. Monk, K.R., et al., *Gpr126 is essential for peripheral nerve development and myelination in mammals*. Development, 2011. **138**(13): p. 2673-80.
37. Kuhlbrodt, K., et al., *Sox10, a novel transcriptional modulator in glial cells*. J Neurosci, 1998. **18**(1): p. 237-50.
38. Britsch, S., et al., *The transcription factor Sox10 is a key regulator of peripheral glial development*. Genes Dev, 2001. **15**(1): p. 66-78.
39. Jessen, K.R. and R. Mirsky, *The origin and development of glial cells in peripheral nerves*. Nat Rev Neurosci, 2005. **6**(9): p. 671-82.
40. Mirsky, R. and K.R. Jessen, *Schwann cell development, differentiation and myelination*. Curr Opin Neurobiol, 1996. **6**(1): p. 89-96.
41. Woodhoo, A. and L. Sommer, *Development of the Schwann cell lineage: from the neural crest to the myelinated nerve*. Glia, 2008. **56**(14): p. 1481-90.
42. Syroid, D.E., et al., *Cell death in the Schwann cell lineage and its regulation by neuregulin*. Proc Natl Acad Sci U S A, 1996. **93**(17): p. 9229-34.
43. Garbay, B., et al., *Myelin synthesis in the peripheral nervous system*. Prog Neurobiol, 2000. **61**(3): p. 267-304.
44. Mikoshiba, K., et al., *Structure and Function of Myelin Protein Genes*. Annu Rev Neurosci, 1991. **14**.
45. Romand, R. and M.R. Romand, *Qualitative and quantitative observations of spiral ganglion development in the rat*. Hear Res, 1985. **18**(2): p. 111-20.

46. Song, L., J. McGee, and E.J. Walsh, *Frequency- and level-dependent changes in auditory brainstem responses (ABRS) in developing mice*. J Acoust Soc Am, 2006. **119**(4): p. 2242-57.
47. Buonanno, A. and G.D. Fischbach, *Neuregulin and ErbB receptor signaling pathways in the nervous system*. Curr Opin Neurobiol, 2001. **11**(3): p. 287-96.
48. Pereira, J.A., F. Lebrun-Julien, and U. Suter, *Molecular mechanisms regulating myelination in the peripheral nervous system*. Trends Neurosci, 2012. **35**(2): p. 123-34.
49. Lee, Y.I., et al., *Neuregulin1 displayed on motor axons regulates terminal Schwann cell-mediated synapse elimination at developing neuromuscular junctions*. Proc Natl Acad Sci U S A, 2016. **113**(4): p. E479-87.
50. Michailov, G.V., et al., *Axonal neuregulin-1 regulates myelin sheath thickness*. Science, 2004. **304**(5671): p. 700-3.
51. Chen, S., et al., *Neuregulin 1-erbB signaling is necessary for normal myelination and sensory function*. J Neurosci, 2006. **26**(12): p. 3079-86.
52. Finzsch, M., et al., *Sox10 is required for Schwann cell identity and progression beyond the immature Schwann cell stage*. J Cell Biol, 2010. **189**(4): p. 701-12.
53. Weider, M., et al., *Elevated in vivo levels of a single transcription factor directly convert satellite glia into oligodendrocyte-like cells*. PLoS Genet, 2015. **11**(2): p. e1005008.
54. Breuskin, I., et al., *Glial but not neuronal development in the cochleovestibular ganglion requires Sox10*. J Neurochem, 2010. **114**(6): p. 1827-39.
55. Mao, Y., et al., *Targeted Deletion of Sox10 by Wnt1-cre Defects Neuronal Migration and Projection in the Mouse Inner Ear*. PLoS ONE, 2014. **9**(4): p. e94580.
56. Locher, H., et al., *Distribution and development of peripheral glial cells in the human fetal cochlea*. PLoS One, 2014. **9**(1): p. e88066.
57. Koundakjian, E.J., J.L. Appler, and L.V. Goodrich, *Auditory neurons make stereotyped wiring decisions before maturation of their targets*. J Neurosci, 2007. **27**(51): p. 14078-88.
58. Druckenbrod, N.R. and L.V. Goodrich, *Sequential Retraction Segregates SGN Processes during Target Selection in the Cochlea*. The Journal of Neuroscience, 2015. **35**(49): p. 16221-16235.
59. Huang, L.C., et al., *Spatiotemporal definition of neurite outgrowth, refinement and retraction in the developing mouse cochlea*. Development, 2007. **134**(16): p. 2925-33.

60. Echteler, S.M., T. Magardino, and M. Rontal, *Spatiotemporal patterns of neuronal programmed cell death during postnatal development of the gerbil cochlea*. Brain Res Dev Brain Res, 2005. **157**(2): p. 192-200.
61. Barclay, M., A.F. Ryan, and G.D. Housley, *Type I vs type II spiral ganglion neurons exhibit differential survival and neuritogenesis during cochlear development*. Neural Dev, 2011. **6**: p. 33.
62. Appler, J.M. and L.V. Goodrich, *Connecting the ear to the brain: Molecular mechanisms of auditory circuit assembly*. Prog Neurobiol, 2011. **93**(4): p. 488-508.
63. Katz, L.C. and C.J. Shatz, *Synaptic activity and the construction of cortical circuits*. Science, 1996. **274**(5290): p. 1133-8.
64. Oster, S.F. and D.W. Sretavan, *Connecting the eye to the brain: the molecular basis of ganglion cell axon guidance*. Br J Ophthalmol, 2003. **87**(5): p. 639-45.
65. Tritsch, N.X., et al., *The origin of spontaneous activity in the developing auditory system*. Nature, 2007. **450**(7166): p. 50-5.
66. Wyatt, R.M. and R.J. Balice-Gordon, *Activity-dependent elimination of neuromuscular synapses*. J Neurocytol, 2003. **32**(5-8): p. 777-94.
67. Fujino, K. and D. Oertel, *Bidirectional synaptic plasticity in the cerebellum-like mammalian dorsal cochlear nucleus*. Proc Natl Acad Sci U S A, 2003. **100**(1): p. 265-70.
68. Tzounopoulos, T., et al., *Cell-specific, spike timing-dependent plasticities in the dorsal cochlear nucleus*. Nat Neurosci, 2004. **7**(7): p. 719-25.
69. Schafer, D.P., et al., *Microglia sculpt postnatal neural circuits in an activity and complement-dependent manner*. Neuron, 2012. **74**(4): p. 691-705.
70. Soto, F., et al., *Spontaneous activity promotes synapse formation in a cell-type-dependent manner in the developing retina*. J Neurosci, 2012. **32**(16): p. 5426-39.
71. Wang, C.L., et al., *Activity-dependent development of callosal projections in the somatosensory cortex*. J Neurosci, 2007. **27**(42): p. 11334-42.
72. Lu, C.C., et al., *Developmental Profiling of Spiral Ganglion Neurons Reveals Insights into Auditory Circuit Assembly*. J Neurosci, 2011. **31**(30): p. 10903-18.
73. Mosser, D.M. and J.P. Edwards, *Exploring the full spectrum of macrophage activation*. Nat Rev Immunol, 2008. **8**(12): p. 958-69.
74. Davies, L.C., et al., *Tissue-resident macrophages*. Nat Immunol, 2013. **14**(10): p. 986-95.
75. Gomez Perdiguero, E., et al., *Tissue-resident macrophages originate from yolk-sac-derived erythro-myeloid progenitors*. Nature, 2015. **518**(7540): p. 547-51.

76. van de Laar, L., et al., *Yolk Sac Macrophages, Fetal Liver, and Adult Monocytes Can Colonize an Empty Niche and Develop into Functional Tissue-Resident Macrophages*. *Immunity*, 2016. **44**(4): p. 755-68.
77. Okano, T., et al., *Bone marrow-derived cells expressing Iba1 are constitutively present as resident tissue macrophages in the mouse cochlea*. *J Neurosci Res*, 2008. **86**(8): p. 1758-67.
78. Sato, E., et al., *Expression of fractalkine receptor CX3CR1 on cochlear macrophages influences survival of hair cells following ototoxic injury*. *J Assoc Res Otolaryngol*, 2010. **11**(2): p. 223-34.
79. Tornabene, S.V., et al., *Immune cell recruitment following acoustic trauma*. *Hear Res*, 2006. **222**(1-2): p. 115-24.
80. Kaur, T., et al., *Fractalkine Signaling Regulates Macrophage Recruitment into the Cochlea and Promotes the Survival of Spiral Ganglion Neurons after Selective Hair Cell Lesion*. *J Neurosci*, 2015. **35**(45): p. 15050-61.
81. Warchol, M.E. and B.A. Kaplan, *Macrophage secretory products influence the survival of statoacoustic neurons*. *Neuroreport*, 1999. **10**(4): p. 665-8.
82. Lang, H., et al., *Contribution of bone marrow hematopoietic stem cells to adult mouse inner ear: mesenchymal cells and fibrocytes*. *J Comp Neurol*, 2006. **496**(2): p. 187-201.
83. Ladrech, S., et al., *Macrophage contribution to the response of the rat organ of Corti to amikacin*. *J Neurosci Res*, 2007. **85**(9): p. 1970-9.
84. Fredelius, L. and H. Rask-Andersen, *The role of macrophages in the disposal of degeneration products within the organ of Corti after acoustic overstimulation*. *Acta Otolaryngol*, 1990. **109**(1-2): p. 76-82.
85. Lang, H., et al., *Contributions of Mouse and Human Hematopoietic Cells to Remodeling of the Adult Auditory Nerve After Neuron Loss*. *Mol Ther*, 2016.
86. Hirose, K., et al., *Mononuclear phagocytes migrate into the murine cochlea after acoustic trauma*. *J Comp Neurol*, 2005. **489**(2): p. 180-94.
87. Tong, L., et al., *Selective deletion of cochlear hair cells causes rapid age-dependent changes in spiral ganglion and cochlear nucleus neurons*. *J Neurosci*, 2015. **35**(20): p. 7878-91.
88. Gloddek, B., et al., *Induction of MHC class II antigens on cells of the inner ear*. *Audiol Neurootol*, 2002. **7**(6): p. 317-23.
89. Yang, W., et al., *Activation of the antigen presentation function of mononuclear phagocyte populations associated with the basilar membrane of the cochlea after acoustic overstimulation*. *Neuroscience*, 2015. **303**: p. 1-15.

90. Lang, H., et al., *Nuclear factor kappaB deficiency is associated with auditory nerve degeneration and increased noise-induced hearing loss*. J Neurosci, 2006. **26**(13): p. 3541-50.
91. Yamamoto, H., et al., *The influence of NF- κ B signal-transduction pathways on the murine inner ear by acoustic overstimulation*. J Neurosci Res, 2009. **87**(8): p. 1832-40.
92. Patel, M., et al., *Transcriptome characterization by RNA-Seq reveals the involvement of the complement components in noise-traumatized rat cochleae*. Neuroscience, 2013. **248**: p. 1-16.
93. Paolicelli, R.C., et al., *Synaptic pruning by microglia is necessary for normal brain development*. Science, 2011. **333**(6048): p. 1456-8.
94. Berg, A., et al., *Reduced removal of synaptic terminals from axotomized spinal motoneurons in the absence of complement C3*. Exp Neurol, 2012. **237**(1): p. 8-17.
95. Bialas, A.R. and B. Stevens, *TGF-beta signaling regulates neuronal C1q expression and developmental synaptic refinement*. Nat Neurosci, 2013. **16**(12): p. 1773-82.
96. Stevens, B., et al., *The classical complement cascade mediates CNS synapse elimination*. Cell, 2007. **131**(6): p. 1164-78.
97. Cunningham, C.L., V. Martinez-Cerdeno, and S.C. Noctor, *Microglia regulate the number of neural precursor cells in the developing cerebral cortex*. J Neurosci, 2013. **33**(10): p. 4216-33.
98. Shigemoto-Mogami, Y., et al., *Microglia enhance neurogenesis and oligodendrogenesis in the early postnatal subventricular zone*. J Neurosci, 2014. **34**(6): p. 2231-43.
99. Ueno, M., et al., *Layer V cortical neurons require microglial support for survival during postnatal development*. Nat Neurosci, 2013. **16**(5): p. 543-51.
100. Nishiyori, A., et al., *Localization of fractalkine and CX3CR1 mRNAs in rat brain: does fractalkine play a role in signaling from neuron to microglia?* FEBS Lett, 1998. **429**(2): p. 167-72.
101. Truman, L.A., et al., *CX3CL1/fractalkine is released from apoptotic lymphocytes to stimulate macrophage chemotaxis*. Blood, 2008. **112**(13): p. 5026-36.
102. Pagani, F., et al., *Defective microglial development in the hippocampus of Cx3cr1 deficient mice*. Frontiers in Cellular Neuroscience, 2015. **9**: p. 111.
103. Hoshiko, M., et al., *Deficiency of the microglial receptor CX3CR1 impairs postnatal functional development of thalamocortical synapses in the barrel cortex*. J Neurosci, 2012. **32**(43): p. 15106-11.

104. Merle, N.S., et al., *Complement System Part I - Molecular Mechanisms of Activation and Regulation*. Front Immunol, 2015. **6**: p. 262.
105. Sarma, J.V. and P.A. Ward, *The Complement System*. Cell Tissue Res, 2011. **343**(1): p. 227-35.
106. Ramaglia, V., M.R. Daha, and F. Baas, *The complement system in the peripheral nerve: friend or foe?* Mol Immunol, 2008. **45**(15): p. 3865-77.
107. Morgan, B.P. and C.L. Harris, *Complement, a target for therapy in inflammatory and degenerative diseases*. Nat Rev Drug Discov, 2015. **14**(12): p. 857-77.
108. Colten, H.R., et al., *Regulation of complement protein biosynthesis in mononuclear phagocytes*. Ciba Found Symp, 1986. **118**: p. 141-54.
109. de Jonge, R.R., et al., *Expression of complement components in the peripheral nervous system*. Hum Mol Genet, 2004. **13**(3): p. 295-302.
110. Fonseca, M.I., et al., *Cell-specific deletion of C1qa identifies microglia as the dominant source of C1q in mouse brain*. J Neuroinflammation, 2017. **14**(1): p. 48.
111. Gasque, P., et al., *The receptor for complement anaphylatoxin C3a is expressed by myeloid cells and nonmyeloid cells in inflamed human central nervous system: analysis in multiple sclerosis and bacterial meningitis*. J Immunol, 1998. **160**(7): p. 3543-54.
112. Levi-Strauss, M. and M. Mallat, *Primary cultures of murine astrocytes produce C3 and factor B, two components of the alternative pathway of complement activation*. J Immunol, 1987. **139**(7): p. 2361-6.
113. Hudspeth, A.J. and M. Konishi, *Auditory neuroscience: development, transduction, and integration*. Proc Natl Acad Sci U S A, 2000. **97**(22): p. 11690-1.
114. Bohlson, S.S., et al., *Complement, C1q, and C1q-related molecules regulate macrophage polarization*. Frontiers in Immunology, 2014. **5**.
115. Erway, L.C., Zheng, Q. Y. and Johnson, K. R., *Inbred strains of mice for genetics of hearing in mammals: Searching for genes for hearing loss*, in *Handbook of Mouse Auditory Research: From Behavior to Molecular Biology*, J.F. Willott, Editor. 2001, CRC Press: Boca Raton. p. 429-439.
116. Zheng, Q.Y., K.R. Johnson, and L.C. Erway, *Assessment of hearing in 80 inbred strains of mice by ABR threshold analyses*. Hear Res, 1999. **130**(1-2): p. 94-107.
117. Cailhier, J.F., et al., *Conditional macrophage ablation demonstrates that resident macrophages initiate acute peritoneal inflammation*. J Immunol, 2005. **174**(4): p. 2336-42.

118. Matsumoto, M., et al., *Abrogation of the alternative complement pathway by targeted deletion of murine factor B*. Proc Natl Acad Sci U S A, 1997. **94**(16): p. 8720-5.
119. Pekna, M., et al., *Mice deficient for the complement factor B develop and reproduce normally*. Scand J Immunol, 1998. **47**(4): p. 375-80.
120. Zhang, W., et al., *Perivascular-resident macrophage-like melanocytes in the inner ear are essential for the integrity of the intrastrial fluid-blood barrier*. Proc Natl Acad Sci U S A, 2012. **109**(26): p. 10388-93.
121. Lang, H., et al., *Neural stem/progenitor cell properties of glial cells in the adult mouse auditory nerve*. Sci Rep, 2015. **5**: p. 13383.
122. Lang, H., et al., *Sox2 up-regulation and glial cell proliferation following degeneration of spiral ganglion neurons in the adult mouse inner ear*. J Assoc Res Otolaryngol, 2011. **12**(2): p. 151-71.
123. Lang, H., et al., *Chronic reduction of endocochlear potential reduces auditory nerve activity: further confirmation of an animal model of metabolic presbycusis*. J Assoc Res Otolaryngol, 2010. **11**(3): p. 419-34.
124. Yu, W.-M., et al., *A Gata3–Mafb transcriptional network directs post-synaptic differentiation in synapses specialized for hearing*. eLife, 2013. **2**: p. e01341.
125. Coate, T.M., et al., *Neuropilin-2/Semaphorin-3F-mediated repulsion promotes inner hair cell innervation by spiral ganglion neurons*. eLife, 2015. **4**: p. e07830.
126. Jyothi, V., et al., *Unmyelinated auditory type I spiral ganglion neurons in congenic Ly5.1 mice*. J Comp Neurol, 2010. **518**(16): p. 3254-71.
127. Brown, L.N., et al., *Macrophage-Mediated Glial Cell Elimination in the Postnatal Mouse Cochlea*. Frontiers in Molecular Neuroscience, 2017. **10**(407).
128. Marrs, G.S. and G.A. Spirou, *Embryonic assembly of auditory circuits: spiral ganglion and brainstem*. J Physiol, 2012. **590**(Pt 10): p. 2391-408.
129. Echterler, S.M. and Y.C. Nofsinger, *Development of ganglion cell topography in the postnatal cochlea*. J Comp Neurol, 2000. **425**(3): p. 436-46.
130. Echterler, S.M., *Developmental segregation in the afferent projections to mammalian auditory hair cells*. Proc Natl Acad Sci U S A, 1992. **89**(14): p. 6324-7.
131. Hansen, M.R., et al., *Reciprocal signaling between spiral ganglion neurons and Schwann cells involves neuregulin and neurotrophins*. Hear Res, 2001. **161**(1-2): p. 87-98.

132. Stankovic, K., et al., *Survival of adult spiral ganglion neurons requires erbB receptor signaling in the inner ear*. J Neurosci, 2004. **24**(40): p. 8651-61.
133. Jeon, E.J., et al., *Influence of central glia on spiral ganglion neuron neurite growth*. Neuroscience, 2011. **177**: p. 321-34.
134. Miron, V.E., et al., *M2 microglia and macrophages drive oligodendrocyte differentiation during CNS remyelination*. Nat Neurosci, 2013. **16**(9): p. 1211-8.
135. Guipponi, M., et al., *Mice deficient for the type II transmembrane serine protease, TMPRSS1/hepsin, exhibit profound hearing loss*. Am J Pathol, 2007. **171**(2): p. 608-16.
136. Akil, O., et al., *Spiral ganglion degeneration and hearing loss as a consequence of satellite cell death in saposin B-deficient mice*. J Neurosci, 2015. **35**(7): p. 3263-75.
137. Tang, W., et al., *Connexin29 is highly expressed in cochlear Schwann cells, and it is required for the normal development and function of the auditory nerve of mice*. J Neurosci, 2006. **26**(7): p. 1991-9.
138. Bas, E., et al., *Spiral ganglion cells and macrophages initiate neuro-inflammation and scarring following cochlear implantation*. Frontiers in Cellular Neuroscience, 2015. **9**(303).
139. Fuentes-Santamaría, V., et al., *The Role of Glia in the Peripheral and Central Auditory System Following Noise Overexposure: Contribution of TNF- α and IL-1 β to the Pathogenesis of Hearing Loss*. Frontiers in Neuroanatomy, 2017. **11**(9).
140. Calton, M.A., et al., *A lack of immune system genes causes loss in high frequency hearing but does not disrupt cochlear synapse maturation in mice*. PLoS One, 2014. **9**(5): p. e94549.
141. Bank, L.M., et al., *Macrophage migration inhibitory factor acts as a neurotrophin in the developing inner ear*. Development, 2012. **139**(24): p. 4666-74.
142. Porter, A.G. and R.U. Janicke, *Emerging roles of caspase-3 in apoptosis*. Cell Death Differ, 1999. **6**(2): p. 99-104.
143. Janicke, R.U., et al., *Caspase-3 is required for DNA fragmentation and morphological changes associated with apoptosis*. J Biol Chem, 1998. **273**(16): p. 9357-60.
144. Hall, P.A., *Assessing apoptosis: a critical survey*. Endocr Relat Cancer, 1999. **6**(1): p. 3-8.
145. Astigarraga, S., et al., *Three Drosophila liprins interact to control synapse formation*. J Neurosci, 2010. **30**(46): p. 15358-68.

146. Dunah, A.W., et al., *LAR receptor protein tyrosine phosphatases in the development and maintenance of excitatory synapses*. Nat Neurosci, 2005. **8**(4): p. 458-67.
147. Yoshikawa, M., et al., *Contribution of the Runx1 transcription factor to axonal pathfinding and muscle innervation by hypoglossal motoneurons*. Dev Neurobiol, 2015.
148. Konig, N., et al., *Forced Runx1 expression in human neural stem/progenitor cells transplanted to the rat dorsal root ganglion cavity results in extensive axonal growth specifically from spinal cord-derived neurospheres*. Stem Cells Dev, 2011. **20**(11): p. 1847-57.
149. Thams, S., A. Oliveira, and S. Cullheim, *MHC class I expression and synaptic plasticity after nerve lesion*. Brain Res Rev, 2008. **57**(1): p. 265-9.
150. Bahrini, I., et al., *Neuronal exosomes facilitate synaptic pruning by up-regulating complement factors in microglia*. Scientific Reports, 2015. **5**: p. 7989.
151. Ohsawa, K., et al., *Involvement of Iba1 in membrane ruffling and phagocytosis of macrophages/microglia*. J Cell Sci, 2000. **113 (Pt 17)**: p. 3073-84.
152. Sasaki, Y., et al., *Iba1 is an actin-cross-linking protein in macrophages/microglia*. Biochem Biophys Res Commun, 2001. **286**(2): p. 292-7.
153. Kaur, C., S.T. Dheen, and E.A. Ling, *From blood to brain: amoeboid microglial cell, a nascent macrophage and its functions in developing brain*. Acta Pharmacol Sin, 2007. **28**(8): p. 1087-96.
154. Parakalan, R., et al., *Transcriptome analysis of amoeboid and ramified microglia isolated from the corpus callosum of rat brain*. BMC Neurosci, 2012. **13**: p. 64.
155. Hume, D.A., V.H. Perry, and S. Gordon, *The mononuclear phagocyte system of the mouse defined by immunohistochemical localisation of antigen F4/80: macrophages associated with epithelia*. Anat Rec, 1984. **210**(3): p. 503-12.
156. Austyn, J.M. and S. Gordon, *F4/80, a monoclonal antibody directed specifically against the mouse macrophage*. Eur J Immunol, 1981. **11**(10): p. 805-15.
157. Barros, M.H., et al., *Macrophage polarisation: an immunohistochemical approach for identifying M1 and M2 macrophages*. PLoS One, 2013. **8**(11): p. e80908.
158. Bennett, M.L., et al., *New tools for studying microglia in the mouse and human CNS*. Proc Natl Acad Sci U S A, 2016. **113**(12): p. E1738-46.
159. Hickman, S.E., et al., *The microglial sensome revealed by direct RNA sequencing*. Nat Neurosci, 2013. **16**(12): p. 1896-1905.

160. Stoneman, V., et al., *Monocyte/Macrophage Suppression in CD11b Diphtheria Toxin Receptor Transgenic Mice Differentially Affects Atherogenesis and Established Plaques*. *Circ Res*, 2007. **100**(6): p. 884-93.
161. Wang, J., et al., *Myelination of the postnatal mouse cochlear nerve at the peripheral-central nervous system transitional zone*. *Front Pediatr*, 2013. **1**: p. 43.
162. Zhang, F., et al., *Characterization and inflammatory response of perivascular-resident macrophage-like melanocytes in the vestibular system*. *J Assoc Res Otolaryngol*, 2013. **14**(5): p. 635-43.
163. Stevens, S.M., et al., *Heptanol application to the mouse round window: a model for studying cochlear lateral wall regeneration*. *Otolaryngol Head Neck Surg*, 2014. **150**(4): p. 659-65.
164. Mizutani, K., et al., *Late-phase recovery in the cochlear lateral wall following severe degeneration by acute energy failure*. *Brain Res*, 2011. **1419**: p. 1-11.
165. Li, Y., et al., *Characterization of slow-cycling cells in the mouse cochlear lateral wall*. *PLoS One*, 2017. **12**(6): p. e0179293.
166. Zhu, B., et al., *Drosophila neurotrophins reveal a common mechanism for nervous system formation*. *PLoS Biol*, 2008. **6**(11): p. e284.
167. Purves, D., W.D. Snider, and J.T. Voyvodic, *Trophic regulation of nerve cell morphology and innervation in the autonomic nervous system*. *Nature*, 1988. **336**(6195): p. 123-8.
168. Kang, H., et al., *Terminal Schwann cells participate in neuromuscular synapse remodeling during reinnervation following nerve injury*. *J Neurosci*, 2014. **34**(18): p. 6323-33.
169. Kim, J.H., R. Renden, and H. von Gersdorff, *Dysmyelination of auditory afferent axons increases the jitter of action potential timing during high-frequency firing*. *J Neurosci*, 2013. **33**(22): p. 9402-7.
170. Dixon-Salazar, T.J., et al., *MHC class I limits hippocampal synapse density by inhibiting neuronal insulin receptor signaling*. *J Neurosci*, 2014. **34**(35): p. 11844-56.
171. Chen, Z., et al., *Microglial displacement of inhibitory synapses provides neuroprotection in the adult brain*. *Nat Commun*, 2014. **5**: p. 4486.
172. Zusso, M., et al., *Regulation of postnatal forebrain amoeboid microglial cell proliferation and development by the transcription factor Runx1*. *J Neurosci*, 2012. **32**(33): p. 11285-98.
173. Elliott, M.R., et al., *Nucleotides released by apoptotic cells act as a find-me signal for phagocytic clearance*. *Nature*, 2009. **461**(7261): p. 282-286.

174. Salt, A.N., I. Melichar, and R. Thalmann, *Mechanisms of endocochlear potential generation by stria vascularis*. Laryngoscope, 1987. **97**(8 Pt 1): p. 984-91.
175. Takeuchi, S., M. Ando, and A. Kakigi, *Mechanism generating endocochlear potential: role played by intermediate cells in stria vascularis*. Biophys J, 2000. **79**(5): p. 2572-82.
176. Juhn, S.K., B.A. Hunter, and R.M. Odland, *Blood-labyrinth barrier and fluid dynamics of the inner ear*. Int Tinnitus J, 2001. **7**(2): p. 72-83.
177. Zhang, W., et al., *Perivascular-resident macrophage-like melanocytes in the inner ear are essential for the integrity of the intrastrial fluid–blood barrier*. Proceedings of the National Academy of Sciences of the United States of America, 2012. **109**(26): p. 10388-10393.
178. Ricklin, D., et al., *Complement: a key system for immune surveillance and homeostasis*. Nat Immunol, 2010. **11**(9): p. 785-97.
179. Bianco, C., O. Gotze, and Z.A. Cohn, *Regulation of macrophage migration by products of the complement system*. Proc Natl Acad Sci U S A, 1979. **76**(2): p. 888-91.
180. Elvington, A., et al., *The alternative complement pathway propagates inflammation and injury in murine ischemic stroke*. J Immunol, 2012. **189**(9): p. 4640-7.
181. Qiao, F., et al., *The alternative and terminal pathways of complement mediate post-traumatic spinal cord inflammation and injury*. Am J Pathol, 2010. **177**(6): p. 3061-70.
182. Ramaglia, V., et al., *C3-dependent mechanism of microglial priming relevant to multiple sclerosis*. Proceedings of the National Academy of Sciences, 2012. **109**(3): p. 965-970.
183. Stephan, A.H., et al., *A dramatic increase of C1q protein in the CNS during normal aging*. J Neurosci, 2013. **33**(33): p. 13460-74.
184. Hong, S., et al., *Complement and microglia mediate early synapse loss in Alzheimer mouse models*. Science, 2016. **352**(6286): p. 712-716.
185. Lian, H., et al., *Astrocyte-Microglia Cross Talk through Complement Activation Modulates Amyloid Pathology in Mouse Models of Alzheimer's Disease*. J Neurosci, 2016. **36**(2): p. 577-89.
186. Ramaglia, V., et al., *Complement inhibition accelerates regeneration in a model of peripheral nerve injury*. Mol Immunol, 2009. **47**(2-3): p. 302-9.
187. Hourcade, D.E. and L.M. Mitchell, *Access to the Complement Factor B Scissile Bond Is Facilitated by Association of Factor B with C3b Protein*. J Biol Chem, 2011. **286**(41): p. 35725-32.
188. Miller, C.A., P.J. Abbas, and B.K. Robinson, *The use of long-duration current pulses to assess nerve survival*. Hear Res, 1994. **78**(1): p. 11-26.

189. Zhou, R., P.J. Abbas, and J.G. Assouline, *Electrically evoked auditory brainstem response in peripherally myelin-deficient mice*. *Hear Res*, 1995. **88**(1-2): p. 98-106.
190. Prado-Guitierrez, P., et al., *Effect of interphase gap and pulse duration on electrically evoked potentials is correlated with auditory nerve survival*. *Hear Res*, 2006. **215**(1-2): p. 47-55.
191. Brasko, C., et al., *Expression of Kir4.1 and Kir5.1 inwardly rectifying potassium channels in oligodendrocytes, the myelinating cells of the CNS*. *Brain Struct Funct*, 2017. **222**(1): p. 41-59.
192. Neusch, C., et al., *Kir4.1 potassium channel subunit is crucial for oligodendrocyte development and in vivo myelination*. *J Neurosci*, 2001. **21**(15): p. 5429-38.
193. Pangburn, M.K. and H.J. Muller-Eberhard, *Initiation of the alternative complement pathway due to spontaneous hydrolysis of the thioester of C3*. *Ann N Y Acad Sci*, 1983. **421**: p. 291-8.
194. Leinhase, I., et al., *Reduced neuronal cell death after experimental brain injury in mice lacking a functional alternative pathway of complement activation*. *BMC Neurosci*, 2006. **7**: p. 55.
195. Leinhase, I., et al., *Inhibition of the alternative complement activation pathway in traumatic brain injury by a monoclonal anti-factor B antibody: a randomized placebo-controlled study in mice*. *J Neuroinflammation*, 2007. **4**: p. 13.
196. Wise, A.K., et al., *Structural and Ultrastructural Changes to Type I Spiral Ganglion Neurons and Schwann Cells in the Deafened Guinea Pig Cochlea*. *J Assoc Res Otolaryngol*, 2017. **18**(6): p. 751-769.
197. Ando, M. and S. Takeuchi, *Immunological identification of an inward rectifier K⁺ channel (Kir4.1) in the intermediate cell (melanocyte) of the cochlear stria vascularis of gerbils and rats*. *Cell Tissue Res*, 1999. **298**(1): p. 179-83.
198. Hibino, H., et al., *An ATP-dependent inwardly rectifying potassium channel, KAB-2 (Kir4.1), in cochlear stria vascularis of inner ear: its specific subcellular localization and correlation with the formation of endocochlear potential*. *J Neurosci*, 1997. **17**(12): p. 4711-21.
199. Rozengurt, N., et al., *Time course of inner ear degeneration and deafness in mice lacking the Kir4.1 potassium channel subunit*. *Hear Res*, 2003. **177**(1-2): p. 71-80.
200. Nataf, S., et al., *Attenuation of experimental autoimmune demyelination in complement-deficient mice*. *J Immunol*, 2000. **165**(10): p. 5867-73.
201. Hu, X., et al., *Therapeutic inhibition of the alternative complement pathway attenuates chronic EAE*. *Mol Immunol*, 2013. **54**(3-4): p. 302-8.

202. Wan, G. and G. Corfas, *Transient auditory nerve demyelination as a new mechanism for hidden hearing loss*. Nat Commun, 2017. **8**: p. 14487.
203. Valadbeigi, A., et al., *Central auditory processing and word discrimination in patients with multiple sclerosis*. Eur Arch Otorhinolaryngol, 2014. **271**(11): p. 2891-6.
204. Knopp, M., et al., *Optic and auditory pathway dysfunction in demyelinating neuropathies*. Acta Neurol Scand, 2014. **130**(1): p. 53-7.
205. Rance, G., et al., *Auditory function in children with Charcot-Marie-Tooth disease*. Brain, 2012. **135**(Pt 5): p. 1412-22.
206. A.O.Dulamea, *Role of Oligodendrocyte Dysfunction in Demyelination, Remyelination and Neurodegeneration in Multiple Sclerosis.*, in *Multiple Sclerosis: Bench to Bedside*. 2017, Springer. p. 91-121.
207. Kocsis, J.D. and S.G. Waxman, *Schwann cells and their precursors for repair of central nervous system myelin*. Brain, 2007. **130**(Pt 8): p. 1978-80.
208. Ellwardt, E. and F. Zipp, *Molecular mechanisms linking neuroinflammation and neurodegeneration in MS*. Exp Neurol, 2014. **262 Pt A**: p. 8-17.
209. Gonzalez-Scarano, F. and G. Baltuch, *Microglia as mediators of inflammatory and degenerative diseases*. Annu Rev Neurosci, 1999. **22**: p. 219-40.
210. Lee, H., et al., *Necrotic neuronal cells induce inflammatory Schwann cell activation via TLR2 and TLR3: implication in Wallerian degeneration*. Biochem Biophys Res Commun, 2006. **350**(3): p. 742-7.
211. Arthur-Farraj, P.J., et al., *c-Jun reprograms Schwann cells of injured nerves to generate a repair cell essential for regeneration*. Neuron, 2012. **75**(4): p. 633-47.
212. Catenaccio, A., et al., *Molecular analysis of axonal-intrinsic and glial-associated co-regulation of axon degeneration*. Cell Death Dis, 2017. **8**(11): p. e3166.
213. Beirowski, B., *Concepts for regulation of axon integrity by enwrapping glia*. Front Cell Neurosci, 2013. **7**: p. 256.
214. Jung, J., et al., *Actin polymerization is essential for myelin sheath fragmentation during Wallerian degeneration*. J Neurosci, 2011. **31**(6): p. 2009-15.
215. Murinson, B.B., et al., *Degeneration of myelinated efferent fibers prompts mitosis in Remak Schwann cells of uninjured C-fiber afferents*. J Neurosci, 2005. **25**(5): p. 1179-87.
216. Bijl, M., et al., *Reduced uptake of apoptotic cells by macrophages in systemic lupus erythematosus: correlates with decreased serum levels of complement*. Ann Rheum Dis, 2006. **65**(1): p. 57-63.

217. Silverman, S.M., et al., *C1q propagates microglial activation and neurodegeneration in the visual axis following retinal ischemia/reperfusion injury*. Mol Neurodegener, 2016. **11**: p. 24.
218. Lichtman, J.W. and H. Colman, *Synapse elimination and indelible memory*. Neuron, 2000. **25**(2): p. 269-78.
219. van Lookeren Campagne, M., C. Wiesmann, and E.J. Brown, *Macrophage complement receptors and pathogen clearance*. Cell Microbiol, 2007. **9**(9): p. 2095-102.
220. Janeway CA Jr, T.P., Walport M et al., *The complement system and innate immunity*, in *Immunobiology: The Immune System in Health and Disease*. 2001, Garland Science: New York.
221. Perry, V.H. and V. O'Connor, *C1q: the perfect complement for a synaptic feast?* Nat Rev Neurosci, 2008. **9**(11): p. 807-11.
222. Hernandez-Encinas, E., et al., *Complement component 3 (C3) expression in the hippocampus after excitotoxic injury: role of C/EBPbeta*. J Neuroinflammation, 2016. **13**(1): p. 276.
223. Luo, L. and D.D. O'Leary, *Axon retraction and degeneration in development and disease*. Annu Rev Neurosci, 2005. **28**: p. 127-56.
224. Dai, S., et al., *Fine tuning inflammation at the front door: macrophage complement receptor 3-mediates phagocytosis and immune suppression for Francisella tularensis*. PLoS Pathog, 2013. **9**(1): p. e1003114.
225. Srivastava, R., et al., *Potassium channel KIR4.1 as an immune target in multiple sclerosis*. N Engl J Med, 2012. **367**(2): p. 115-23.
226. Djukic, B., et al., *Conditional knock-out of Kir4.1 leads to glial membrane depolarization, inhibition of potassium and glutamate uptake, and enhanced short-term synaptic potentiation*. J Neurosci, 2007. **27**(42): p. 11354-65.
227. Watkins, L.M., et al., *Complement is activated in progressive multiple sclerosis cortical grey matter lesions*. J Neuroinflammation, 2016. **13**(1): p. 161.
228. Oliveira, A.L., et al., *A role for MHC class I molecules in synaptic plasticity and regeneration of neurons after axotomy*. Proc Natl Acad Sci U S A, 2004. **101**(51): p. 17843-8.
229. Zanon, R.G. and A.L. Oliveira, *MHC I upregulation influences astroglial reaction and synaptic plasticity in the spinal cord after sciatic nerve transection*. Exp Neurol, 2006. **200**(2): p. 521-31.
230. Huh, G.S., et al., *Functional requirement for class I MHC in CNS development and plasticity*. Science, 2000. **290**(5499): p. 2155-9.
231. Mantegazza, A.R., et al., *Presentation of phagocytosed antigens by MHC class I and II*. Traffic, 2013. **14**(2): p. 135-52.

232. Joffre, O.P., et al., *Cross-presentation by dendritic cells*. Nat Rev Immunol, 2012. **12**(8): p. 557-69.
233. Leone, P., et al., *MHC class I antigen processing and presenting machinery: organization, function, and defects in tumor cells*. J Natl Cancer Inst, 2013. **105**(16): p. 1172-87.